NOTICE

The quality of this microform is heavily dependent upon the quality of the original thesis submitted for microfilming. Every effort has been made to ensure the highest quality of reproduction possible.

If pages are missing, contact the university which granted the degree.

Some pages may have indistinct print especially if the original pages were typed with a poor typewriter ribbon or if the university sent us an inferior photocopy.

Previously copyrighted materials (journal articles, published tests, etc.) are not filmed.

Reproduction in full or in part of this microform is governed by the Canadian Copyright Act, R.S.C. 1970, c. C-30.

AVIS

La qualité de cette microforme dépend grandement de la qualité de la thèse soumise au microfilmage. Nous avons tout fait pour assurer une qualité supérieure de reproduction.

S'il manque des pages, veuillez communiquer avec l'université qui a conféré le grade.

La qualité d'impression de certaines pages peut laisser à désirer, surtout si les pages originales ont été dactylographiées à l'aide d'un ruban usé ou si l'université nous a fait parvenir une photocopie de qualité inférieure.

Les documents qui font déjà l'objet d'un droit d'auteur (articles de revue, tests publiés, etc.) ne sont pas microfilmés.

La reproduction, même partielle, de cette microforme est soumise à la Loi canadienne sur le droit d'auteur, SRC 1970, c. C-30.

Canada

FLOW VISUALIZATION OF CAVITATING, HIGH-SPEED, SUBMERGED WATER JETS

by

MICHEL SZYMCZAK

A thesis
presented to the University of Ottawa
on May 3, 1988
in partial fulfillment of the
requirement for the degree of
MASTER of APPLIED SCIENCE
in
MECHANICAL ENGINEERING

OTTAWA, Ontario, 1988

ISBN 0-315-46860-2

UNIVERSITÉ D'OTTAWA
UNIVERSITY OF OTTAWA

ABSTRACT

The performance of high-speed submerged water jets has generally shown encouraging results in cleaning, cutting, drilling and industrial applications. A number of publications have reported tests of the jet performance under various conditions, but fundamental studies dealing with the jet structure and the rationalization of its erosive properties are relatively few.

Simple visualization techniques involving stroboscopic and laser-sheet illumination were developed to investigate the cavitation characteristics of jets issuing from three geometrically similar nozzles, one of which was equipped with an obstruction. Short and long-time-exposures were recorded using a 35 mm reflex camera and high-speed black-and-white film.

The presence of the jet's potential core as well as the inception, transport and collapse of the cavities were visible. As the nozzle pressure increased, consequently increasing the jet velocity, the cavitation region not only intensified but also expanded both radially and axially.

A cavitation coefficient, k, was defined to describe the probability of cavitation inception in the submerged jets, taking into account the mean and fluctuating static pressure fields. The coefficient was found to grow quadratically with axial distance from the nozzle. The axial extent of the cavitation region was correlated

with the various flow variables.

ACKNOWLEDGEMENTS

I would like to express my gratitude to my advisors, Professors S. Tavoularis and A. Fahim for initiating this research. I am particularly grateful to Professor S. Tavoularis for his added time, help and guidance throughout the study.

Thanks are also due to the Natural Sciences and Engineering Research Council of Canada for granting me a Graduate Scholarship and to my supervisors for further financial assistance.

Permission to use the research facilities of the Gas Dynamics Laboratory, National Research Council of Canada and helpful interaction during this work were kindly provided by Dr. M.M. Vijay. I also wish to acknowledge the technical assistance offered by Mr. N. Paquette and Mr. J. Lancaster also of the National Research Council of Canada.

To my family, friends and colleagues, I am greatly indebted for the moral support and encouragements they have given me throughout this research thesis.

NOMENCLATURE

C_p	pressure coefficient
$C_{p,min}$	minimum pressure coefficient
$C_{p'}$	r.m.s. pressure coefficient
$C_{\bar{p}}$	mean pressure coefficient
D	diameter of nozzle
D_e	equivalent diameter of nozzle
D_p	pin diameter of nozzle
k	cavitation coefficient
k_{col}	cavitation coefficient at cavity collapse
k_i	cavitation inception coefficient
O_2	oxygen
p	pressure fluctuation
p'	r.m.s. pressure fluctuation
P	local static pressure
$\bar{P}$	mean static pressure
P_{amb}	ambient pressure
P_N	pressure upstream of nozzle
P_v	vapor pressure
r	radial distance from jet axis

R	radius of nozzle
Re_D	Reynolds number based on diameter
Re_{D_e}	Reynolds number based on equivalent diameter
T_{H_2O}	temperature of water
U	local velocity
$\overline{U}_m$	jet centerline velocity
U_o	jet velocity at nozzle exit
x	downstream distance from nozzle
$\left(\frac{x}{D}\right)_{col}$	downstream distance of cavity collapse
γ	specific weight of water
ρ	fluid density
σ	cavitation index
σ_i	incipient cavitation index
σ_d	cavitation desintence index

TABLE OF CONTENTS

List of Tables

List of Plates

List of Figures

Chapter 1

INTRODUCTION

1.1 Preamble

As early as the Roman times, a law governing the discharge rate from orifices supplying public water was defined. Jets issuing from fountains, faucets and fire hose nozzles have been studied systematically at least since the days of Renaissance.

Liquid jets have been used in industry in a wide variety of applications. For example, atomization jets in carburetors have been developed to improve engine efficiency and to reduce fuel consumption; subcutaneous injections are possible with liquid jets under the trade name of 'Hypospray' ; and jets of abrasive particles have been used for drilling holes in teeth.

The invention of the jet pump by James Thomson in 1852 gradually led to the technology of jet propulsion, first developed for boats and, more recently, for aircraft and rockets. On a large scale, meteorologists have also observed 'jet streams' of air in the stratosphere, with speeds from 160 to 480 km/h (100-300 mph) (Birkhoff and Zarantonello, 1957).

High-speed water jets have recently been developed for use in the cleaning, cutting and drilling industries. Applications include the removal of oil and rubber

off airport runways, the peeling of chewing gum off sidewalks, and the scouring of rust from industrial boilers and heat exchangers (Gronauer, 1972; Harris and Brierley, 1972; Torpey, 1972).

Materials ranging from candy bars to composite materials are cut by needle-thin jets of water forced out of nozzles at pressures of up to 380 MPa (55 000 psi) and velocities equivalent to three times the speed of sound in air. With the addition of abrasive particles such as silica to the water, materials such as glass and metal which once were thought to be impossible to cut with water jets are now cut routinely (Yie, 1987). There are many advantages in using high-speed water jets instead of conventional methods. The suppression of dust and the relatively small quantity of debris produced by these jets result in safer cutting and cleaning operations (Saunders, 1982). Unlike saws, water jets can cut along complicated contours. Furthermore, water jets can cut materials without generating heat encountered in plasma, laser and torch cutting, and, therefore, cutting does not alter the physical properties of the material.

1.2 Objectives and Scope of the Present Research

Although water jets have been studied since the early 1900's, the advent of technology has brought new questions to be resolved. The commercial applications of various types of high-speed water jets in cleaning, cutting and drilling a diverse selection of materials has sparked great interest in the industry.

Since the time of the first international symposium on jet cutting technology, held in Coventry, England, in 1972, it has been realized that prediction and improvement of jet operation requires an understanding of basic flow conditions,

such as turbulence level, shear magnitude and, also, in the case of submerged water jets, cavitation characteristics. Unfortunately, there still exists a shortage of information on the basic characteristics of cavitating jets despite their realized potential.

Athough cavitation is a detrimental and destructive phenomenon in most applications (i.e. pumps, propellers, spillways, etc.), its presence appears to improve jet performance at least in certain applications such as rock cutting (Johnson et al., 1968; Vijay and Brierley, 1979). The increased erosive power of cavitating, submerged water jets relative to water jets issuing in air at the same nozzle pressures can be possibly attributed to the high magnitude stresses caused by the impact of microjets created in the proximity of the specimen surface during cavity collapse.

The main objective of the present study was to develop flow visualization techniques suitable for the study of cavitation in submerged high-speed water jets of the type used in cleaning, cutting and drilling applications. Since previous techniques have only revealed the surface structure of high-speed water jets, emphasis in the present study was placed on developing techniques to reveal the jet's internal structure. The intention was to apply such visualization techniques to cavitating high-speed submerged water jets generated at different operating conditions and by nozzles of varying geometry and diameter and to record the images on photographic film, which could be possibly used to qualitatively describe and explain the structure of the jet and its cavitation characteristics.

A second objective of this thesis was to examine the possibility of predicting cavitation in high-speed water jets using results from earlier investigations. Since no directly relevant measurements could be found, this aspect was expected to be

of very rough nature. Results of such predictions, combined with a few case studies of flow visualization, would constitute the first study specifically addressing this problem and could provide an impetus for future quantitative studies.

Chapter 2

LITERATURE SURVEY

Jets, in general have been extensively studied and in consequence, well documented.

In view of the vast amount of information concerning jets and the specific nature of the present study, the literature survey will be presented in four sections. The first section treats jets in general with emphasis on high-speed water jets. It is followed by a brief section dealing with the general phenomenon of cavitation. The next section summarizes the research and developments concerning submerged and cavitating water jets and, finally, the last section covers visualization studies of water jets.

Although some papers and reports contain material relevant to two or three sections, it was found best to present them in this manner, because this permits a self-contained summary of previous work related to each different aspect of the present research.

2.1 Circular Jets

Early studies by Corrsin (1946) and Corrsin and Uberoi (1950,1951) in heated, axisymmetric air jets, provided detailed measurements of the mean and turbulent

velocity and temperature fields using hot-wire anemometry.

Mean axial and radial velocities, mean static pressure, turbulence intensities, turbulent shear stresses, and pressure fluctuations have also been measured and analyzed by various authors. Davies et al. (1962) studied the turbulence in the mixing region whereas Sami et al. (1967) performed similar tests in the flow-establishment region of an air jet. In the latter study it was found that low frequency small-scale eddies are located near the axis of the jet while the higher frequency eddies seem to appear in the vicinity of the nominal boundary of the jet.

Extensive measurements of the acoustic and turbulent fields of jets were performed by Lau et al. (1970), Fuchs (1972), Michalke and Fuchs (1975), and Arndt and Nilsen (1971). Comparable tests conducted by Yamamoto and Arndt (1979) detected slight asymmetries in both the jet and the surrounding flow fields and indicated that the true jet axis had the form of a helical wave. More recently, Drubka et al. (1982) studied the role of the jet's helical mode and the instability of the mixing layers in turbulent axisymmetric jets.

Conventional intrusive data collection was complemented in some cases by flow visualization (Crow and Champagne, 1971).

Understanding of the dynamics of relatively slow jets has led to the development of high-speed water jets. Shavlovsky (1972) presented the dynamics and structure of fine continuous water jets at pressures of up to 51 MPa and discussed conditions necessary for the formation of fine, high-speed continuous water jets. A technique for measuring liquid jets travelling at supersonic velocity in air was developed by Kinoshita (1974).

Extensive theoretical and experimental research by Yanaida (1974), and Yanaida and Ohashi (1978, 1980) revealed the pattern of the jet spread, the axial dynamic pressure, and the break-up characteristics in all regions of water jets issuing in air. Eddingfield et al. (1981) also presented an axisymmetric, multi-component mathematical model which couples all the existing flow fields in a water jet.

Expressions describing the length of the initial section, the boundary and the distribution of dynamic pressure in the core of a water jet issuing in air were developed by Zou et al. (1985).

2.2 Cavitation

The cavitation phenomenon occurs in a wide range of applications and has been studied extensively, because of its significant effects on drag, noise, vibration and material erosion. A number of reviews on cavitation are available. In recent years, Plesset and Prosperetti (1977) presented a review focussing on bubble dynamics, whereas Apfel (1981) presented an in-depth outlook on acoustic cavitation. Arndt (1981) has published an extensive review on cavitation in fluid machinery and hydraulic structures, covering a physical description of cavitation, cavitation and bubble dynamics, dissolved gas effects, and thermodynamic effects. Finally Billet (1985) has reviewed cavitation nuclei. A textbook authored by Knapp et al. (1970) also extensively documents cavitation.

Although most of its effects are undesirable, cavitation has also been found useful in certain applications, for example in homogenization of milk and in industrial cleaning (Arndt, 1981). Vijay and Brierley (1978, 1979) and Chahine et

al (1983), among others, have documented the advantages of cavitation in water jets used in cutting and cleaning applications.

2.3 Submerged and Cavitating Water Jets

Submerged water jets are but one form of high-speed water jets used in cutting and cleaning. It appears that in most cases, their erosive power is surprisingly high, compared to that of non-submerged water jets operating at the same nozzle pressure.

Early studies of the diffusion of submerged water jets from slots and orifices by Albertson et al. (1950) resulted in the development of analytical expressions for the distribution of velocity, volume flux, and energy flux in the zones of flow establishment and of established flow.

Due to the problems associated with inserting probes into a liquid flow, Wilson and Prosser (1969) developed a remote optical sensing technique, utilizing two schlieren systems to measure turbulent density fluctuations in a low speed, submerged water jet. Laser-Doppler systems were used by Barker (1973) to obtain detailed measurements in axisymmetric turbulent round jets of water and dilute polymer solutions in water. Reed et al. (1977), and Rankin et al. (1983) also used laser-Doppler instrumentation in the fully developed turbulence of an axisymmetric free jet, and in laminar axisymmetric submerged water jets, respectively.

Studies were also conducted to investigate submerged water jets directed normally at a free surface from below. Ungate et al. (1975) measured jet temperature profiles and turbulent jet dilution in the laminar-turbulent transition of non-buoyant and buoyant round jets. Garrad et al. (1983) measured the axial

velocity distribution and radial velocity distribution on the free surface for round turbulent jets.

It is clear that, at high Reynolds numbers, the mixing layer of a submerged water jet becomes turbulent. Turbulence and large-scale vortices cause positive and negative pressure fluctuations, which have particularly large magnitudes in the mixing layer between the jet and the surrounding fluid. The presence of low pressure regions leads to cavitation.

Turbulence and boundary-layer effects on cavitation inception near solid boundaries have been investigated by Daily and Johnson (1956), who addressed the effect of gas nuclei and by Arndt and Daily (1969), who dealt with the specific problem of turbulence effects on cavitation inception within a turbulent boundary layer on a solid boundary for smooth and rough surfaces. Cavitation was observed by Arndt and Ippen (1968) to occur approximately in the center of the boundary layer, at a point where negative peaks in the static pressure have a magnitude which exceeds five times the root mean square wall pressure fluctuation.

Arndt and George (1979) found that cavitation nuclei in turbulent shear flows are relatively more responsive to a wider range of pressure fluctuations as the scale of the flow increases and that large deviations from the mean pressure are more probable with increasing Reynolds number.

The point of incipient cavitation of submerged water jets was studied by Whitehouse (1952). Photographic evidence confirmed that cavitation occurred in the core of turbulent vortices within the zone of maximum turbulence.

Rouse (1966) demonstrated using flow visualization that the inception of cavitation occurred near the nozzle exit, in the mixing layer between the jet core and

the surrounding fluid.

Johnson et al. (1968) attempted to utilize cavitation damage produced by high-speed water jets in rock tunneling. As preliminary results, the findings were encouraging and required further studies. Cavitation production by means of nozzles with inserts was also studied by Lichtarowicz and Şakkejha (1972).

While evaluating the cutting and drilling performance of cavitating submerged jets, Lichtarowicz (1974), and Vijay and Brierley (1978, 1979) concluded that, in most cases, submerged jets would be more effective than similar jets issuing in air. Summers (1983) pointed out that a disadvantage of submerged jets is that their effectiveness decays very rapidly with increasing distance from the nozzle.

A few attempts to improve the cavitation characteristics of water jets by using various nozzle designs have also been published. Erdmann-Jesnitzer et al. (1978) designed nozzles combining both conical contraction angles and straight cylindrical sections. The submerged jet appeared as a white truncated cone which consisted mainly of a jet conical core, induced cavities, highly disturbed zones with free cavities and turbulence. They concluded that an increase in jet pressure had no influence on the stand-off distance (i.e. distance between nozzle exit and specimen), but it affected the intensity of erosion. Yanaida et al. (1985) found that horn-shaped nozzles (i.e. nozzles with divergent outlets) produced approximately fourteen times the eroded volume produced by hornless nozzles of similar internal geometry.

In order to overcome the difficulty in producing submerged conditions, in many applications, Vijay and Brierley (1978, 1979) and Vickers et al. (1980) examined two methods of artificial submergence for in-air cleaning and cutting operations.

Their results showed an increase in cleaning and cutting efficiency, which was partially attributed to an extended stand-off distance.

Johnson et al. (1982) have developed self-resonating, submerged, cavitating jets in which the flow is caused to pulsate at frequencies corresponding to the predominant frequency of the vertical structures in the jet shear layer. Comparative testing showed that self-resonating cavitating jets can cut rock and perform underwater cleaning more effectively and faster than either conventional jets or non-resonating cavitating jets.

Finally, Vijay (1987) has surveyed the existing literature related to cavitating water jets. He concluded that, although the potential of cavitating jets has been recognized, reliable measurements of their basic characteristics are scant and an understanding of the fluid flow phenomena (i.e. turbulence, cavitation, etc.) involved is incomplete.

2.4 Water Jet Visualization

Direct measurements with probes are difficult in water jets because such probes would disturb the flow or would be damaged by it. Therefore, non-intrusive techniques such as flow visualization are more appropriate for such studies.

Early visual studies of submerged water jets by Rouse (1953) consisted of single and multiple exposures using short duration illumination (1/20000 second). To visualize the radial distribution of the cavities, a condensing lens and a slot were used to produce a thin (6 mm) sheet of light at right angles to the camera axis.

Hoyt and Taylor (1979, 1983) studied water jets in air with a special camera designed and built by J.J. Taylor (1975). They utilized a special photographic

technique, imaging light from an electronic flash through the flow field directly upon the photographic film and recording two subsequent images on the same frame. Flow details such as surface waves, transition and spray eruption were captured. Bubbles of air riding on the surface of water jets and rayon threads added to the water were also clearly visible and demonstrated that the flow inside the jet was turbulent. This technique has a good temporal resolution but is unable to reveal the three-dimensional distribution of cavities since it images a projection of the entire flow.

Hiller and Hägele (1980) visualized hypersonic micro-jets by laser-induced fluorescence and recorded the jet boundaries and the shock wave patterns.

High-speed percussive water jets (i.e. having a modulated flow discharge, resulting in a sequence of high frequency impact forces) were studied by Nebecker and Cramer (1980) and Nebecker (1983) by means of an infrared technique. Penetration of the mist shrouding the jets travelling at velocities of up to 300 m/s was possible thus revealing the 'core' followed by 'bunches' (i.e. intermittent modules of water) which are typical of percussive water jets. Similar results were obtained by Chahine et al. (1983), using dark field illumination and a high speed camera. This technique also showed the bunching and jet contour but could not reveal the jet's internal structure.

The spread of a jet and the small scale structures of liquid (fuel) jets in gas were visualized by Eisfeld (1984), using high-speed cinematography and short time interferometry. Interferometric fringes were visible due to the great temperature and density gradients resulting from the fuel's combustion.

Baev et al. (1985) observed the dynamics of unsteady high-velocity liquid jets

injected into air by methods of high-speed cinematography, roentgenography and microphotography with pulsed lasers and pulsed X-rays. The temporal development of the jet and its non-stationary structure were studied. The jet profile and bunching effect were visible. Photographs by Fiedler et al. (1985) revealed the small scale structure of submerged water jets using a schlieren system, which was sensitive to density differences caused by small temperature variations.

Finally, Ooi (1985) used holography and schlieren photography in an extensive study of cavitating submerged jets. The latter technique provided detailed views of the jet projection, but, again, was unable to resolve the radial distribution of cavities. The cavities at inception were found to be randomly scattered within the fine, grainy, three-dimensional structure of the jet and not in the cores of the large vortex structures within the shear layer.

From the literature review, it was clear that the performance of cavitating, high-speed, submerged water jets has not yet been fully understood and explained. In view of the potential of cavitating, high-speed, submerged water jets in cutting, cleaning and drilling applications, it was felt that further understanding of their properties would be desirable. Therefore, this visualization study was undertaken. A qualitative analysis, combining both visualization of high-speed jets and rough predictions of cavitation by extrapolating data collected by previous investigators under different jet conditions, is presented. Based on this study, plans for future work, to quantify the investigation can be made.

Chapter 3

BACKGROUND INFORMATION

3.1 The Circular Turbulent Jet

A circular (axisymmetric) jet is a fluid flow produced by a pressure difference across a circular orifice. In general, this flow may be laminar, turbulent or a combination of the two. The jet issuing from a nozzle is not enclosed by solid boundary walls but is surrounded by a fluid whose velocity is less than its own. The two fluids may or may not be the same.

A stream of liquid surrounded by a gas is known as a free jet; its structure is affected by gravity. A submerged jet is a stream of liquid surrounded by a liquid; if the jet and the surrounding fluid have the same density, gravity does not influence the jet structure.

Consider a circular jet discharging from a nozzle of diameter D with a uniform velocity U_o into a large stagnant mass of the same fluid. A mixing region develops at the edge of the jet, which grows progressively with downstream distance both inwards toward the jet axis and outwards into the external fluid, as shown in figure 1.

Two distinct regions can be distinguished near the discharge of a submerged jet. a)The region of flow development or establishment, which contains an essentially

irrotational core of flow with undiminished velocity equal to U_o, known as the potential core, and a mixing or shear layer between the core and the surrounding fluid. b) The region of established or fully developed flow, which starts at the position where the shear layer reaches the jet's axis. The jet continually diffuses, gradually reducing the maximum velocity and dissipating the jet energy.

As is the case of air jets, formation of vortices and generation of turbulence occurs in the shear layer of high Reynolds number, submerged water jets. As a result, a pressure field with positive and negative fluctuations is created. Direct measurements have shown that large pressure fluctuations, associated with turbulence, occur in the jet's shear layer (Arndt, 1981). The negative pressure peaks occur relatively frequently and have a duration that is sufficiently long for cavities to form. The experiments of Rouse (1953,1966) and Sami et al. (1967) in submerged water jets have indeed demonstrated that cavitation occurs in the jet's shear layer.

Figures 2 and 3 illustrate mean pressure and r.m.s. pressure fluctuation profiles at various downstream distances of an air jet issuing at about 10.7 m/s (35 ft/s) from a 0.305 m (1.0 ft) diameter nozzle into still air, as presented by Sami et al. (1967). The same results have also been presented by Rouse (1966) in the form of iso-contours (Figures 4 and 5). It can be clearly seen that the highest shear stresses, the most intense turbulence, and the largest pressure fluctuations are contained in the shear layer in the flow development region.

Detailed pressure fluctuation measurements are not available beyond the flow development region. It is possible, however, to estimate the r.m.s. pressure fluctuation from velocity measurements. Figures 6 and 7 present measurements of the centerline mean velocity and axial turbulent intensity, respectively, of sub-

merged water jets (Barker, 1973). These measurements extend up to x/D=50, but can be extrapolated to higher x/D by noting that the ratio $U_o/\overline{U}_m$ ($\overline{U}_m$ is the centerline velocity) grows linearly with downstream distance, while the intensity $u'/\overline{U}_m$ remains constant beyond x/D$\approx$30 (self-preserving flow). Pressure fluctuations can be estimated from velocity fluctuations using theories developed by Batchelor (1953) for isotropic turbulence, as

$$p' = 0.58\rho u'^2 \tag{3.1}$$

or by Kraichnan (1956), for uniformly sheared isotropic turbulence, as

$$p' = 0.73\rho u'^2 \tag{3.2}$$

Although these theories were developed for idealized turbulence, their approximate validity for shear flows has been confirmed by several investigators (Arndt, 1981). These expressions are useful, as below, in explaining the phenomenon of cavitation.

3.2 Cavitation Index

Cavitation is a phenomenon distinguished by the formation of one or more pockets of gas (or cavities) in a liquid (Apfel, 1981). In submerged water jets, cavitation may be gaseous or vaporous. The former, also termed degassing, occurs when gas-filled bubbles, usually minute air bubbles entrapped in the liquid, expand due to a local or ambient pressure reduction or temperature rise. As the pressure increases or decreases, these bubbles contract or expand.

Vaporous cavitation (i.e. formation of vapour cavities) is caused by pressure reduction due to dynamic effects at essentially constant temperature. As a result

of vaporization in the cavity, the bubble growth can be 'explosive' . If a bubble is subjected to a pressure increase, its growth will be arrested and reversed. A cavity may collapse and possibly disappear by absorption of gases and condensation of vapor. The collapse occurs 'implosively' for a vapor-filled cavity with negligible gas content and less dramatically for cavities with higher gas content.

Many variables in the flow can affect the cavitation process in submerged water jets. The critical pressure at which a cavity will be formed depends on the properties of the fluid (i.e. density, viscosity, surface tension and vaporization characteristics), and on the concentration of solid or gaseous contaminants which may be entrained or dissolved in the liquid. In the case of large cavities, hydrostatic pressure gradients are also important. It has become a general practice to describe cavitation by a basic dimensionless parameter, called 'cavitation index' .

A definition of the cavitation index, which is suitable for submerged water jets will be presented in the following. The difference between the local static pressure, P, at a point in the jet and the pressure in the undisturbed liquid, P_{amb}, can be nondimensionalized with the dynamic pressure at the exit, in the form of a pressure coefficient C_p,

$$-C_p = \frac{P_{amb} - P}{\rho U_o^2/2} \tag{3.3}$$

The pressure coefficient at the position of minimum static pressure, P_{min}, is defined as

$$C_{p,min} = \frac{P_{amb} - P_{min}}{\rho U_o^2/2} \tag{3.4}$$

In a jet flow where cavitation exists, the cavitation index can be defined as the pressure coefficient corresponding to the internal cavity pressure. If one further assumes that the internal cavity pressure is equal to the vapor pressure, P_v, then

the cavitation index is expressed as

$$\sigma = \frac{P_{amb} - P_v}{\rho U_o^2/2} \tag{3.5}$$

In the above form, the cavitation index is a macroscopic flow parameter, that can be defined whether cavitation occurs or not. If, in a given experiment, one reduces the value of C_p, inception (i.e. beginning) of cavitation will occur when P_{min} equals P_v. The value of σ at which $P_{min} = P_v$ is called the 'cavitation inception' index, σ_i.

If the value of σ for a given flow field is such that $\sigma < \sigma_i$, cavitation should be expected with the degree of cavitation depending on the magnitude of $(\sigma_i - \sigma)$ (i.e. higher values of σ_i relative to σ result in more intense cavitation). If, however, in a cavitating flow, C_p is increased, cavitation will disappear when $\sigma > \sigma_d$, where σ_d is the 'cavitation desinence' index. In general, σ_d is somewhat larger than σ_i. For example, Lienhard and Goss (1971) reported values of σ_d about 15% larger than those of σ_i, for several cases of submerged water jets.

3.3 Cavitation in Turbulent Jets

Turbulent fluid motion is defined by Hinze (1975) as an irregular condition of flow in which the various quantities show a random variation with time and space coordinates, so that statistically distinct average values can be discerned. The fluctuating pressure at a point in a statistically stationary flow (i.e. a flow whose statistics are independent of time) may be represented as a function of time by figure 8, where P is the instantaneous pressure; $\bar{P}$ is the average pressure; p is the pressure fluctuation, defined as $p = P - \bar{P}$, and p' is the root-mean-square pressure fluctuation.

It can be seen that if p' is large enough, the instantaneous pressure will occasionally drop below the fluid's vapor pressure, P_v, even if the average pressure is much higher than P_v. Thus, cavitation will occur when $P \leq P_v$.

The probability for the presence of cavities at a particular point in a flow field with fluctuating pressure has not yet been quantified. It is therefore necessary to introduce a novel approach. In the following, the coefficient k will be defined by the relationship

$$\bar{P} - kp' = P_v \tag{3.6}$$

It is clear that, the lower the value of k is in a given flow, the higher the probability for cavitation would be, since the occurrence of pressure values below P_v would be more frequent. Of course, the exact dependence of cavitation inception on k would depend on the probability density function and the frequency content of the random pressure field as well as on other parameters, such as the Reynolds number and the gas content.

Further introducing the mean and r.m.s. pressure fluctuation coefficients as,

$$-C_{\bar{p}} = \frac{P_{amb} - \bar{P}}{\rho U_o^2/2} \tag{3.7}$$

and,

$$C_{p'} = \frac{p'}{\rho U_o^2/2} \tag{3.8}$$

and multiplying all terms by the characteristic dynamic pressure, $\rho U_o^2/2$, equation [3.6] may be re-written, as

$$C_{\bar{p}} - kC_{p'} = -\sigma \tag{3.9}$$

From this last expression, k may be evaluated at any location in a turbulent jet

as,

$$k = \frac{1}{C_{p'}}(C_{\bar{p}} + \sigma) \tag{3.10}$$

The local values of the coefficients, $C_{\bar{p}}$ and $C_{p'}$ could be estimated from earlier measurements in jets while σ is a constant for each particular set of test conditions.

Although the introduction of the coefficient k appears to be novel, a similar approach has been followed by earlier investigators (see the review by Arndt, 1981), who, however, focussed upon the particular case of cavitation inception. In this case, the coefficient k_i was defined as

$$k_i = \frac{1}{C_{p'}}(C_{\bar{p},min} + \sigma_i) \tag{3.11}$$

where $C_{p'}$, $C_{\bar{p},min}$ and σ_i are obtained at conditions of cavitation inception in the flow. Measured values of k_i in submerged water jets were about 10 (Rouse, 1953).

Chapter 4

EXPERIMENTAL FACILITIES

A diagram of the experimental facility is shown in figure 9. The apparatus consisted of the test section, the water supply system, the illumination sources, the optical components, the photographic equipment, and the measuring instruments.

4.1 Water Supply System

The high-pressure water flow was produced by a Union Quintuplex pump, rated at 69 MPa (10 000 psi) and 0.83 l/s (13 gpm). Two pressure gauges were mounted to monitor both the low and high pressure ends of the pump. The pump was supplied directly from the city water line.

High-pressure flexible hosing linked the pump to the lance. The steel lance consisted of two sections at approximately 30 degrees from one another to permit internal axial illumination of the jet. The nozzles were secured to the downstream end of the lance with a specially designed threaded nut. The nozzle pressure was monitored with a gauge mounted at the lance inlet, approximately 1.5 m upstream of the nozzle.

4.2 Test Section and Nozzles

The test section consisted of a transparent channel with a 140 x 140 mm square cross-section. The walls were made of 12.7 mm (1/2 inch) Plexiglas with the corners reinforced and braced by 3.2 mm by 25.4 mm (1/8 x 1 inch) aluminum angles. The section was sealed with silicone along the inside corners and between the aluminum angles and the Plexiglas to prevent leakage.

The channel was composed of two straight sections and a converging/draining section. The sections were joined by means of flanges and rubber gaskets. The first module and its end plate, which supported the lance and water inlet valves, were 0.305 m (12 in.) long. Four inlet valves upstream of the jet nozzles were used to fill the channel and to maintain a slow water stream, co-flowing with the jet. The second module was 1.09 m (43 in.) long and allowed clear visualization of the nozzle and the jet. The converging square cone at the end of the test section permitted a smooth flow transition from the square cross- sectional area to a 38 mm (1.5 in.) diameter copper drain pipe.

The channel could be slightly pressurized, up to about 138 kPa (20 psi) above atmospheric pressure. The pressurizing and draining of the channel were controlled with two gate valves situated on the bottom of the section and at the end of the drain pipe. Two pressure gauges, each equipped with a needle valve, were mounted at the two ends of the test section. The valves permitted fine adjustments of the pressure and a means for the air to escape as the section was filled with water.

The test section was supported by a wooden frame. Western red cedar was chosen since it would offer some vibration dampening, strength and water resistance with minimal twisting and swelling. The entire structure rested on aluminum L-

shaped channels for added stability and, if need be, as a means of securing the entire set-up to the concrete floor.

Among the number of nozzles with different shapes and sizes that were available, three were chosen for the present study. As shown in figure 10, all three nozzles were geometrically similar, with a 20 degrec conical entry. Two plain conical entry nozzles with 4.01 mm and 1.02 mm diameters were tested. The third nozzle consisted of a plain conical entry nozzle equipped with a cylindrical pin mounted transversely near the orifice exit. The orifice and pin diameters were 3.05 mm and 1.96 mm, respectively.

4.3 Illumination Sources and Optical Components

The main source of illumination was a 13 Watt Argon-ion continuous laser (Control Laser Corp., model 556). In view of the high voltage and current involved in driving such a laser and the high humidity in the test room, it was found best to place the laser source and power pack on the roof of the test room (but within the building).

To measure the beam power, the laser's built-in power pack meter was calibrated with a Spectra Physics power meter (model 404, serial number 46169 1754).

The beam was contained on the roof and passed through a copper pipe to the optics inside the room. The mirrors and lenses were also contained or covered to prevent accidental exposure to the beam.

By reflecting the beam and passing it through the optical window of the lance, internal jet illumination was possible. To correct the laser beam's divergence, a double convex focusing lens (B and L No.DCX-5-015, focal length = 666 mm) was

placed prior to the lance. With careful adjustments of the mirrors, this permitted the entire beam to pass unobstructed through the lance and the nozzle.

External illumination was achieved by intercepting the beam prior to the lance' entry with mirrors and passing it through lenses. A combination of a converging and a cylindrical lens produced the desired sheet illumination. The position of the double concave focusing lens (focal length = 1 000 mm) determined the thickness of the laser beam. A beam thickness of approximately 0.5 to 1.5 mm was thus obtained at the jet. The conversion of the laser beam to a sheet of light was achieved by placing a cylindrical lens (focal distance = 41 mm) immediately following the focusing lens. The resulting plane sheet of light illuminating the jet was approximately 1 mm thick and 110 mm wide. Occasionally, the thickness of the sheet was further reduced by a slit.

The cylindrical lens was mounted in a rotating brace to permit control of the orientation of the light sheet. Finally the sheet of light was reflected toward the jet by means of a mirror mounted on a track.

Full-field illumination was possible with the use of a stroboscope (General Radio Strobotac, Type 1538A) mounted on top of the test section. The light frequency could be varied from 110 to 150 000 pulses per minute. As the frequency increased, the light duration was shortened and its intensity diminished. For single flash mode operation, the light duration was approximately 3 μs.

4.4 Photographic Equipment

Jet visualization was recorded with a Nikon F2 35 mm single reflex camera. The aperture and shutter speed (as small as 0.5 ms) were controlled manually to

best suit the exposure. The desirable field of view was obtained with a Vivitar 2X macro focusing teleconverter lens and a Nikon Nikkor 50ϕ mm 1:1.4 lens mounted in series.

Events were recorded on Kodak Recording Film 2475. The developing of the high-speed (1000 ASA) black-and-white film and the printing of stills was undertaken in the dark room facilities in the Department of Mechanical Engineering at the University of Ottawa.

4.5 Other Measuring Equipment

A Gaertner Scientific Corporation M-911 cathetometer was used for direct observation of the jet and accurate measurements of vertical displacements and distances. It consisted of a tripod stand, a vertical guide bar, and a telescope, horizontally mounted on a carriage. The guide bar was equipped with a Vernier having a resolution of 0.05 mm. The cathetometer's reading was calibrated using a Vernier caliper temporarily positioned on the test section wall. The calibration line is presented in figure 11.

The dissolved oxygen content of the water was measured with a Broadley James Corp. Oxygen Meter, model 1051O, serial No. 5448/1050. The oxygen probe and meter measure oxygen pressure in water and air. The amporometric (Polarographic) probe consists of electrodes, a thermistor and a filling solution (sodium chloride and sodium hydroxide) contained by a membrane. When the probe is inserted in water, the current between the probe electrodes consumes oxygen and reduces the pressure between the membrane and electrode to zero. Because of the pressure differential across the membrane, oxygen diffuses through the membrane.

As a result of this imbalance, the electrochemical reaction within the probe produces a current which is directly proportional to the oxygen being consumed, thus yielding an oxygen content in parts per million or percent of saturation within ± 0.3 ppm or ± 2.4 % of saturation.

Chapter 5

EXPERIMENTAL PROCEDURE

5.1 Preliminary Procedure

Due to the high pressures and velocities involved, great care was required before and during test runs. The following precautions were followed prior to starting the tests.

First, the security of all laser, test section and pump connections was checked. All the pump by-pass valves were fully opened to prevent any pressure surge in the system.

The four inlet water valves mounted on the end plate of the test section were closed whereas the two drain valves and the two air-bleed valves were opened. It was checked that the power to the laser was off and that the sliding shutter was closed.

Once these steps were completed, the water was supplied to the pump and to the Argon-ion laser cooling system and the test section water inlet valves were opened.

5.2 Pressurizing the Test Section

Before operating the jet in submerged conditions, the test section was first completely filled with water and very slightly pressurized. The drain valve on the test section was fully closed while the water level and, therefore, the internal pressure was adjusted by means of the valve mounted at the end of the copper tube. This sequence minimized air circulation within the test section.

The pump was then activated with all by-pass valves fully open always closely monitoring the channel's internal pressure.

After a few minutes, once the system had reached equilibrium, the nozzle pressure was carefully adjusted by slowly closing the pump's by-pass valves as necessary without letting the test section internal pressure rise beyond 138 kPa above atmospheric pressure. If the pressure exceeded this value, it was reduced accordingly by adjusting the drainage valve.

The final internal pressure of the test section was obtained by first adjusting the drainage valve, followed by fine adjustments of the two valves mounted on top of the two extremities of the channel.

When performing repeated tests at the same operating conditions, the drainage valve at the end of the copper tube was fixed so that the filling and pressurizing of the channel was controlled by the three remaining valves.

5.3 Laser and Optics

The laser was activated at its lowest power setting, with the cooling water flowing at a minimum rate of 12 liters per minute (about 3 U.S. gpm). The shutter was then opened to permit free passage of the beam. The prescribed

goggles were worn for protection against eye-beam contact due to beam reflection or misalignment.

Inside the test room, the laser beam was contained from the ceiling to the optical components within a copper tube with an end cap. Safe interruption of the beam from within the room was possible by using this cap.

After being reflected by two mirrors, the beam was focussed by a biconvex lens and then converted into a thin sheet with the use of a cylindrical lens. It was important to obtain a perfect alignment to maximize the beam's intensity.

The dimensions (i.e. thickness and width) of the sheet of light were adjusted to the desired values by placing the converging and cylindrical lenses in the proper locations. Finally, the sheet was reflected towards the jet by a mirror mounted on a track to obtain plane illumination of the jet at various positions downstream of the nozzle.

5.4 Laser-Sheet Alignment

To obtain a sheet of light normal to the jet axis, the projection of the nozzle's exit was marked on the top wall of the test section by placing the sheet of light flush with the nozzle's exit. Orthogonality of the sheet of light and the jet axis was also checked using the cross-hair of the cathetometer. A template, containing a grid, was fixed on the top wall of the test section and was used for determining the orientation and downstream location of the sheet of light. Illumination was usually either on an axial plane or on a transverse plane forming an angle of 60 degrees with the jet axis. The angle of 60 degrees was used instead of 90 degrees in order to provide a view of the jet to the camera, which was set normal to the

channel for minimum light refraction by the walls.

Care had to be taken to obtain identical plane illumination under different internal pressures, since the test section slightly expanded when pressurized.

5.5 Recording of Events

Photographs of the jet were taken with a NIKON F2 camera. In order to reduce distortion through the Plexiglas walls, the camera was mounted on a tripod with the lens plane parallel to the channel wall. The exact positioning of the camera was done with the use of a transparent grid placed on the back wall of the test section which was aligned with the center line of the jet using the cathetometer. These alignments were necessary in order to minimize optical distortion due to differences between refractive indices of air and water.

At each position downstream of the nozzle, a set of photographs was taken. First, the camera was positioned at the closest possible distance from the jet to better capture all details. This distance was limited by the lenses' focal length. Subsequently the camera was moved back to provide an overall view of the cavitation region of the submerged jet. Photographs were taken at different conditions of nozzle inlet pressure and test section internal pressure before the camera was moved.

Because of the variation in cavitation intensity for different nozzles, pressures, and downstream locations, the amount of light reaching the film plane varied. The camera's shutter speed and aperture were adjusted accordingly.

For comparative reasons, all events were recorded at a fixed shutter speed as well as at the fastest possible shutter speed.

Most photographs were taken with half or all the test room lights turned off to obtain a better contrast between the jet's illuminated plane and the black background placed on the outside of the rear wall. Due to the averaging of the camera's light meter over the entire viewing field, smaller apertures than those indicated by the camera had to be used. If the shutter speed and/or aperture settings of the camera were not adjusted accordingly, the small illuminated portion of the jet would appear on the film as a brightly lit area thus nor revealing any jet detail.

For each photograph, the following conditions were recorded:

i) pump outlet pressure,

ii) nozzle inlet pressure,

iii) test section internal pressure,

iv) type of illumination (i.e. room, laser, stroboscope),

v) laser beam power or stroboscope frequency setting,

vi) location of illumination plane, if applicable,

vii) shutter speed,

viii) aperture.

5.6 Full-field Illumination

Photographs of the jet were also obtained by synchronizing the stroboscope with the camera shutter. For best visualization and lighting, the stroboscope was placed on top of the test section directly above the jet.

In view of the low shutter speeds of the camera, compared to the duration of the stroboscope light (approximately 3 μs), the photographs were taken in total

darkness (i.e. with the room lights turned off). Proper aperture settings were obtained by trial and error since the camera's light meter could not be used in total darkness.

All previously mentioned conditions were also recorded during this process.

5.7 Jet Measurements

The spread of the cavitation region was directly measured with the cathetometer, which was positioned on the rear side of the test section opposite to the camera. This permitted simultaneous use of both instruments.

Observation of the jet's cavitation region was possible by focusing the cathetometer's telescope along the jet's center axis at the desired downstream location. Due to the randomness of the motion of cavities defining this region, measurements were taken after an observation time of approximately one minute to account for all cavities. As a result, some subjectiveness was inevitable in defining this boundary.

The cavitation region's internal boundary could only be visualized with transverse laser plane illumination. Measurements were taken at the same time as when each cross-section was photographed.

Stroboscopic illumination proved to be the best method for measurements of the jet's outer cavitation region boundary. With the stroboscope frequency set at approximately 2300 pulses per minute, the overall cavitation region was clearly visible. Measuring locations were the same as those used in the transverse plane illumination. When the latter technique was used, the plane location was marked on the test section wall as seen through the cathetometer. The markings were

used as reference points for stroboscopic jet measurements.

5.8 Oxygen Content Measurements

The oxygen content of the water was measured by analyzing samples drawn from the test section while the experiments were conducted. The samples were carefully isolated from the atmosphere to prevent the water from absorbing or liberating any additional oxygen until measurement was complete.

Before taking measurements, the meter was calibrated. Corrections were applied to account for variations in air temperature and barometric pressure.

Once the calibration was completed, sample measurements were taken. While immersing about half of the probe's length with the membrane end down into the water sample, the meter was set on standby. The meter's switch was then set to O_2 and measurements were taken after the few minutes that were required for the reading to stabilize.

The probe was finally raised from the sample, rinsed well with water, and patted dry with a tissue. The system was then ready for additional measurements.

Chapter 6

PHOTOGRAPHS AND MEASUREMENTS

6.1 Test Conditions

All three nozzles were tested under various conditions, having different values of the water, jet and test section parameters as summarized in table 1. The jet velocities at nozzle exit were calculated by applying Bernouilli's equation between a point upstream of the nozzle and the nozzle exit, thus obtaining the following relationship,

$$U_o = \sqrt{\frac{2g}{\gamma}\Delta P}$$

In view of the qualitative nature of the present study, the pressure losses were neglected and the discharge coefficient was assumed as 1. Although the oxygen content of water was not measured for the first nozzle tested, it appears reasonable to assume that it was within the range of the measurements for the other two nozzles.

The low water temperature reading of 3.7° C for the tests performed with the 4.01 mm diameter plain conical entry nozzle is due to the time at which the tests were conducted. This nozzle was tested in the winter whereas the 1.02 mm diameter nozzle and the nozzle with the pin insert were tested in spring and early summer. The increase in water temperature for the smallest diameter nozzle from

23.6° C at the lower pressure to 27.0° C at the higher pressure can be attributed to an increased internal pump friction due to the load increase.

The test section was slightly pressurized above atmospheric pressure to reduce the number of stray air bubbles in the surrounding water. It was found that, at atmospheric pressure, a great number of air bubbles was present throughout the section seriously reducing the visibility of the jet. The test section pressure was maintained nearly constant for all tests despite the varying nozzle pressures.

Due to the difficulty in reducing the flow rate of the system, it was not possible to obtain critical conditions for cavitation inception (i.e. the threshold between conditions with no cavitation and with detectable cavitation). The lowest possible nozzle pressure and, consequently, jet velocity was achieved with all pump by-pass valves fully open. A higher pressure for each nozzle was attained by gradually closing the by-pass valve(s) as much as the test section's strength or the pump's capacity permitted.

6.2 Photographs

Visualization of the various events was recorded, as previously mentioned, on high-speed 35 mm black and white film. The film was sensitive to all three light sources (i.e. room lights, stroboscope and Ar-ion laser) yielding photographs of good resolution.

The same sequence of photographs is presented for each nozzle. A scale placed at the bottom of the prints defines the jet's downstream distance from the nozzle, whereas the numbers on each print indicate the nozzle pressure and the film exposure time.

The photographs are so arranged as to facilitate the comparison of the jets issuing from a particular nozzle at the two test pressures. When two columns of photographs are presented, the set at the lower pressure is on the left side of the plate and the corresponding set at the higher pressure is on the right.

6.2.1 Stroboscopic Illumination

Full-field illumination was obtained by synchronizing the stroboscope in single flash mode with the camera shutter. The overall views of the jet thus obtained are presented in the first sequence of photographs. Each of these plates presents one photograph of the jet illuminated by room lighting followed by two (Plates 1, 2, 4, 5, 6, 7, 8, 10 and 11) or three (Plate 9) photographs of the jet illuminated by the stroboscope. These latter two or three photographs in each plate were taken at identical operating conditions but at different times; they were included in order to show the variability in the jet's appearance.

At close range, Plates 1 and 2 show typical examples of the jet issuing from the 4.0[illegible] mm diameter plain conical entry nozzle at 1.65 and 3.89 MPa, respectively. The top photograph of each plate shows the jet as seen with room lighting. The parts of the jet that appear as bright are those containing gas and/or vapor bubbles. It was interesting to note that, when issuing under tap pressure ($\sim$ 0.69 MPa), the jet was invisible, thus indicating absence of cavities.

An increase of nozzle pressure from 1.65 to 3.89 MPa resulted in a general increase of the bubble density and the disappearance of an invisible region near the nozzle exit, where, presumably, there are no light scattering bubbles. At 1.65 MPa, the cavities formed clusters of gas and/or vapor filled cavities which were

separated by dark regions. The distribution of cavities near the nozzle exit seem to follow the development of a helical pattern, especially noticeable in the bottom photograph of Plate 1. The spacing between two consecutive coils of the helix was about 3D near the nozzle exit. The cavitation region also appeared to grow monotonically with downstream distance.

As the pressure was increased to 3.89 MPa, the jet appeared as an almost continuous cluster of gas and/or vapor filled cavities. Some bunching or breakdown occurred and as shown in the last photograph of Plate 2, the helical pattern was barely visible.

The same jet characteristics were seen with the entire cavity-filled region of the jet is as visualized in Plate 3. At the lower pressure, cavities are not visible at the nozzle orifice. The pressure increase intensified the amount of cavities and extended their range from approximately 18 diameters downstream of the nozzle at 1.65 MPa to approximately 25 diameters at 3.89 MPa.

As the cavity region diminished in intensity downstream, the jet faded into a 'milky cloud' of small air bubbles, which were mostly carried through the main discharge of the test section or through some of the intermediate valves; larger air pockets sometimes attached to the top of the test section and occasionally broke into smaller bubbles at random time intervals.

When the orifice diameter was reduced while maintaining the same internal nozzle geometry, higher nozzle pressures and jet velocities were reached. Stroboscopic illumination of the jets generated by the 1.02 mm plain conical entry nozzle (Plates 4 and 5) followed the same pattern as described with the 4.01 mm diameter nozzle. Generally, the jet was visible immediately as it emerged from the nozzle

orifice. There appeared to be an initial region of a few diameters in length where the boundary of the cavity filled region grew smoothly, after which this boundary became ragged.

As the pressure increased from 19.4 to 55.3 MPa, the initial 'smooth' region was prolonged, the bubble density increased and the jet boundary's monotonic growth appeared to increase at a higher rate.

The almost complete disruptions of the gas and/or vapor filled cavities observed at the lower pressure (Plate 6) did not appear at 55.3 MPa (Plate 7). The pressure increase also generated a greater amount of cavities in the surrounding fluid, which appeared in the photographs as soft white (off-focus) circular shapes of varying size.

The background bubbles became more apparent when the entire cavity filled region was photographed (Plates 6 and 7) as a result of the increasing depth-of-field of the camera. It was apparent that, at the higher nozzle pressure, these background bubbles not only increased in population but also in size. These photographs also revealed that the large cavities collapsed at approximately 120 to 160 diameters downstream of the nozzle at 19.4 and 55.3 MPa, respectively. Once again, as the vapor cavities collapsed, the jet faded into a 'milky cloud' of small air bubbles.

The nozzle with the cylindrical pin mounted transversely near the orifice exit, (2.34 mm equivalent diameter) produced a rather complex jet. Plates 8 and 9 clearly show the gas and/or vapor filled cavity region of the jet. Again, the jet has a milky appearance with room lighting. The presence of the pin is revealed as the jet emerges from the nozzle by a dark area which is very rapidly engulfed by the

brighter white region which grows both inwards and outwards. With stroboscopic illumination, this void space is clearly seen at the lower pressure of 9.41 MPa but not as well at the higher pressure.

The intensity of cavitation in this case appeared to be greater than that produced by the plain conical entry nozzles. Bunching of the cavities was recorded as intermittent puffs, as shown in Plates 10 and 11.

The cavity-filled region grew at a moderate rate for approximately one diameter as the jet emerged from the nozzle and then its growth rate underwent a sudden dramatic increase. After considerable growth, the cavity region eventually faded into a cloud of small air bubbles at about 50 diameters at 9.41 MPa and 65 diameters at 24.2 MPa.

Finally, stroboscopic illumination was used to show the effect of decreasing the test section's internal pressure to atmospheric pressure. As can be seen in Plate 12, this change greatly hampered the jet visualization because it resulted in a sharp increase of the stray (presumably, air) bubble content of the surrounding fluid, Background bubbles of different sizes appeared both individually and in clusters.

6.2.2 Axial Laser-Sheet Illumination

The internal structure of the jet was observed and recorded by utilizing the laser-sheet illumination along an axial plane coinciding with the jet axis. The laser sheet was transmitted from the top of the jet toward the bottom of the test section; as a result, the upper boundary of the jet was illuminated better than the lower boundary. Shutter speed and aperture were adjusted according to lighting conditions.

Plate 13 presents photographs using axial laser-sheet illumination for the jet issuing from the 4.01 mm diameter plain conical entry nozzle. The gas and/or vapor-filled cavities appear bright in contrast to the dark background.

At the lower pressure of 1.65 MPa, no cavities were seen very close to the nozzle. They first appeared in the mixing layer of the jet but the cavitation region spread both outward and inward toward the jet axis until the entire jet became visible. A few cavities were observed separating from the apparent outer boundary of the jet into the surrounding low-speed fluid. Further downstream (at approximately 12D, Plate 13b), the cavities became fewer and broke up into filaments. As this occurred, the jet became a 'milky cloud' of small air bubbles, as also seen with stroboscopic illumination. When the pressure was increased to 3.89 MPa, the cavities became visible in the mixing layer right at the orifice exit. The definition of the cavity filled region was not as sharp as that seen at the lower pressure, perhaps due to the relatively long exposure time. As a result, it was difficult to distinguish any cavities possibly detaching from the boundary and to differentiate gas and/or vapor-filled cavities from the small air bubbles farther downstream from the nozzle.

Lower resolution was also observed in the case of the jet discharging from the 1.02 mm diameter nozzle (Plate 14). As a result of the increase in jet velocity, shorter exposure times would have been desirable to capture instantaneous events. However, even at the shortest possible exposure time of the camera (i.e. 0.5 ms), the cavitation region in the photographs appeared blurred. At both tested pressures of 19.4 and 55.3 MPa, cavities were visible throughout the entire cross-section. The outer boundary appeared rougher and had a faster growth at the higher pressure.

Photographs for the jet emerging from the plain conical nozzle equipped with a transverse pin are presented in Plate 15a at close range and, from further away, in Plate 15b.

A small dark triangular area could be slightly detected very close to the nozzle orifice, suggesting the wake of the pin. High cavity population appeared to occur at the boundary of this wake and at the jet's outer mixing-layer, which were very bright. The entire jet cross-section was quickly filled by the cavities, and the cavity filled region's outer boundary presented a sudden increase of its growth rate as in the plain nozzle case.

As the jet progressed downstream from the nozzle, the outer boundary became irregular, followed by a break-down of the cavitation region into isolated filaments which completely disappeared farther downstream, leaving only minute air bubbles visible within the jet (Plate 15b).

6.2.3 Transverse Laser-Sheet Illumination

Internal details of the jets were obtained with laser-sheet illumination along a transverse plane forming an angle of 60 degrees with the jet axis. Cross-sections of the jets were thus obtained at various downstream distances from the nozzle.

The first set of photographs were taken at the closest range. Cross-sections were obtained at 3 mm and 6 mm up to a distance of 32 mm in increments of approximately 6 mm as shown in Plate 16.

The cavity-filled region appeared in a 'donut' shape. This bears out the observations made with axial laser-sheet illumination by showing what appears to be the cavity-free core. This core diminished in size with downstream distance as

the 'donut' expanded both inward towards the jet axis and outward towards the surrounding fluid.

The cavity region progressed from a bright well defined region to a ragged shape due to the appearance of individual cavities or small clusters of gas and/or vapor-filled cavities along the outer boundary. Further downstream, the cavities occupied the entire cross-section of the jet.

The camera was then moved back to obtain a larger field of view with width between 32 mm and 76 mm as shown in Plate 17. The illuminated region was seen to expand radially and revealed a decrease in cavity population until none or very few could be seen. Once again, an increase in nozzle pressure and downstream distance made it more difficult to distinguish the gas and/or vapor-filled cavities from the residual small air bubbles in the jet.

Due to the great velocities encountered in the jets issuing from the 1.02 mm diameter plain conical entry nozzle, the cavity filled region appeared blurred. Cavities were visible in the entire cross-section. Photographs had to be taken in three sets to cover the entire range. Plate 18 describes the jet at 3mm and 6 mm up to a distance of 25 mm in 6 mm increments, Plate 19 from 32 mm to 51 mm and Plate 20 from 64 mm to 102 mm in 13 mm increments. Beyond 64 mm, the cavities could not be distinguished from the 'milky cloud' of small air bubbles in the jet and a greater amount of air bubbles were present in the surrounding fluid.

Similar observations were made for the jet issuing from the nozzle with the pin insert. Plates 21, 22, and 23 reveal a blurred cavity filled region where, at times, it is very difficult to distinguish the cavities from the surrounding fluid and jet's air bubbles. The sudden expansion of the region's outer boundary was the only

unique jet characteristic visible in these photographs.

6.3 Measurements

The boundaries of the cavitation regions for all test conditions were determined using the cathetometer. The results are summarized in figures 12, 13 and 14. Only the upper half of the jets is presented in the figures since it was much more visible than the lower half.

The cavitation region was measured using transverse laser-sheet illumination for the jet issuing from the 4.01 mm diameter nozzle and stroboscopic illumination for the jets issuing from the other two nozzles. As mentioned in Section 5.7, measurements of the cavitation region of each jet were taken after an observation time of approximately one minute, which yielded the boundary of the cavity containing region in both radial and axial directions. Evidently, this procedure introduces some subjectiveness in the definition of the boundary; the uncertainty of the measurements is estimated to be less than $\pm$ 0.25 r/D.

The transverse laser-sheet clearly revealed the entire cavity region of the jet at the lower nozzle pressure of 1.65 MPa but only up to 20D at the higher pressure (Figure 12). Beyond this distance, scattered light illuminated the entire test section, rendering the cavities indistinguishable to the bare eye from the surrounding fluid. This may be due to the increasing concentration of minute bubbles in the jet and surrounding fluid. As seen in the photographs though (Plate 3), the cavitation region did extend to approximately 25D at the higher pressure.

The outer boundary of the cavitation region grew monotonically up to a certain distance, where it stabilized momentarily and then, suddenly ended due to the

absence of cavities. Its radial expansion was somewhat greater at the higher than at the lower pressure. The inner boundary shrank radially, but more slowly for the higher pressure revealing a potential core in that case. No cavities were visible from the jet axis to the inner boundary, presumably due to the absence of pressure fluctuations in the potential core.

The outer boundaries of the cavity regions generated by the jets issuing from the 1.02 mm diameter nozzle, showed similar trends (Figure 13). The axial spread of the cavitation region also increased with increasing pressure for the jet issuing from the 1.02 mm diameter nozzle. The region grew monotonically up to about 65D and then stabilized at r/D=8 for P_N = 19.4 MPa and r/D=9 for P_N = 55.2 MPa. As visualized in the photographs, no inner boundary was visible, perhaps due to the small size of this region or because of light loss in the outer boundary.

Finally, figure 14 reveals the cavity region produced by the jets issuing from the plain conical entry nozzle with the pin insert. As the nozzle pressure increased from 9.41 MPa to 24.2 MPa, the cavitation region expanded in both radial and axial directions. The axial expansion was initially very rapid, then it gradually stabilized and, finally, it decreased. The short inner boundary of the cavities probably coincided with the initial wake of the pin. The nozzle pressure increase caused a noticeable increase in the radial expansion of this boundary.

Chapter 7

ANALYSIS AND DISCUSSION OF RESULTS

7.1 General comments

The main variables that affect the inception and subsequent character of cavitation in submerged high-speed water jets are the nozzle type (i.e. geometry, obstructed or unobstructed) and orifice size, as well as the flow variables, namely the nozzle and ambient pressures, and the critical pressure at which a cavity can be formed and maintained. The latter depends on the properties of the fluid (i.e. density, viscosity, surface tension and vaporization characteristics) and on the concentration of solid or gaseous contaminants which may be entrained or dissolved in the liquid.

Most of the research on cavitation in submerged water jets has been focussed upon cavitation inception at relatively slow jet velocities. In the present study it was not possible to study this inception condition, because the flow rate to the nozzle system could not be reduced to obtain critical conditions for cavitation inception.

The range of the flow was, however, suitable for cavitation studies applicable to water jet technology. As discussed in the literature survey, cavitation, in most cases, enhances the jet's erosive power. Cavitating water jets are currently used

in cleaning and cutting applications.

Since it was not possible to obtain conditions appropriate to produce cavitation inception in the present facility, one can only estimate the cavitation inception index, σ_i from previous studies. Lienhard and Goss (1971) observed the incipient cavitation index to vary from 0.15 to 0.66 in water flowing through 0.80 to 6.35 mm orifices, whereas Rouse (1953) found a value of 0.55 for a jet issuing from a 38.1 mm diameter nozzle and Ooi (1985) obtained σ_i values ranging from 0.03 to 0.27 with nozzles of 3.17 to 6.35 mm in diameter. Ooi (1985) found σ_i to inversely vary with dissolved air content. Considerable uncertainty in the determination of σ_i is introduced by differences in experimental techniques (i.e. definition of the point of incipience), and in nozzle geometry.

Even though it is very difficult to extrapolate previous findings to the present cases, which have much higher velocities, it is clear that the cavitation index as summarized in table 1, falls below any reasonable estimate of σ_i (for example $\sigma_i \approx 0.20$), therefore suggesting the presence of intense cavitation.

The present facility was also unsuitable for measuring the desinent cavitation index, σ_d. As a guide, one may use Lienhard and Goss's (1971) measurements that indicate σ_d to be approximately 15% higher than σ_i.

7.2 The axial extent of the cavitation region

The coefficient, k, for a turbulent flow has been defined in Chapter 3 as,

$$k = \frac{1}{C_{p'}}(C_{\bar{p}} + \sigma)$$

The mean pressure and pressure fluctuations coefficients obtained by Sami et

al. (1967) are presented in figures 15 and 16, respectively. It is clear that both the mean and the r.m.s. pressures depend on the jet velocity, U_o, since they scale with the mean dynamic pressure $1/2\rho U_o^2$. The r.m.s. pressure fluctuations in a turbulent flow are proportional to the r.m.s. velocity fluctuations, u' (Batchelor, 1951; Kraichnan, 1956). If one assumes that the turbulence intensity $u'/\bar{U}$ remains constant as U_o varies, then higher p' would correspond to higher jet speeds.

Farther downstream, the mean pressure gradually reaches the test section's ambient pressure whereas the axial turbulence intensity along the centerline asymptotically reaches a value of $u'/\overline{U}_m = 0.19$ (Barker, 1973). In the absence of transverse profiles, one may assume that the maximum p' at a given x/D is comparable to the centerline value. Figure 17 presents the r.m.s. pressure fluctuations on the jet axis as a function of downstream distance. Sami et al. (1967) results were obtained from an air jet issuing in air whereas Barker (1973) tested a submerged water jet. In the latter case, the average value between Batchelor's (1951) and Kraichnan's (1956) theories was used to obtain p' from the u' measurements. The discrepancy between the two curves of the figure (in the range $10 \leq$ x/D ≤ 20) can be attributed to differences in test conditions, nozzle diameter and geometry, as well as to the considerable uncertainty in the r.m.s. pressure estimates.

The estimated variation of the coefficient k near the nozzle is presented in figure 18 for the jet issuing from the 4.01 mm diameter nozzle and in figure 19 for the 1.02 mm diameter nozzle. The nozzle with the pin insert was not represented since no relevant measurements of the pressure field are available. The two figures present the two extreme cases, corresponding to velocities of 55.5 and 331. m/s. As explained earlier, it is expected that in regions with low values of k, the chance of cavitation is high. A value of k=0 occurs when $\bar{P}$=P_v, which implies that

cavitation will almost always occur. According to equation [3.6], negative values of k are unrealistic since they imply that the average pressure $\bar{P}$ would fall below the fluid's vapor pressure, P_v. But it can be assumed that cavitation will be present within regions where such values occur; in fact, the presence of cavities is expected to modify the pressure field, such that the local static pressure will never fall below P_v.

The iso-curves of the coefficient k follow a pattern consistent with the development of the jet's mixing layer, with the lowest values contained in the approximate center of this layer. As the jet velocity is increased from 55.5 m/s to 331. m/s, the k value is greatly diminished. The only significant region with relatively large values of k (i.e. $k > 10$) is in the potential core of the lower speed jet. This is in good agreement with the photographic evidence of absence of cavities in that region.

Estimates of k far from the nozzle are subject to relatively large errors because they were based on estimated and not measured pressure values and, also, because the intense cavitation is expected to modify the downstream pressure field. The value of k, for any given condition was defined by equation [3.10]. The values of $C_{p'}$ were estimated from Barker's (1973) velocity measurements in the range 10 $\leq$ x/D $\leq$ 50 by first calculating u'. As shown in figure 6, the development of the centerline velocity can be fitted by a power law as

$$\frac{\overline{U}_m}{U_o} \approx 6.8 \left(\frac{x}{D}\right)^{-1}$$

while the centerline axial turbulence intensity (Figure 7) attains the nearly constant value

$$\frac{u'}{\overline{U}_m} \approx 0.19$$

Thus, one may imply that

$$\frac{u'}{U_m} \approx 1.3\left(\frac{x}{D}\right)^{-1}$$

As discussed earlier, the r.m.s. pressure fluctuations p' can be obtained from u' as the average of the two estimates based on Batchelor's (1951) and Kraichnan's (1956) theories. As figure 15 indicates, it can be also assumed that, far downstream, $C_{\bar{p}} \approx 0$. The measurements were extrapolated to downstream distances beyond x/D=50 by assuming self-preservation of the turbulence structure.

Using the above expressions, it is possible to derive an expression for the far downstream development of the coefficient k as

$$k = 0.46\sigma\left(\frac{x}{D}\right)^2 \tag{7.1}$$

This expression, plotted in figure 20 for the various test conditions, illustrates that the value of k increases (and, therefore, the probability of cavitation presence decreases) with increasing distance from the origin and increasing value of the cavitation index, σ. Thus, for a given nozzle and a given x/D, it is anticipated that cavitation will cease as soon as σ exceeds a certain value, namely when the jet velocity U_o decreases below a certain threshold. For a given nozzle and jet speed, cavitation will cease as soon as x/D exceeds a certain value. Plate 3 and Plates 6 and 7 confirm this prediction for the 4.01 mm and 1.02 mm diameter nozzles, respectively. Cavitation is expected to diminish and eventually disappear as the cavities are transported downstream in the jet. As the turbulent kinetic energy is gradually dissipated, the velocity and pressure fluctuations also decrease in magnitude. Therefore, the chance of the instantaneous local pressure being maintained at the fluid vapor pressure keeps decreasing until it vanishes, in which case no vapor cavity can be maintained.

Similar observations apply to the nozzle with a pin insert (Plates 10 and 11). In figure 20, the nozzle is represented by two curves, for the two corresponding nozzle pressures. The calculations were based on an equivalent diameter D_e, defined as

$$D_e = \sqrt{D^2 - D_p^2}$$

From the photographs, it was also possible to estimate the distance at which cavities collapse. These values of $(x/D)_{col}$ for the six cases studied are included in Table 2. The corresponding values, k_{col}, of the coefficient k at the point of collapse are shown by the various symbols along the k-curves in figure 20; they have also been included in Table 2. These values extend over a wide range.

For the jets issuing from the 4.01 mm diameter nozzle and the obstructed nozzle, the values of k_{col} were of the same order of magnitude as k_i in Rouse's (1953) experiments.

In the case of the jet issuing from the 1.02 mm diameter nozzle, k_{col} appears to be measurably higher than that obtained from the jets produced by the other two nozzles but still within the same order of magnitude. This increase in k_{col} may be partly attributed to an increased distortion of the pressure field due to the presence of cavities. Comparison of the values of k_{col} for each nozzle at two different jet speeds indicate a decrease of k_{col} with increasing jet speed.

Another concern for the obstructed nozzle is that the pressure field would also depend on the size and shape of obstructions, although less so far downstream of the nozzle when distances are normalized with an 'appropriate' diameter. Since the definition of an 'appropriate' diameter is not clear, a quantitative comparison of results corresponding to obstructed and unobstructed nozzles is very difficult.

A correlation of the extent of the cavitation region with the various flow pa-

rameters would be useful in water jet applications. As shown in figure 21, $(x/D)_{col}$ increased with increasing Reynolds number for a given nozzle. On the other hand, figure 22 shows a systematic decrease of $(x/D)_{col}$ with increasing cavitation index σ for all three nozzles. Furthermore, the results for all three nozzles appear to follow a trend. Whether this is coincidental or systematic deserves further study.

7.3 Effect of other parameters

Nozzle velocity, shape and diameter are not the only parameters affecting the degree of cavitation in submerged water jets. Fluid properties such as temperature, gas content and the ambient pressure have to be included in a full description of the cavitation process.

Suppression of cavitation with an increase in P_{amb} was observed in all the jets. For demonstrative purposes, Plate 12 shows this effect for the submerged jet issuing from the 1.02 mm diameter nozzle. The ambient pressure was atmospheric. Not only did cavitation appear to be more intense than that observed at greater ambient pressures (Plates 4, 5, 6 and 7) but the population of gas filled bubbles in the surrounding fluid was also greater. The bubbles appeared individually and in clusters. Their density increased with downstream distance, greatly hampering visualization of the cavitation region of the jet.

Water temperature and gas content also affect cavitation. Both were measured and recorded (the gas content could be estimated from the oxygen content) even though their effect was not studied. Water density, viscosity, tensile strength, and vapor pressure are all a function of temperature. Ooi (1985) discouraged the past practice of using the dissolved air content as a direct indication of the nuclei

distribution; nevertheless, he has shown that a decrease of the incipient cavitation index occurs with a decrease in dissolved air content.

7.4 Evolution of the cavitation region of the jet

7.4.1 Stroboscopic illumination

As the jet progresses downstream from the nozzle, the vapor and/or gas filled cavities appear to change in size and shape.

The overall view of the entire cavity-filled region was best visualized with the stroboscope as the lighting source. The full-field illumination of the jet presented in Plates 3, 6, 7, 10 and 11 captured the cavities from their formation near or at the nozzle exit up to their collapse and eventual disappearance. The cavities were visible at the nozzle exit in all the jets except the jet issuing from the 4.01 mm diameter nozzle at the lower velocity of 55.5 m/s.

As described in Chapter 6, the jets contain an initial region of a few diameters in length where the boundary of the cavity-filled region grows relatively smoothly, after which this boundary becomes ragged. Finally, the cavity region diminishes in intensity as the cavities attain a streaky appearance (Plates 3 and 6), collapse and fade into a 'milky cloud' comprised of small air bubbles.

It appears that the jet, based on the cavity-filled region, can be divided into three sections. First, the jets issuing from the plain conical entry nozzles will be considered since the structure of the cavity-filled region differs from the nozzle with the pin insert.

The first region where the boundary of the cavity-filled region grows smoothly may be considered as the initial section. This smooth growth suggests developing

flow conditions containing the entire flow development region and a portion of the jet's developed flow region as defined in figure 1. Cavities are generated only within this region where the r.m.s. pressure fluctuations are the greatest. These fluctuations are maintained for a sufficiently long time to promote the formation and growth of vapor cavities.

As the flow progresses, the turbulence due to shear, decays resulting in a gradual decrease of the local pressure fluctuations. Fewer or no gas-filled cavities are generated because of the lower frequency and magnitude of these pressures. The cavity-filled region appears to bunch-up creating intermittent voids containing few cavities within the jet. Thus, only some cavities will be sustained whereas others will collapse. This section can be defined as the transport region.

Finally, the collapse region comprises the tail end of the cavity-filled region. As a result of the further turbulence decay, negative pressure fluctuations are of diminishing magnitude. As a result, the local static pressure is maintained above P_v, so that the cavities can no longer exist and collapse.

The cavity-filled region produced by the jet issuing from the nozzle with the pin insert can also be broken-down in the generating, transport and collapse regions. Because of the pin and the greater turbulence levels, bunching of the cavities in intermittent puffs occurs close to the nozzle orifice (Plate 8) perhaps suggesting a short but intense cavity generating region. The cavity-filled region then progresses similarly to the ones in the jets issuing from the unobstructed nozzles.

7.4.2 Laser-sheet illumination

Due to the relatively long exposure times when compared to the jet velocities,

instantaneous photographs were difficult to obtain.

Laser-sheet illumination along an axial plane coinciding with the jet center axis revealed mainly the boundary of the cavitation region (Plates 13a, 14 and 15a). Only far from the nozzle exit is the evolution of individual cavities distinguishable (Plates 13b, 14 and 15b). The possible trajectories of cavities during or just prior to collapse are visible at lower jet velocities. At higher velocities, the cavity-filled region appears as a bright cloud, probably due to the superposition of several events.

Transverse laser-sheet illumination revealed more details of the cavitation region's internal structure. Distinct cavities were visible only for the jets issuing from the 4.01 mm diameter plain conical entry nozzle. Due to the relatively long shutter speed, the cavitation regions produced by the other two nozzles appears as a bright cloud.

The cavitation generation region of the jet appears to be comprised of a large amount of minute cavities. As the jet further evolves, the cavities, in the transport region of the jet, grow in size and eventually populate the region's cross-section. Finally, in the collapse region, fewer cavities are visible until they completely vanish.

7.5 Some Practical Considerations for Cutting and Cleaning Jets

Submerged cavitating jets should generate higher erosive power than water jets issuing in air operating at identical conditions due to the great forces imparted to a specimen when the cavities collapse near or on the surface. It is very important,

however, to keep in perspective that when a specimen is introduced in front of the jet, the pressure field will, naturally, be altered.

The presence of cavitation has proved to improve jet performance at least in certain applications such as rock cutting (Johnson et al., 1968; Vijay and Brierley, 1979). Therefore cavitating jets could be designed for lower operating pressures, with the advantages of safer operation, extended life of the equipment and lower start-up and maintenance costs.

Submerged conditions for cavitation naturally occur in certain situations such as vertical drilling and underwater drilling and cleaning (i.e. cleaning ship hulls, swimming pools, etc.). When submerged conditions are not met, perhaps artificial submergence for in-air cleaning and cutting operations could be applied such as suggested by Vijay and Brierley (1979) and Vickers et al. (1980).

Cavitation may be further enhanced by the appropriate nozzle. One may anticipate that nozzle shape and obstructions would also affect performance. Further systematic experiments and analysis are necessary in order to resolve these issues.

Chapter 8

CONCLUSIONS

The present study has investigated the cavitation process involved in high-speed submerged water jets issuing from axisymmetric nozzles. Briefly, the following may be concluded:

1. The simple flow visualization techniques developed during the research proved efficient in capturing the cavitation phenomenon in high-speed submerged water jets.

2. Full-field illumination, using a stroboscope as lighting source synchronized with a single lens reflex camera, permitted the recording of short duration events, but could only reveal the surface structure.

3. Visualization of the internal structure of the submerged jet's cavitation region was possible with laser-sheet illumination. The presence of the jet's potential core as well as the evolution and collapse of the cavities were visible. The visual resolution was reduced at higher jet velocities.

4. An increase in ambient pressure reduced the intensity of cavitation. Slightly pressurized conditions for the surrounding fluid were desirable for optimum visualization of the cavitation region.

5. As the nozzle pressure increased, consequently increasing the jet velocity, the cavitation region not only intensified but also expanded both radially and axially.

6. Cavitation inception and desinence were not studied. The cavitation index in the present flows was much lower than any estimate of σ_i, based on previous studies.

7. A coefficient related to cavitation in a fluctuating pressure field has been defined as

$$k = \frac{1}{C_{p'}}(C_{\bar{p}} + \sigma)$$

taking into account the r.m.s. pressure fluctuations and the mean static pressure. It is found that the probability of cavitation at a point in a flow increases with decreasing value of k.

8. The estimated variation of the coefficient k near the nozzle was found to follow contours similar to those of $C_{p'}$ and $C_{\bar{p}}$, with minimum values near the center of the jet's shear layer. At distances greater than x/D = 30, the minimum value of k was expected to be on the jet axis; it was observed to follow the asymptotic law,

$$k = 0.46\sigma\left(\frac{x}{D}\right)^2$$

9. The axial extent of the cavitation region for the three nozzles was found to systematically decrease with increasing cavitation index.

Chapter 9

RECOMMENDATIONS FOR FUTURE WORK

The present work can be viewed as a starting point for the documentation of the cavitation process within high-speed, submerged water jets and its effects in cutting and cleaning applications. Although the developed flow visualization techniques were found generally suitable for the study of cavitation, it also appears that further improvements of these techniques are possible. In particular, it would be desirable to record the evolution of single cavities within the jet and its surrounding from inception to collapse. This would require a higher temporal resolution, which can be obtained by using a) higher camera or external shutter speeds, b) pulsed-laser illumination and/or, c) high-speed cinematography.

Research can also be extended by studying jets produced within a wider range of operating conditions including those corresponding to cavitation inception and desinence. This would require some changes in the water supply system and the use of additional nozzles. Such results would further clarify the relationship between cavitation and parameters, such as σ, Re, and nozzle shape and size. To fully evaluate the effect of obstructions within nozzles, the performance of obstructed and unobstructed nozzles of the same orifice diameter and operating at the same nozzle pressure should be compared.

An aspect not considered until now but deserving full investigation is the inter-

action of a cavitating jet with a solid surface in its path, which, of course, would be the configuration with practical interest. Some preliminary estimation of the coefficient k could be based on the existing measurements in turbulent jets impinging on flat surfaces. Furthermore, the present facility could be modified in order to accommodate samples positioned at different distances from the nozzle. The visualization techniques would have to be adapted to this configuration in order to provide a view of the cavitating region and the collapse of cavities near the wall and, when appropriate, of the process of material removal from the surface.

References

Albertson, M.L., Dai, Y.B., Jensen, R.A. and Rouse, H. 1950 Diffusion of submerged jets. Trans. of the American Soc. of Mech. Engrs., vol. 115, 639.

Apfel, R.E. 1981 Acoustic cavitation. Methods of Experimental Physics, vol. 19, Marton, L. and Marton, C., editors-in-chief, 355.

Arndt, R.E.A. 1981 Cavitation in fluid machinery and hydraulic structures. Ann. Rev. Fluid Mech., vol. 13, 273.

Arndt, R.E.A. 1981 Recent advances in cavitation research. Advances in Hydroscience, vol. 12, Ven Te Chow, editor, Academic Press.

Arndt, R.E.A. and Daily, J.W. 1969 Cavitation in turbulent boundary layers. Cavitation State of Knowledge, ASME, 64.

Arndt, R.E.A. and George, W.K. 1979 Pressure fields and cavitation in turbulent shear flows. Twelfth Symposium on Naval Hydrodynamics, Natl. Acad. of Sciences, Natl. Res. Council, 327.

Arndt, R.E.A. and Ippen, A.T. 1968 Rough surface effects on cavitation inception. American Soc. of Mech. Engrs., New York, U.S.A., ASME Paper No. 68-FE-6.

Arndt, R.E.A. and Nilsen, A.W. 1971 On the measurement of fluctuating pressure in the mixing zone of a round jet. American Soc. of Mech. Engrs., New York, U.S.A., ASME Paper No. 71-FE-31.

Baev, V.K., Bazhaikin, A.N., Buzukov, A.A., Timoshenko, B.P., Bichenko, E.I. and Rabinovich, R.L. 1986 Experimental study of the development and structure of high-velocity liquid jets in air. Progress in Astronautics and Aeronautics, Martin Summerfield, editor-in-chief, vol. 105, 104.

Barefoot, G.L. 1972 Fluctuating pressure characteristics of perturbed and unperturbed round free jets. M.S. Thesis, Pennsylvania State Univ., University Park, Pa., U.S.A.

Barker, S.J. 1973 Laser-Doppler measurements on a round turbulent jet in dilute polymer solutions. J. Fluid Mech., vol. 60, part 4, 721.

Batchelor, G.K. 1951 Pressure fluctuations in isotropic turbulence. Proc. of the Cambridge Philosophical Soc., vol. 47, 359.

Billet, M.L. 1985 Cavitation nuclei measurements - A review. Cavitation and Multiphase Flow Forum, ASCE/ASME Mechanics Conference, Albuquerque, New Mexico, U.S.A., 31.

Birkhoff, G. and Zarantonello, E.H. 1957 Jets, Wakes, and Cavities. Academic Press Inc., New York.

Chahine, G.L., Conn, A.F., Johnson, Jr. V.E. and Frederick, G.S. 1983 Cleaning and cutting with self-resonating pulsed water jets. Second U.S. Water Jet Conference, Univ. of Missouri-Rolla, Missouri, U.S.A., 167.

Corrsin, S. 19434 Investigation of the flow in an axially symmetrical heated jet of air, NACA ACR 3L23.

Corrsin, S. and Uberoi, M.S. 1950 Further experiments on the flow and heat transfer in a heated turbulent air jet, NACA Report 998.

Corrsin, S. and Uberoi, M.S. 1951 Spectra and diffusion in a round turbulent jet, NACA Report 1040.

Crow, S.C. and Champagne, F.H. 1971 Orderly structure in jet turbulence. J. Fluid Mech., vol. 48, part 3, 547.

Daily, J.W. and Johnson, Jr. V.E. 1956 Turbulence and boundary-layer effects on cavitation inception from gas nuclei. Trans. of the American Soc. of Mech. Engrs., vol. 78, 1695.

Daugherty, R.L. and Franzini, J.B. 1977 Fluid Mechanics with Engineering Applications. Seventh Edition, McGraw-Hill, Inc.

Davies, P.O.A.L., Fisher, M.J. and Barrat, M.J. 1963 The characteristics of the turbulence in the mixing region of a round jet. J. Fluid Mech., vol. 15, 337.

Drubka, R.E., Nagib, H.M., Arndt, R.E. and George, W.K. 1982 Cooperative investigation of jet flows. Annual Technical Report, Illinois Institute of Technology, Chicago, Illinois, U.S.A.

Eddingfield, D.L., Evers, J.L. and Setork, A. 1981 Mathematical modeling of high velocity water jets. First U.S. Water Jet Symposium, Golden, Colorado, U.S.A.

Eisfeld, F. 1984 The investigation of the penetration of liquid jets in gas by the methods of high speed cinematography and short time interferometry. SPIE High Speed Photography, vol. 491, 329.

Erdmann-Jesnitzer, F., Hassan, A.M. and Louis, H. 1978 A study of the effect of nozzle configuration on the performance of submerged water jets. Fourth International Symposium on Jet Cutting Technology, BHRA, Bedford, England, Paper A2, 21.

Fiedler, H., Nottmeyer, K., Wegener, P.P. and Raghu, S. 1985 Schlieren photography of water flow. Experiments in Fluids 3, 145.

Fuchs, H.V. 1972 Measurement of pressure fluctuations within subsonic turbulent jets. J. of Sound and Vibration, vol. 22, no. 3, 361.

Fuchs, H.V. 1972 Space correlations of the fluctuating pressure in subsonic turbulent jets. J. of Sound and Vibration, vol. 23, no. 1, 77.

Fuchs, H.V. 1974 Resolution of turbulent jet pressure into azimuthal components. AGARD-CP-131, Paper 27.

Garrad, A.D. and Patrick, M.A. 1983 The velocity field produced by a submerged jet directed upwards at a free surface. Int. J. Heat Mass Transfer, vol. 26, no. 7, 1029.

George, W.K., Arndt, R.E.A. and Nagib, H.M. 1980 Cooperative investigation of the noise producing region of an axisymmetric jet. State Univ. of New York, Buffalo, New York, U.S.A.

Gronauer, R.W. 1972 Cleaning and descaling of equipment with high pressure water. First International Symposium on Jet Cutting Technology, BHRA, Cranfield, Bedford, England, Paper D3, 25.

Hägele, J. and Hiller, W.J. 1980 Visualization of hypersonic micro-jets by laser-induced fluorescence. Second International Symposium on Flow Visualization, Bochum, West Germany, 427.

Harris, H.D. and Brierley, W.H. 1972 Application of water jet cutting. First International Symposium on Jet Cutting Technology, BHRA, Cranfield, Bedford, England, Paper D3, 25.

Hinze, J.O. 1979 Turbulence. Second Edition, McGraw-Hill, Inc.

Hoyt, J.W. and Taylor, J.J. 1979 Effect of nozzle shape and polymer additives on water jet appearance. Transactions of the ASME, vol. 101, 304.

Johnson, V.E., Jr. 1963 Mechanics of cavitation. Jour. of the Hydraulics Division, Proc. of the American Soc. of Civil Engrs., vol. 89.

Johnson, V.E., Conn, A.F., Lindenmuth, W.T., Chahine, G.L. and Frederick, G.S. 1982 Self-resonating cavitating jets. Sixth International Symposium on Jet Cutting Technology, BHRA, Cranfield, Bedford, England, Paper A1, 1.

Johnson, Jr. V.E., Thiruvengadam, A. and Kohl, R.E. 1968 Rock tunneling with high-speed water jets utilizing cavitation damage. American Soc. of Mech. Engrs., New York, U.S.A., ASME Paper No. 68-FE-42.

Kinoshita, T. 1974 An investigation of the mechanism of a high speed liquid jet and its practical application. Second International Symposium on Jet Cutting Technology, BHRA, Cranfield, Bedford, England, Paper B4, 47.

Knapp, R.T., Daily, J.W. and Hammitt, F.G. 1970 Cavitation. McGraw-Hill, Inc.

Kraichnan, R.H. 1956 Pressure field within homogeneous unisotropic turbulence. Journal of the Acoustical Society of America, 28.

Lau, J.C., Fuchs, H.V. and Fisher, M.J. 1970 A study of pressure and velocity fluctuations associated with jet flows. Institute of Sound and Vibration Research, University of Southampton, Technical Report No. 28.

Lichtarowicz, A. 1974 Experiments with cavitating jets. Second International Symposium on Jet Cutting Technology, BHRA, Cranfield, Bedford, England, Paper D1, 1.

Lichtarowicz, A. and Sakkejha, M.F. 1972 Cutting with cavitating jets. First International Symposium on Jet Cutting Technnology, BHRA, Cranfield, Bedford, England, Paper G6, 61.

Lienhard, J.H. and Goss, C.D. 1971 Influence of size and configuration on cavitation in submerged orifice flows. American Soc. of Mech. Engrs., New York, U.S.A., ASME Paper No. 71-FE-39.

List, E.J. 1982 Turbulent jets and plumes. Ann. Rev. Fluid Mech., vol. 14, 189.

Michalke, A. and Fuchs, H.V. 1975 On turbulence and noise of an axisymmetric shear flow. J. Fluid Mech., vol. 70, part 1, 179.

Nebeker, E.B. 1983 Standoff distance improvement using percussive jets. Second U.S. Water Jet Conference, Univ. of Missouri-Rolla, Missouri, U.S.A., 25.

Nebeker, E.B. and Cramer, J.B. 1983 Visualization of the central core of high-speed water jets - An infrared tecnique. Second U.S. Water Jet Conference, Univ. of Missouri-Rolla, Missouri, U.S.A., 75.

Ooi, K.K. 1985 Scale effects on cavitation inception in submerged water jets: A new look. J. Fluid Mech., vol. 151, 367.

Plesset, M.S. and Prosperetti, A. 1977 Bubble dynamics and cavitation. Ann. Rev. Fluid Mech. 9, 145.

Rajaratnam, N. 1976 Turbulent Jets. Elsevier Scientific Publishing Company, Amsterdam, Netherlands.

Rankin, G.W., Sridhar, K., Arulraja, M. and Kumar, K.R. 1983 An experimental investigation of laminar axisymmetric submerged jets. J. Fluid Mech., vol. 133, 217.

Reed, X.B., Spiegel, L. and Hartland, S. 1977 Some measurements of spatial correlations in an axisymmetric turbulent jet. Selected Papers from the First Interna-

tional Symposium on Turbulent Shear Flows, Pennsylvania State Univ., University Park, Pennsylvania, U.S.A.

Rouse, H. 1953 Cavitation in the mixing zone of a submerged jet. La Houille Blanche, 8, no. 1, 9.

Rouse, H. 1966 Jet diffusion and cavitation. J. of the Boston Society of Civil Engineers, vol. 53, no. 3, 255.

Sami, S., Carmody, T. and Rouse, H. 1967 Jet diffusion in the region of flow establishment. J. Fluid Mech., vol. 27, part 2, 231.

Saunders, D.H. 1982 A safe method of cutting steel and rock. Sixth International Symposium on Jet Cutting Technology, BHRA, Cranfield, Bedford, England, Paper K5, 503.

Schlichting, H. 1968 Boundary Layer Theory. Sixth Edition, McGraw-Hill, Inc.

Shavlovsky, D.S. 1972 Hydrodynamics of high pressure fine continuous jets. First International Symposium on Jet Cutting Technology, BHRA, Cranfield, Bedford, England, Paper A6, 81.

Summers, D.A. 1983 Considerations in the comparison of cavitating and plain water jets. Second U.S. Water Jet Conference, Univ. of Missouri-Rolla, Missouri, U.S.A., 153.

Szymczak, M., Tavoularis, S., Fahim, A. and Vijay, M.M. 1987 Flow visualization of high-speed submerged water jets. Fourth U.S. Water Jet Conference, Univ. of Berkeley, California, U.S.A.

Taylor, J.J. 1975 Camera apparatus for making photographic images on moving cut film pieces. U.S. Patent 3,925,796.

Taylor, J.J. and Hoyt, J.W. 1983 Water jet photography - Techniques and methods. Experiments in Fluids 1, 113.

Torpey, P. 1972 Some experiences in the manufacture and application of high pressure water cleaning equipment. First International Symposium on Jet Cutting Technology, BHRA, Cranfield, Bedford, England, Paper G1, 1.

Ungate, C.D., Harleman, D.R.F. and Jirka, G.H. 1975 Mixing of submerged turbulent jets at low Reynolds numbers. MIT, School of Engineering, Cambridge, Massachusetts, Report No. 197.

Vickers, G.W., Harrison, P.W. and Houlston, R. 1980 Extending the range of cavitation cleaning jets. Fifth International Symposium on Jet Cutting Technology, BHRA, Hanover, FRG, Paper J1, 403.

Vijay, M.M. 1987 Some aspects of high speed cavitating water jets. International Water Jet Symposium, Beijing, China, 1987.

Vijay, M.M. and Brierley, W.H. 1978 Cutting rocks and other materials by cavitating and non-cavitating jets. Fourth International Symposium on Jet Cutting Technology, BHRA, Cranfield, Bedford, England, Paper C5, 51.

Vijay, M.M. and Brierley, W. H. 1979 A study of erosion by high-pressure cavitating and noncavitating waterjets. American Soc. for Testing and Materials, Special Technical Publication 664, 512.

Whitehouse, J.P. 1952 An investigation into the point of incipient cavitation of submerged jets. M.S. Thesis, State Univ. of Iowa.

Wilson, L.N. and Prosser, D.W. 1969 Measurements of density fluctuations in submerged water jets. Proc. of Symposium on Turbulence Measurements in Liquids, Univ. of Missouri-Rolla, Missouri, U.S.A., 38.

Yamamoto, K. and Arndt, R.E.A. 1979 Asymmetry of a circular jet observed in near and far fields. AIAA Journal, vol. 17, no. 1, 533.

Yanaida, K. 1974 Flow characteristics of water jets. Second International Symposium on Jet Cutting Technology, BHRA, Cranfield, Bedford, England, Paper A2, 19.

Yanaida, K., Nakaya, M., Eda, K. and Nishida, N. 1985 Water jet cavitation performance of submerged horn shaped nozzles. Third U.S. Water Jet Conference, Univ. of Pittsburgh, Pittsburgh, U.S.A., 336.

Yanaida, K. and Ohashi, A. 1978 Flow characterristics of water jets in air. Fourth International Symposium on Jet Cutting Technology, BHRA, Cranfield, Bedford, England, Paper A3, 39.

Yanaida, K. and Ohashi, A. 1980 Flow characteristics of water jets in air. Fifth International Symposium on Jet Cutting Technology, BHRA, Cranfield, Bedford, England, Paper A3, 33.

Yie, G.G. 1987 Some novel applications of abrasive water jets. Proceedings of the International Waterjet Symposium, Beijing, China, Paper 4-3, 34.

Zou, C., Dang. L., Duan, X. and Cheng, D. 1985 Investigation on anatomy of continuous waterjet for updating jet performance. Third U.S. Water Jet Conference, Univ. of Pittsburgh, Pittsburgh, U.S.A., 160.

D mm	P_N MPa	P_{amb} MPa	U_o m/s	T_{H_2O} $°C$	ρ kg/m^3	P_v kPa	O_2 ppm	Re_D x10^5	σ
4.01	1.65	0.161	55.5	3.7	999.95	0.80	N.A.	1.40	0.104
	3.89	0.188	86.8	3.7	999.95	0.80	N.A.	2.19	0.050
1.02	19.4	0.213	196.	23.6	997.30	2.94	8.1	2.05	0.011
	55.2	0.212	331.	27.0	996.50	3.60	8.2	3.84	0.004

a) Plain conical entry nozzles

D_e mm	P_N MPa	P_{amb} MPa	U_o m/s	T_{H_2O} $°C$	ρ kg/m^3	P_v kPa	O_2 ppm	Re_D x10^5	σ
2.34	9.41	0.208	137.	19.7	998.30	2.30	7.8	3.17	0.022
	24.2	0.207	220.	19.7	998.30	2.30	7.7	5.09	0.009

b) Plain conical entry nozzle with pin insert

Table 1. Test conditions

D mm	U_o m/s	$(x/D)_{col}$	k_{col}
4.01	55.5	18	24
	86.8	25	17
1.02	196.	120[a]	70
	331.	160	41

a) Plain conical entry nozzles

D_e mm	U_o m/s	$(x/D)_{col}$	k_{col}
2.34	137.	50	22
	220.	65	14

b) Plain conical entry nozzle with pin insert

Table 2. Estimated values of k at positions of cavity collapse

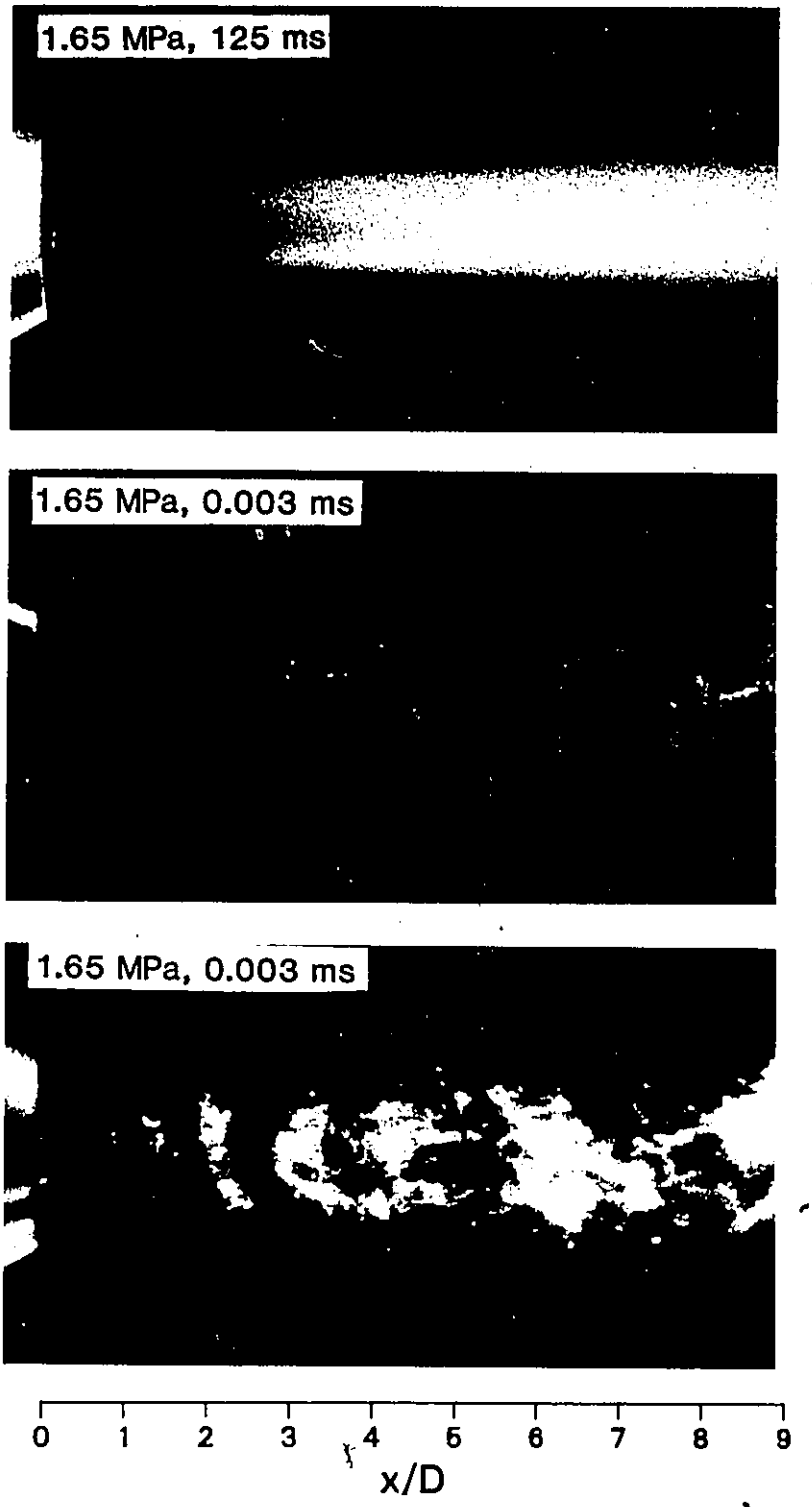

Plate 1. Jet issuing from plain conical entry nozzle, D=4.01 mm, U_o=55.5 m/s, illuminated by room lighting (top) and stroboscope

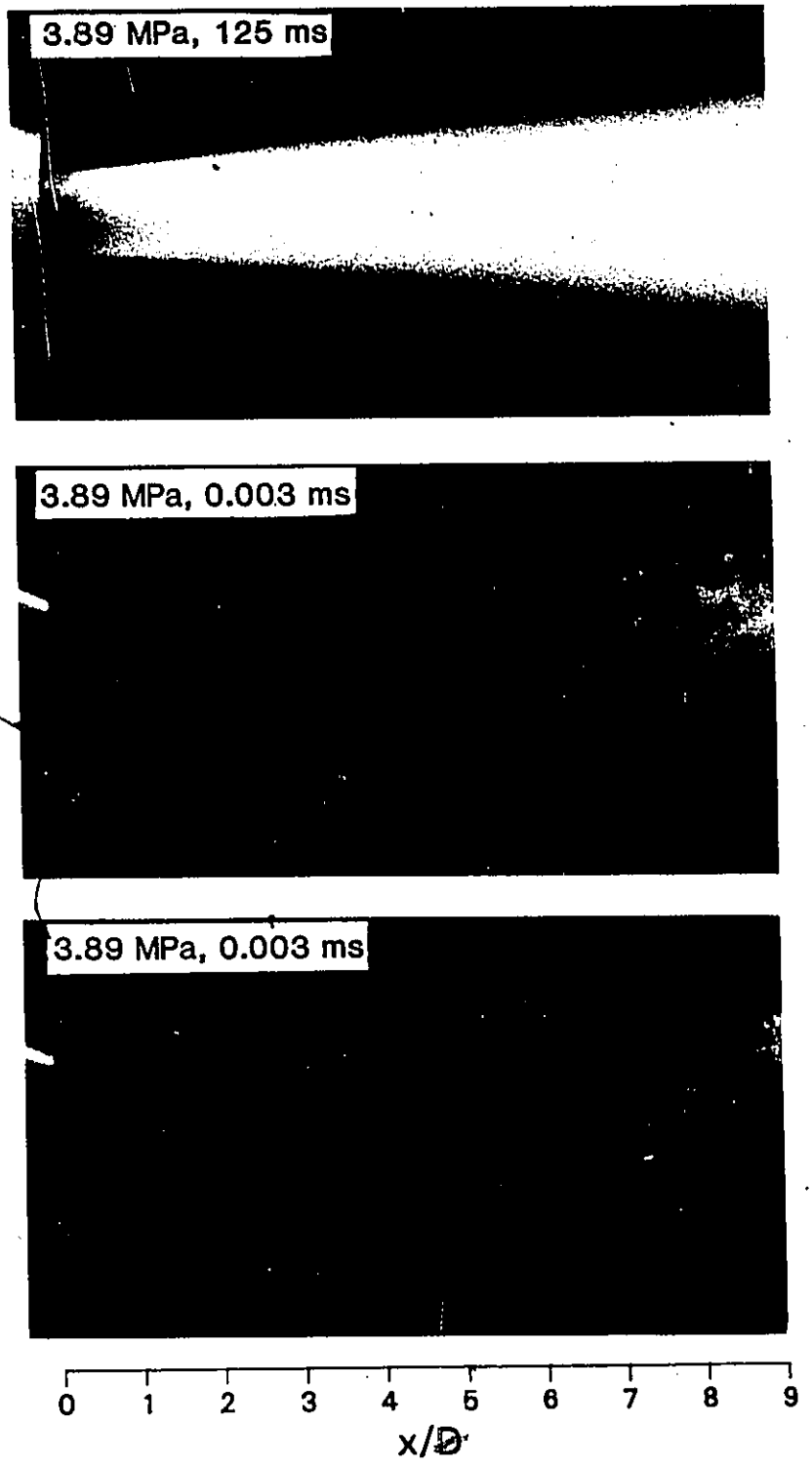

Plate 2. Jet issuing from plain conical entry nozzle, D=4.01 mm, U_o=86.8 m/s, illuminated by room lighting (top) and stroboscope

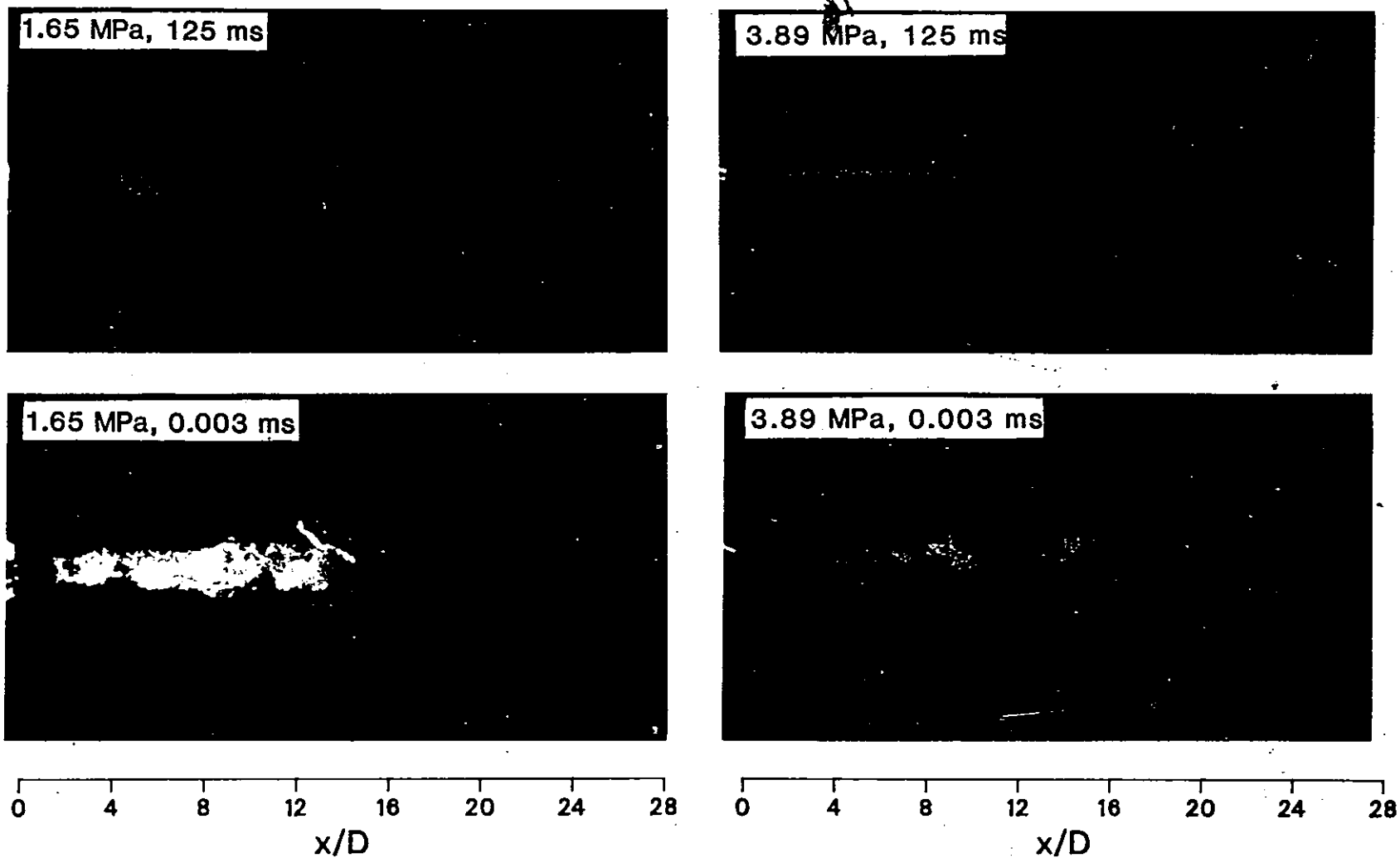

Plate 3. Jet issuing from plain conical entry nozzle, D=4.01 mm, illuminated by room lighting (top) and stroboscope

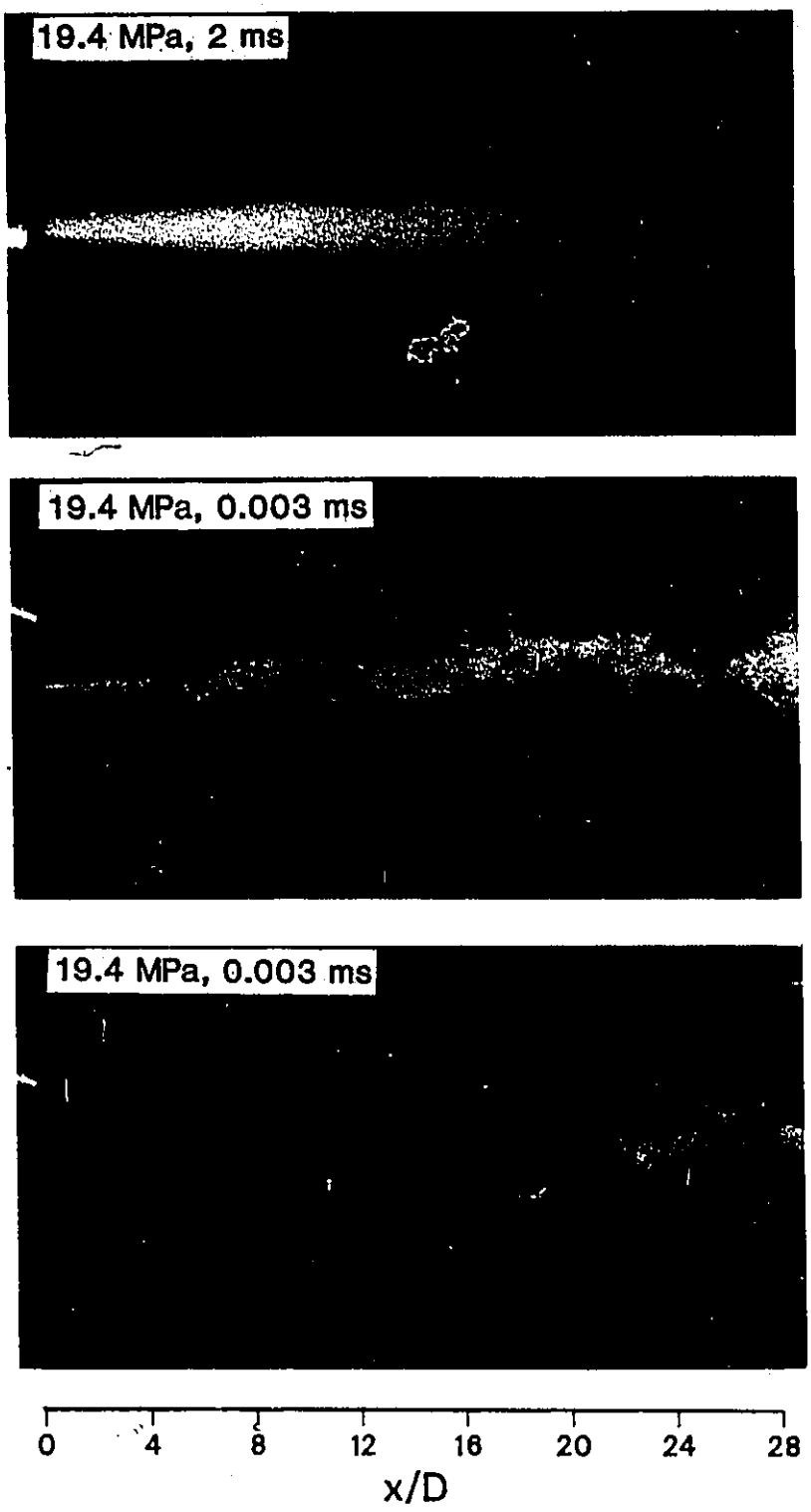

Plate 4. Jet issuing from plain conical entry nozzle, D=1.02 mm, U_o=196. m/s, illuminated by room lighting (top) and stroboscope

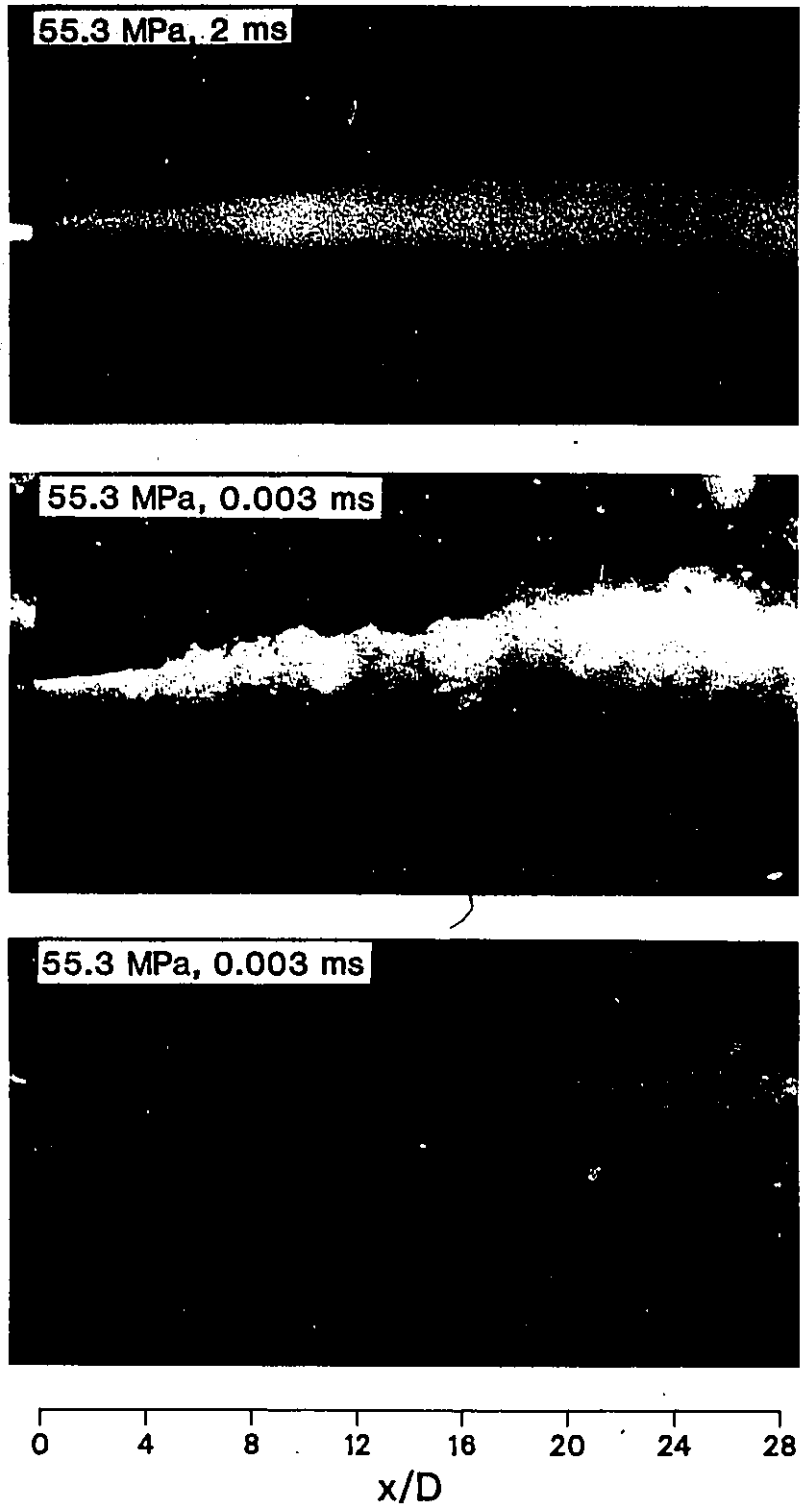

Plate 5. Jet issuing from plain conical entry nozzle, D=1.02 mm, U_o=331. m/s, illuminated by room lighting (top) and stroboscope

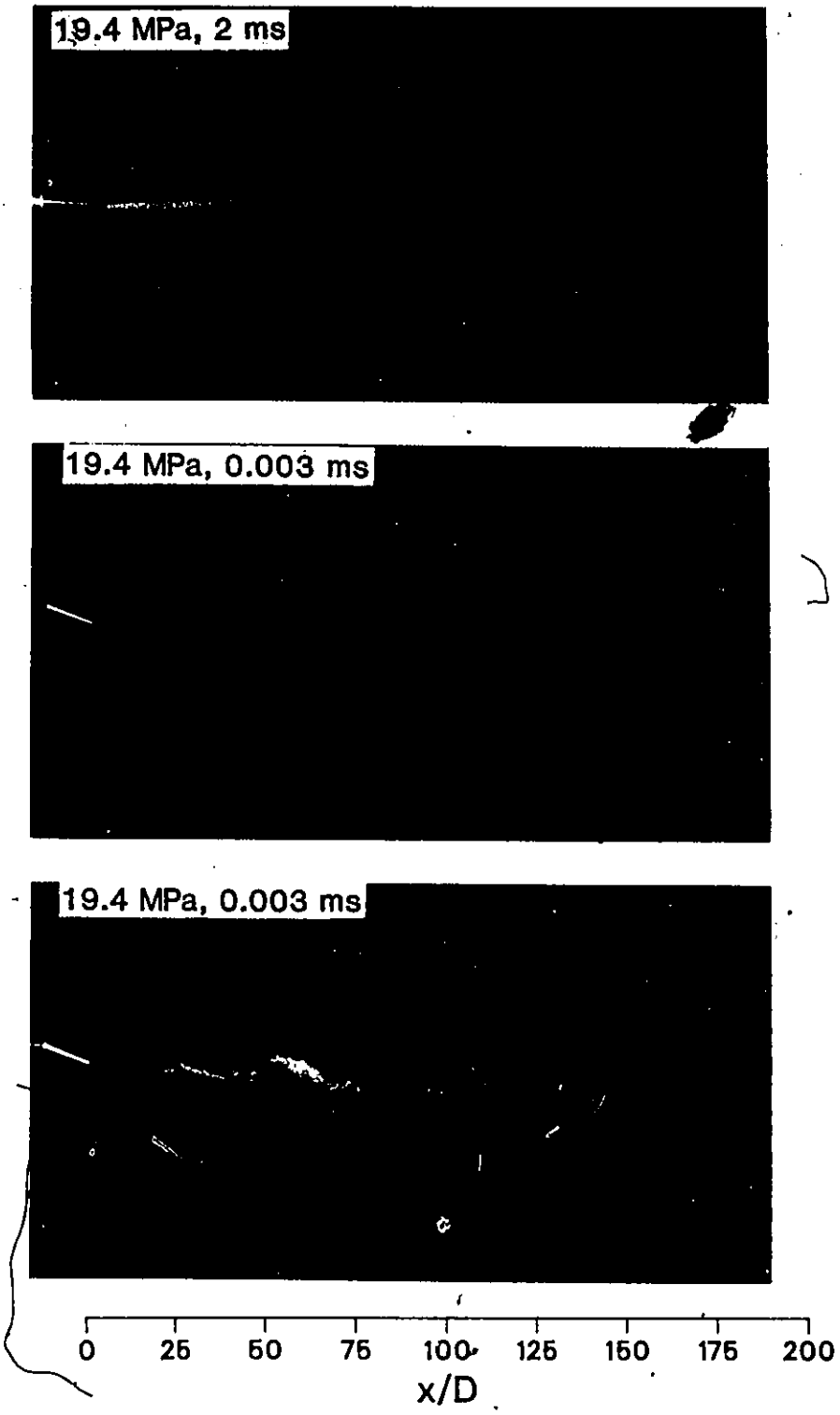

Plate 6. Jet issuing from plain conical entry nozzle, D=1.02 mm, U_o=196. m/s, illuminated by room lighting (top) and stroboscope

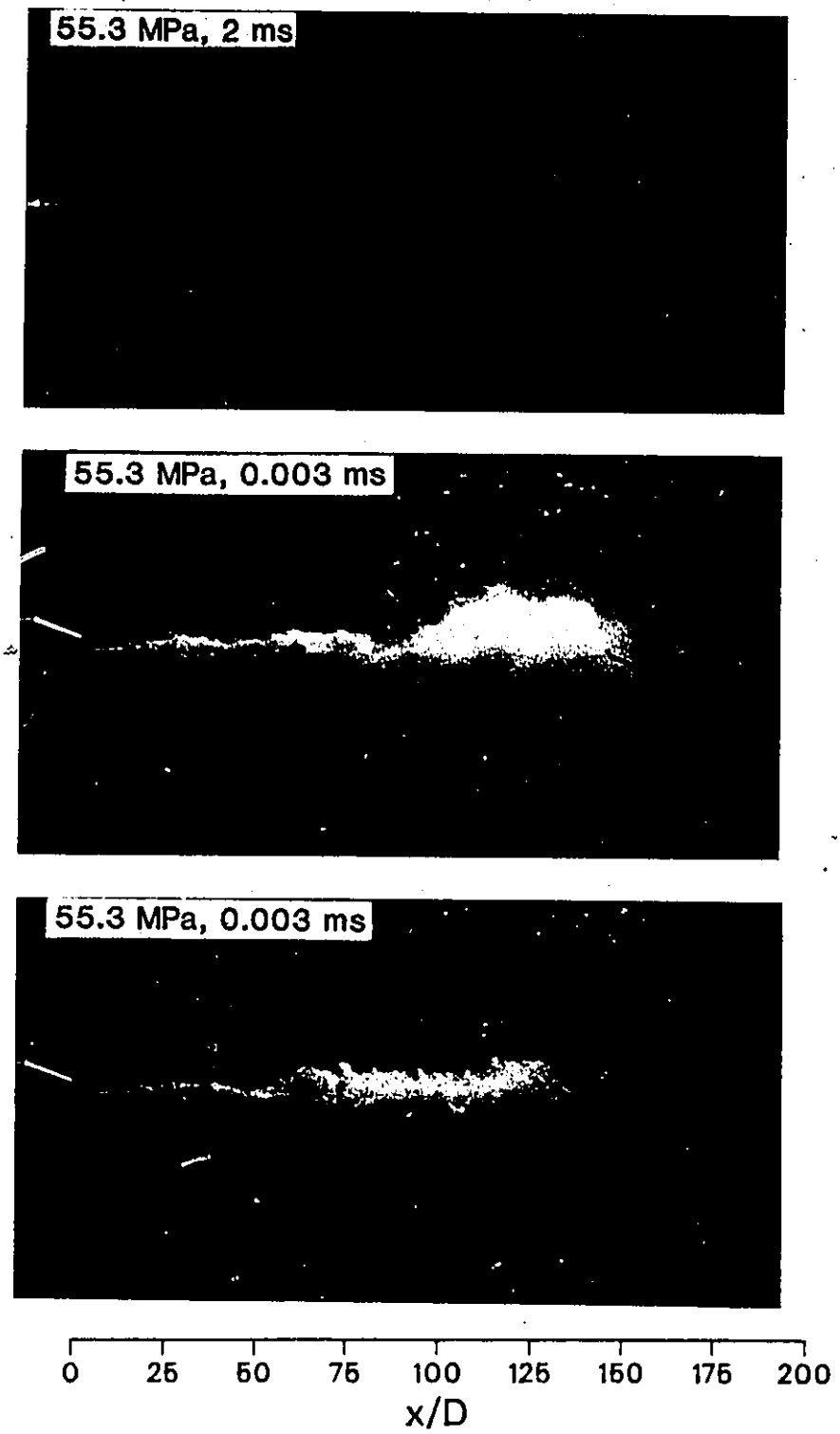

Plate 7. Jet issuing from plain conical entry nozzle, D=1.02 mm, U_o=331. m/s, illuminated by room lighting (top) and stroboscope

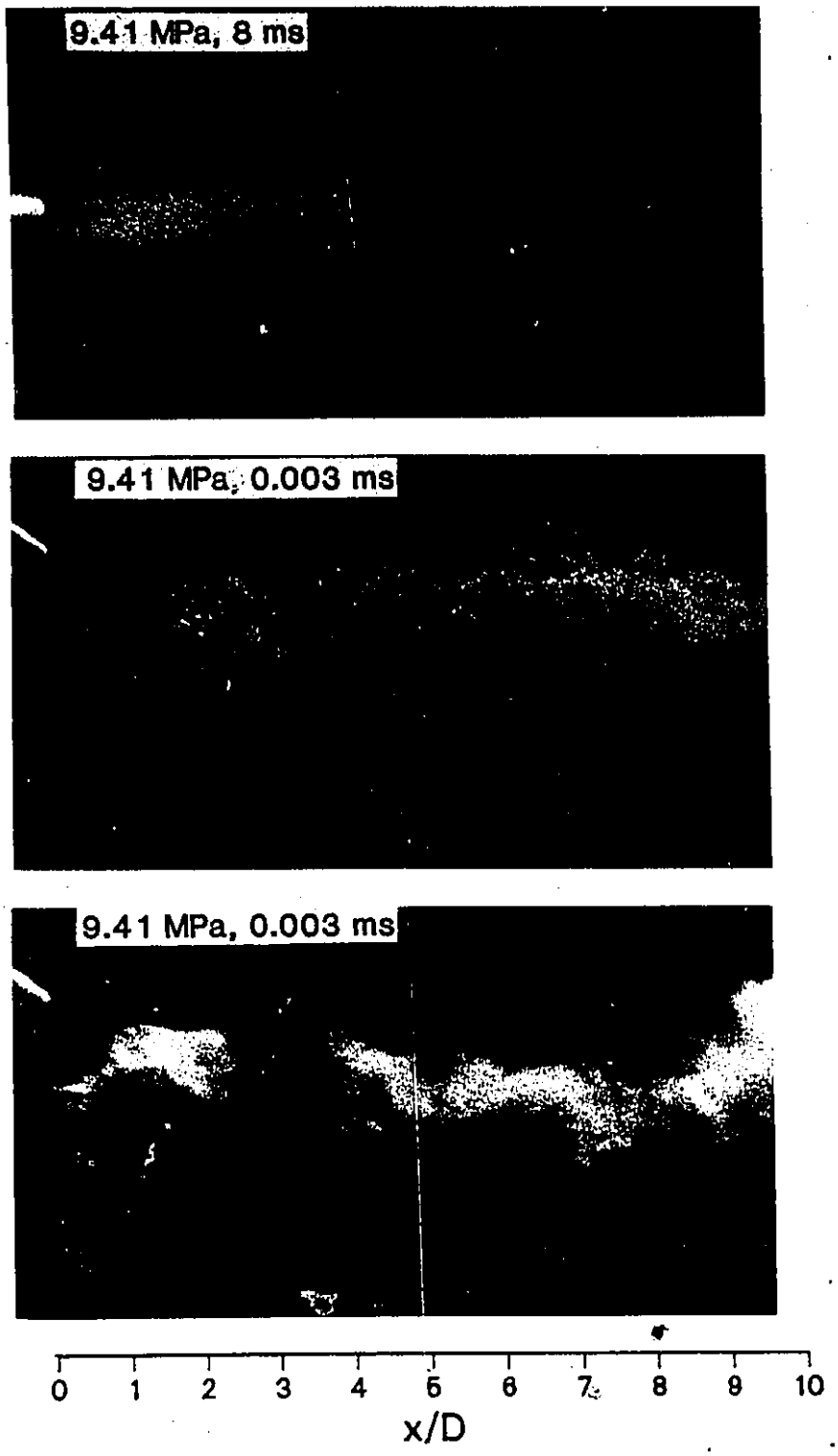

Plate 8. Jet issuing from plain conical entry nozzle with pin insert, D_e=2.34 mm, U_o=137. m/s, illuminated by room lighting (top) and stroboscope

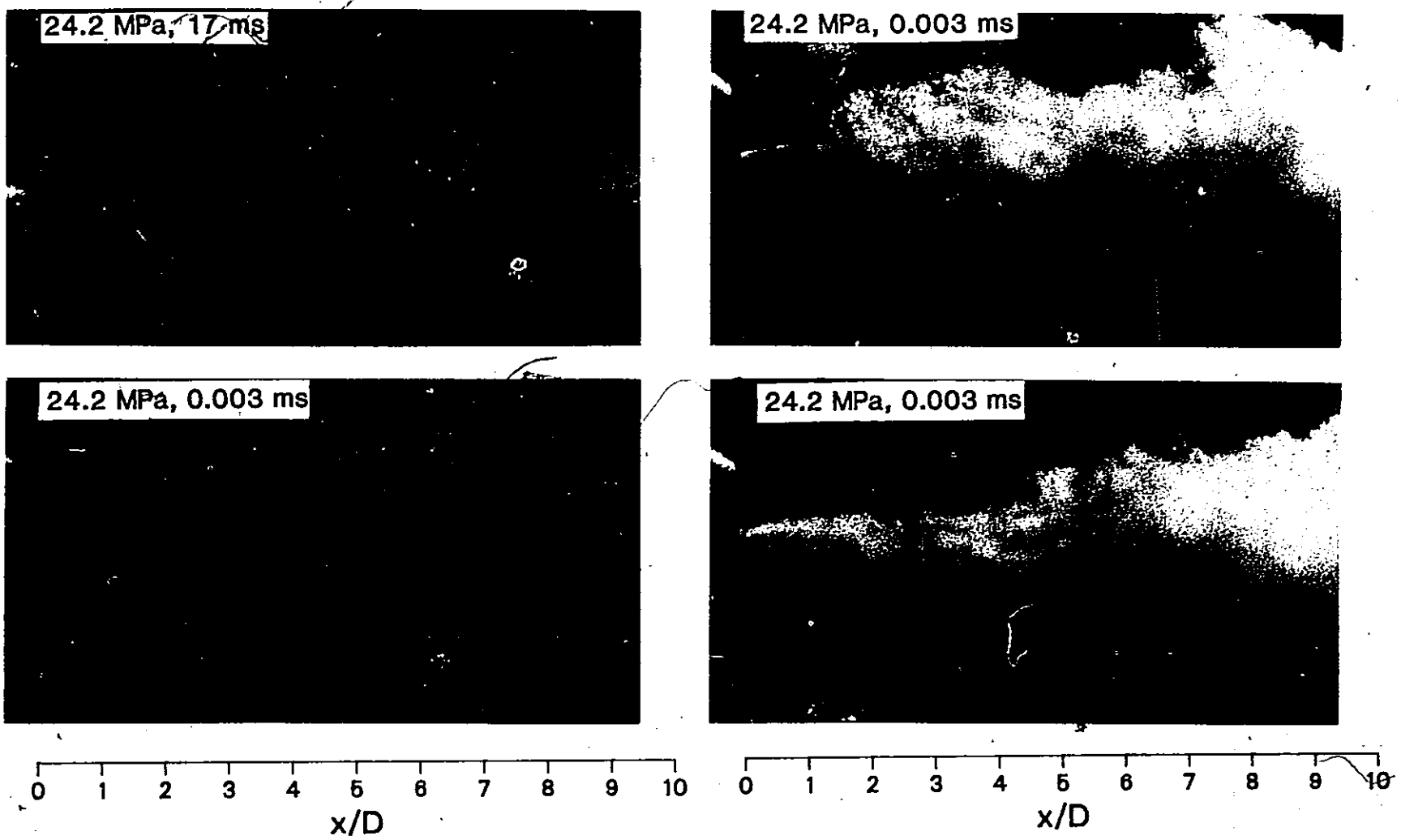

Plate 9. Jet issuing from plain conical entry nozzle with pin insert, D_e=2.34 mm, U_o=220. m/s, illuminated by room lighting (top) and stroboscope

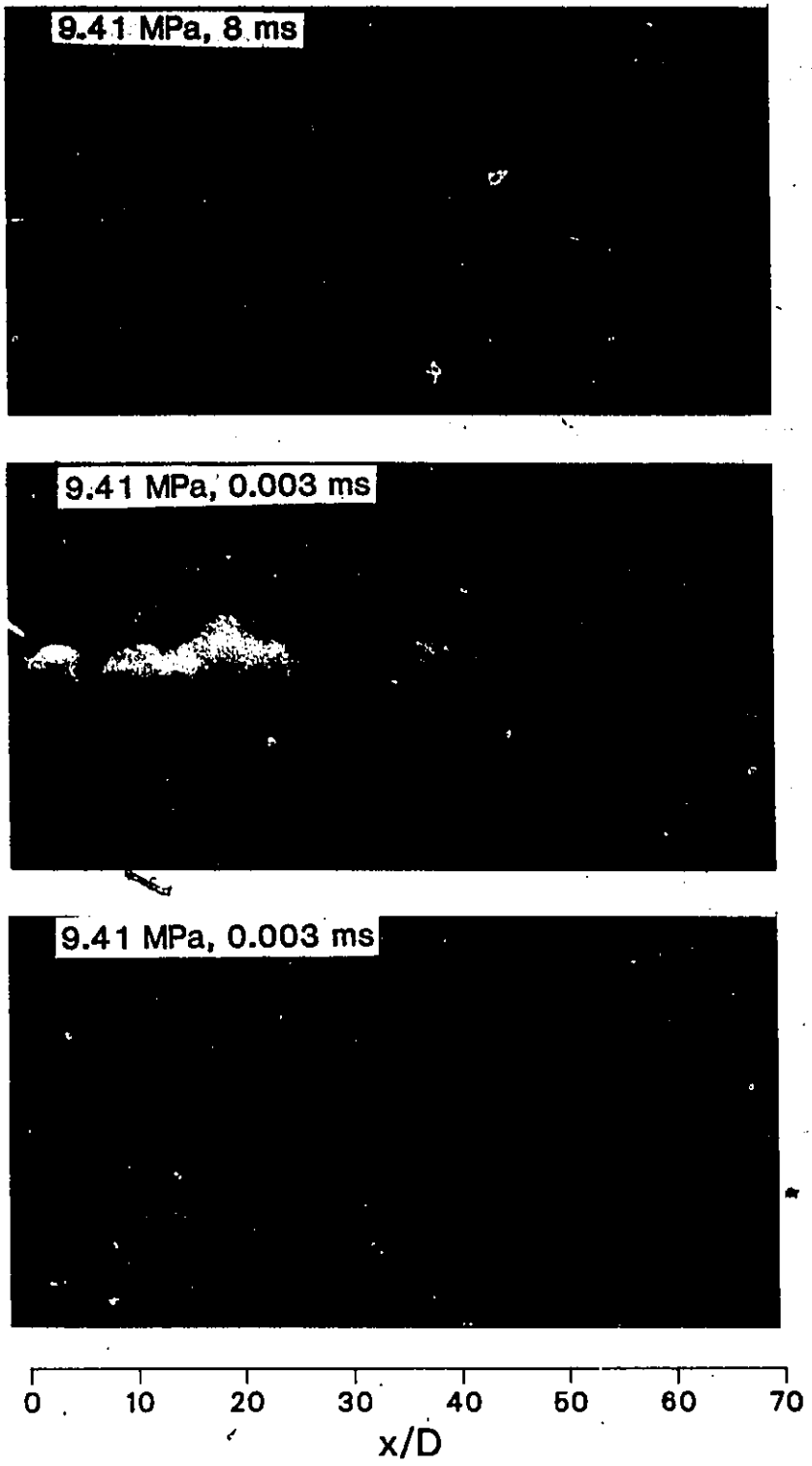

Plate 10. Jet issuing from plain conical entry nozzle with pin insert, D_e=2.34 mm, U_o=137. m/s, illuminated by room lighting (top) and stroboscope

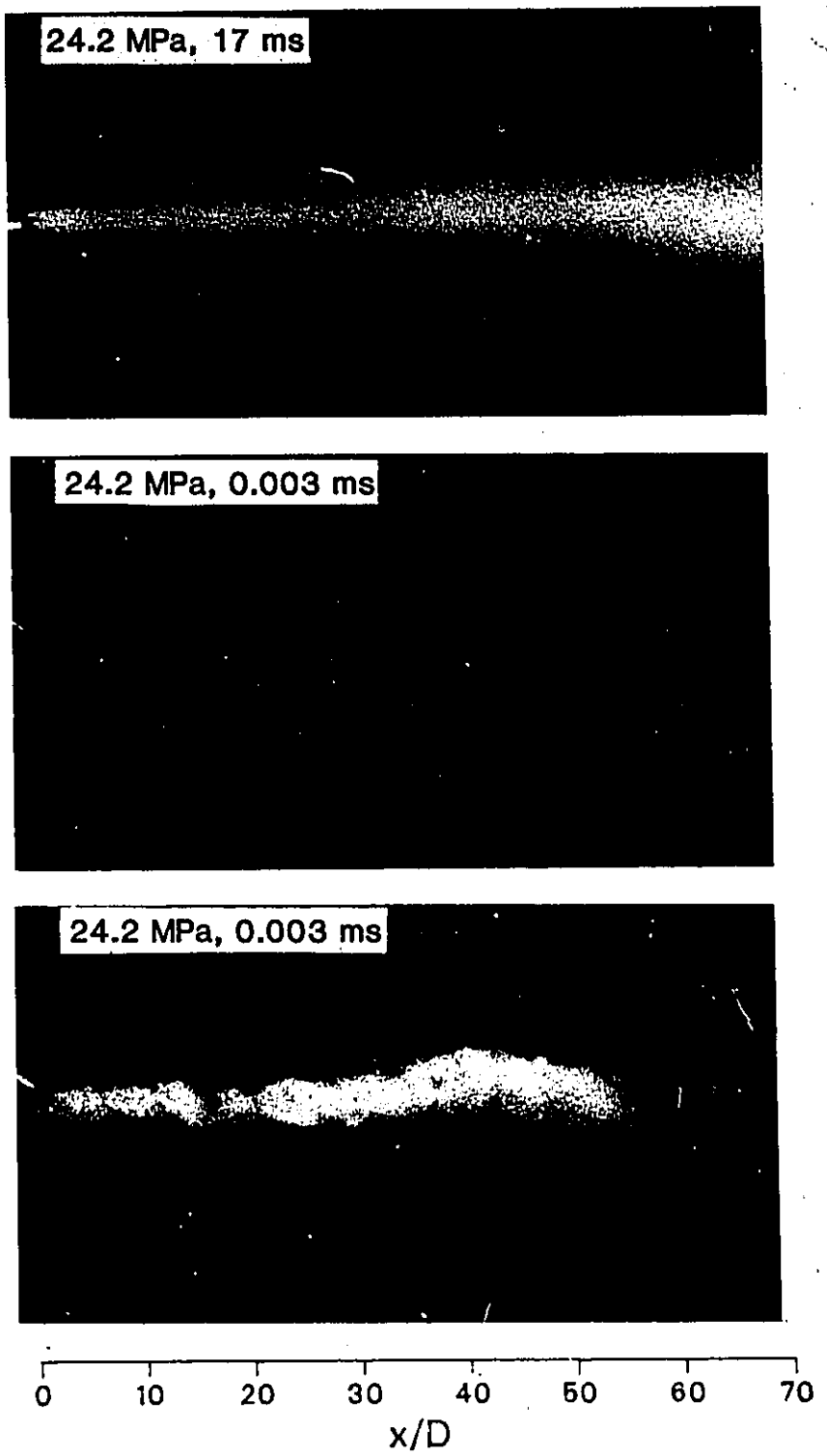

Plate 11. Jet issuing from plain conical entry nozzle with pin insert, D_e=2.34 mm, U_o=220. m/s, illuminated by room lighting (top) and stroboscope

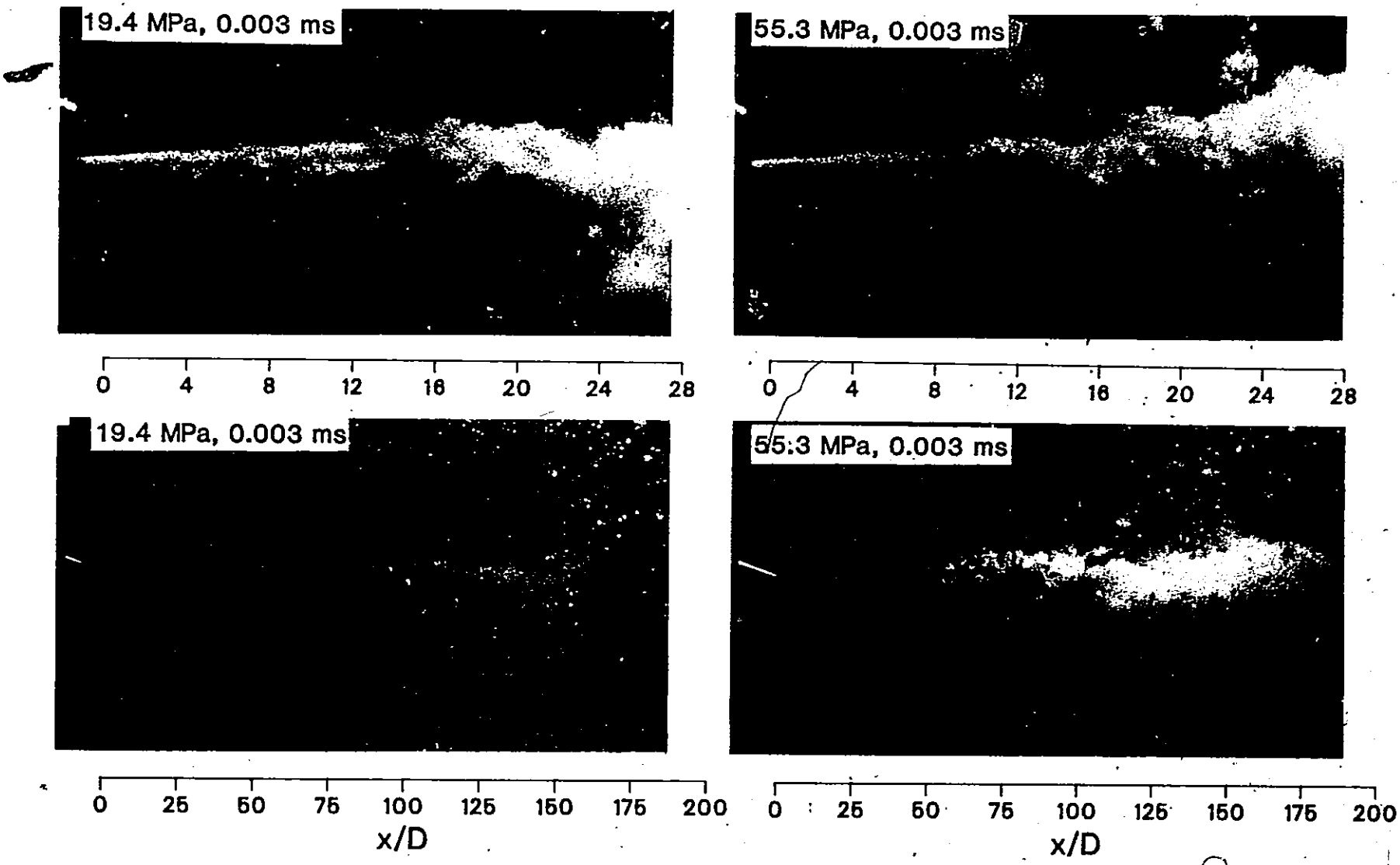

Plate 12. Jet issuing from plain conical entry nozzle, D=1.02 mm, P_{amb}=atm, illuminated by stroboscope

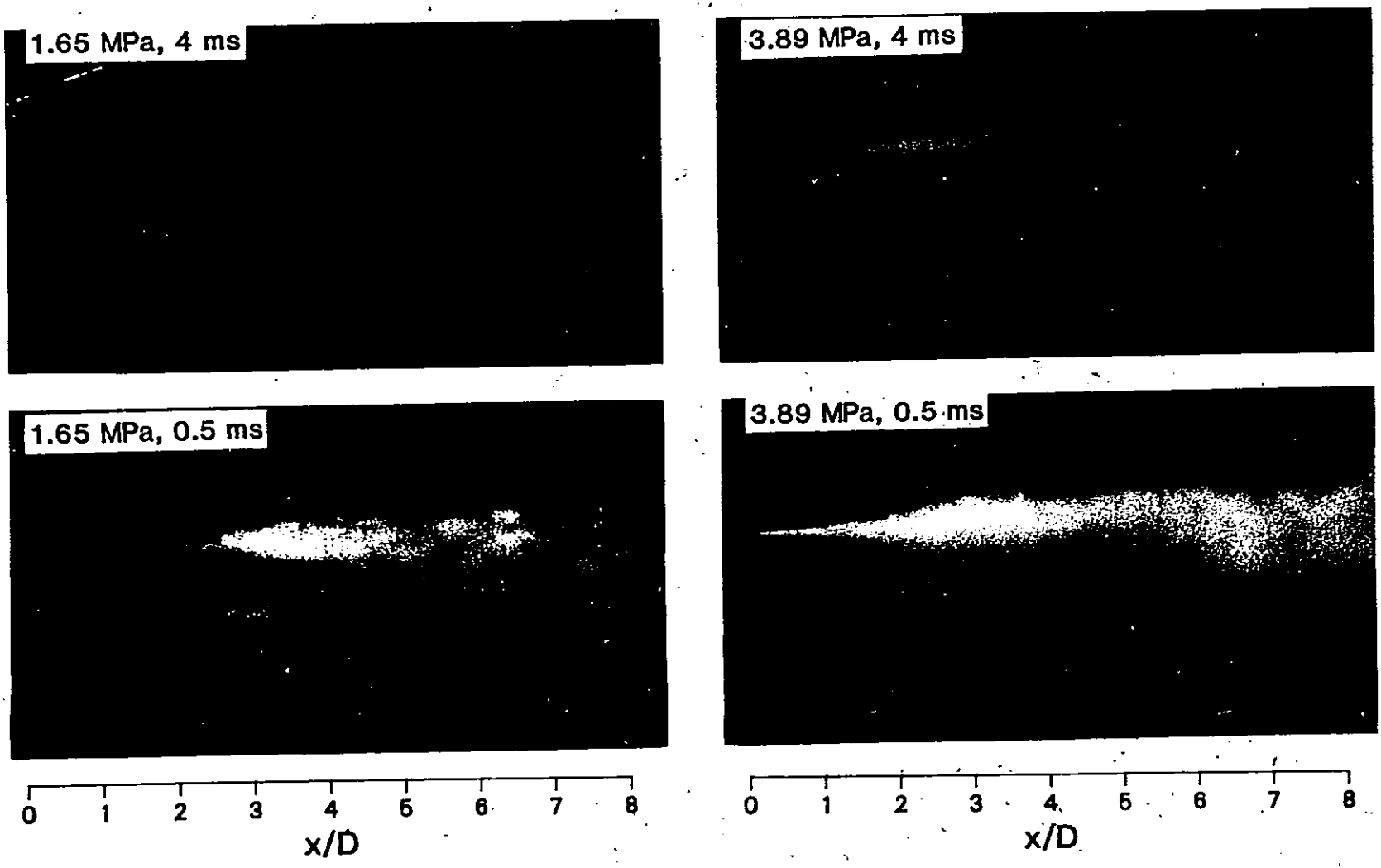

Plate 13a. Jet issuing from plain conical entry nozzle, D=4.01 mm, illuminated by axial laser-sheet

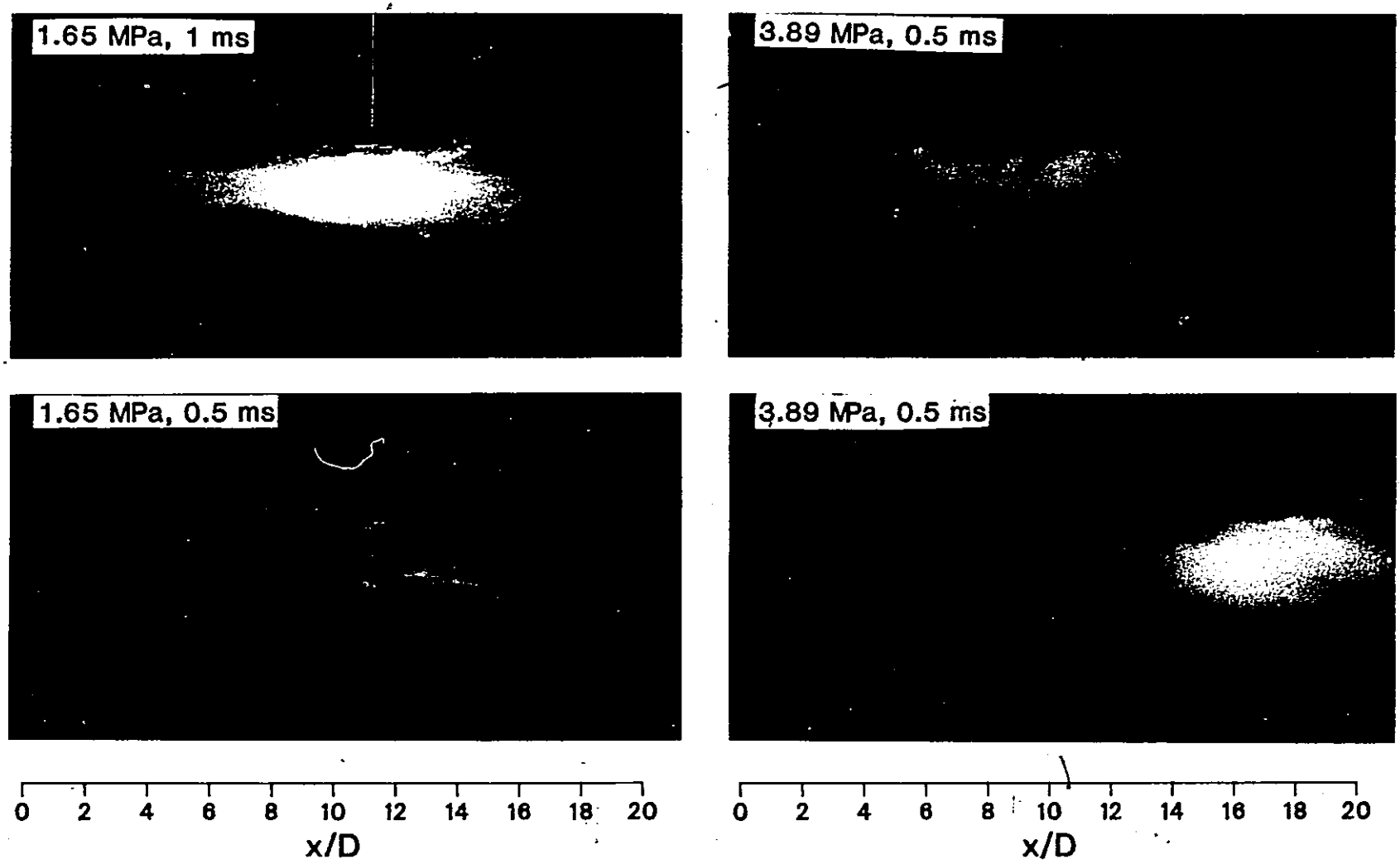

Plate 13b. Jet issuing from plain conical entry nozzle, D=4.01 mm, illuminated by axial laser-sheet

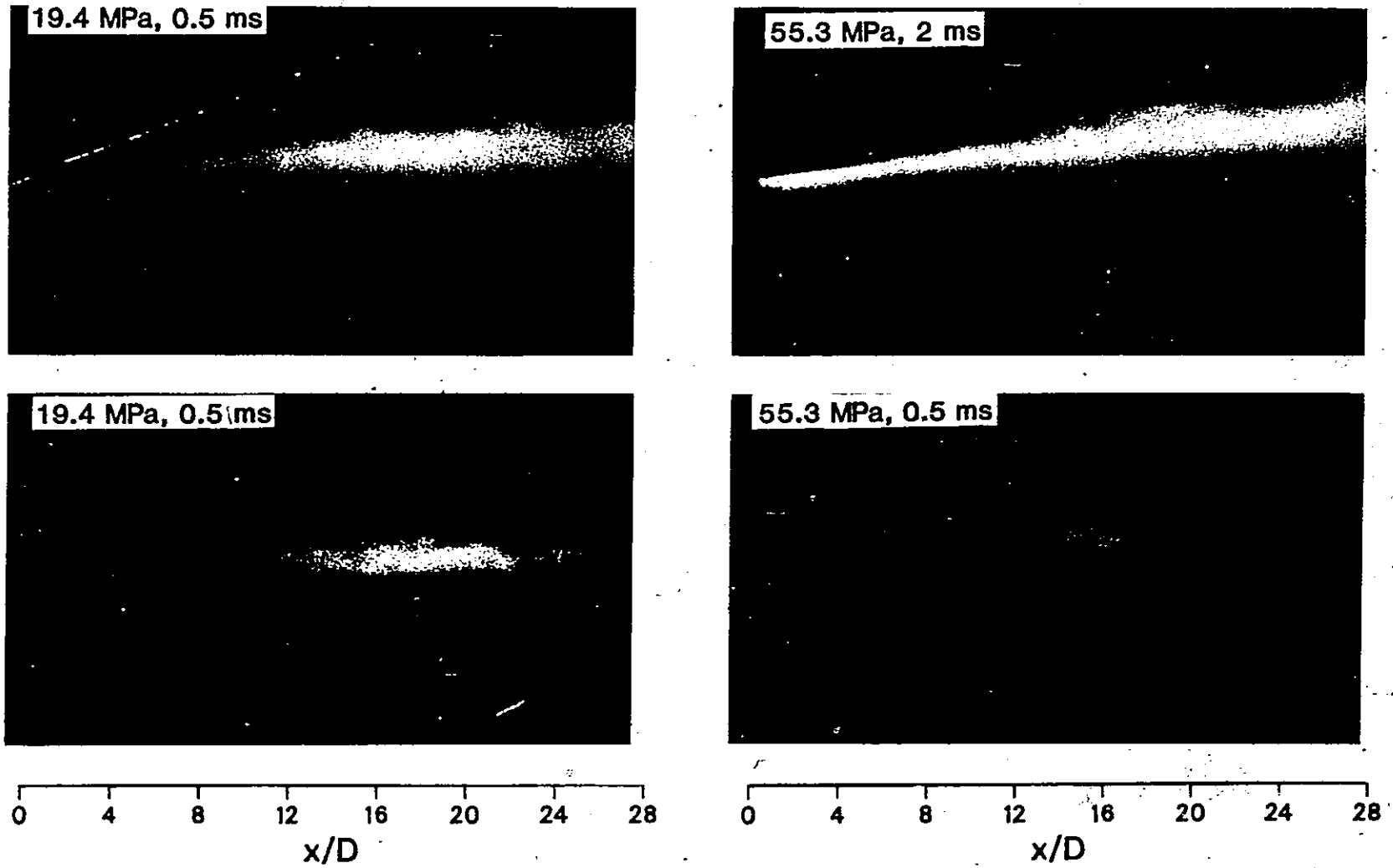

Plate 14. Jet issuing from plain conical entry nozzle, D=1.02 mm, illuminated by axial laser-sheet

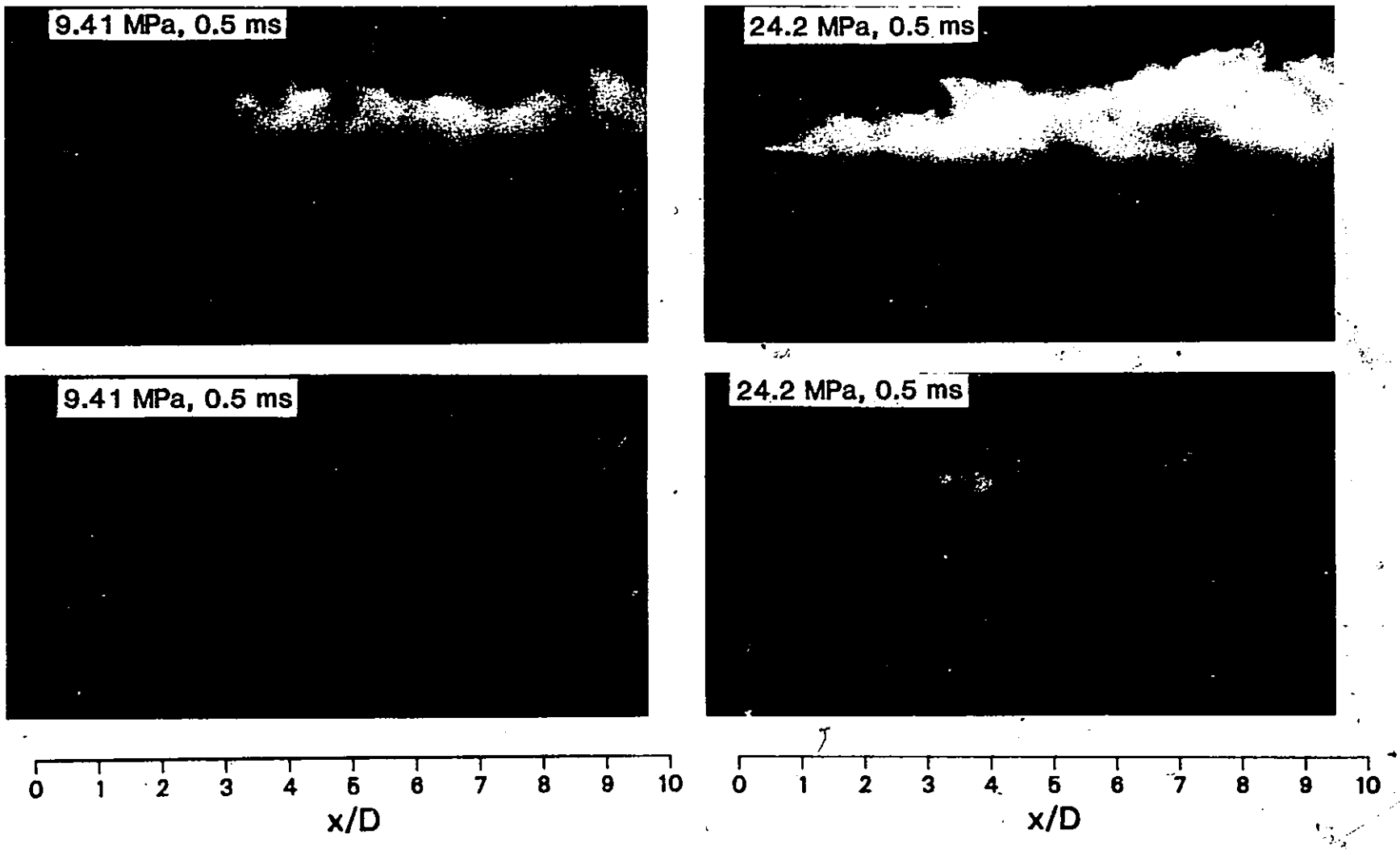

Plate 15a. Jet issuing from plain conical entry nozzle with pin insert, D_e=2.34 mm, illuminated by axial laser-sheet

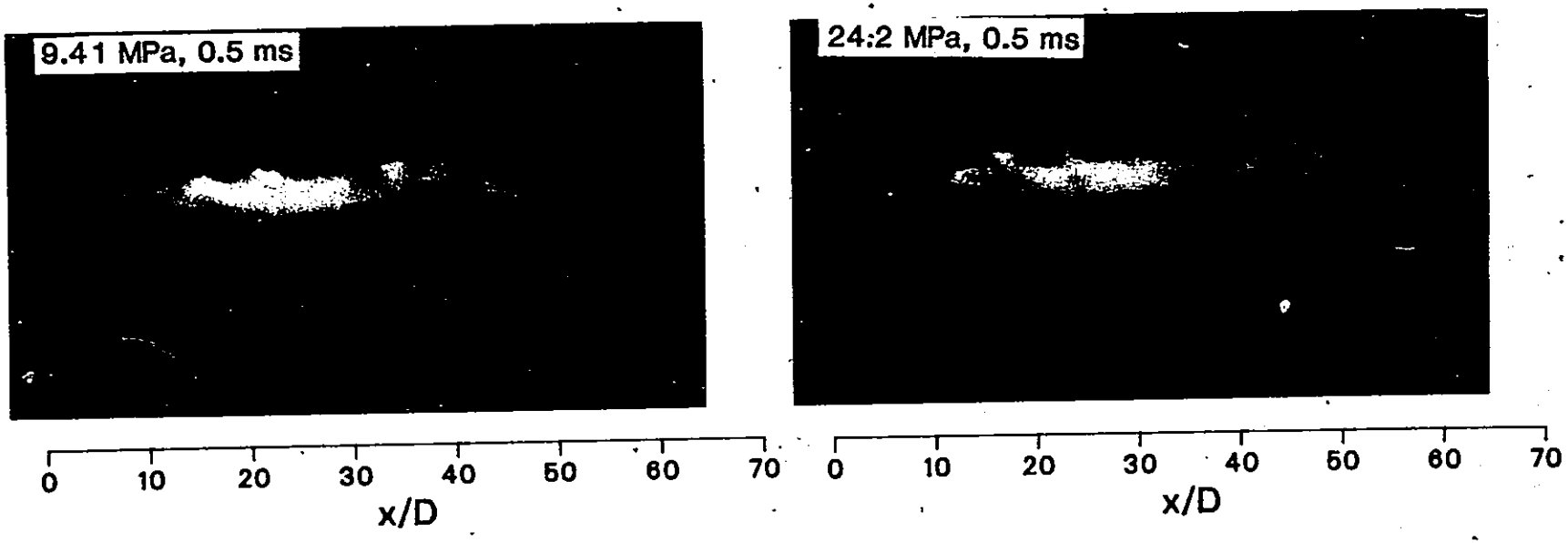

Plate 15b. Jet issuing from plain conical entry nozzle with pin insert, D_e=2.34 mm, illuminated by axial laser-sheet

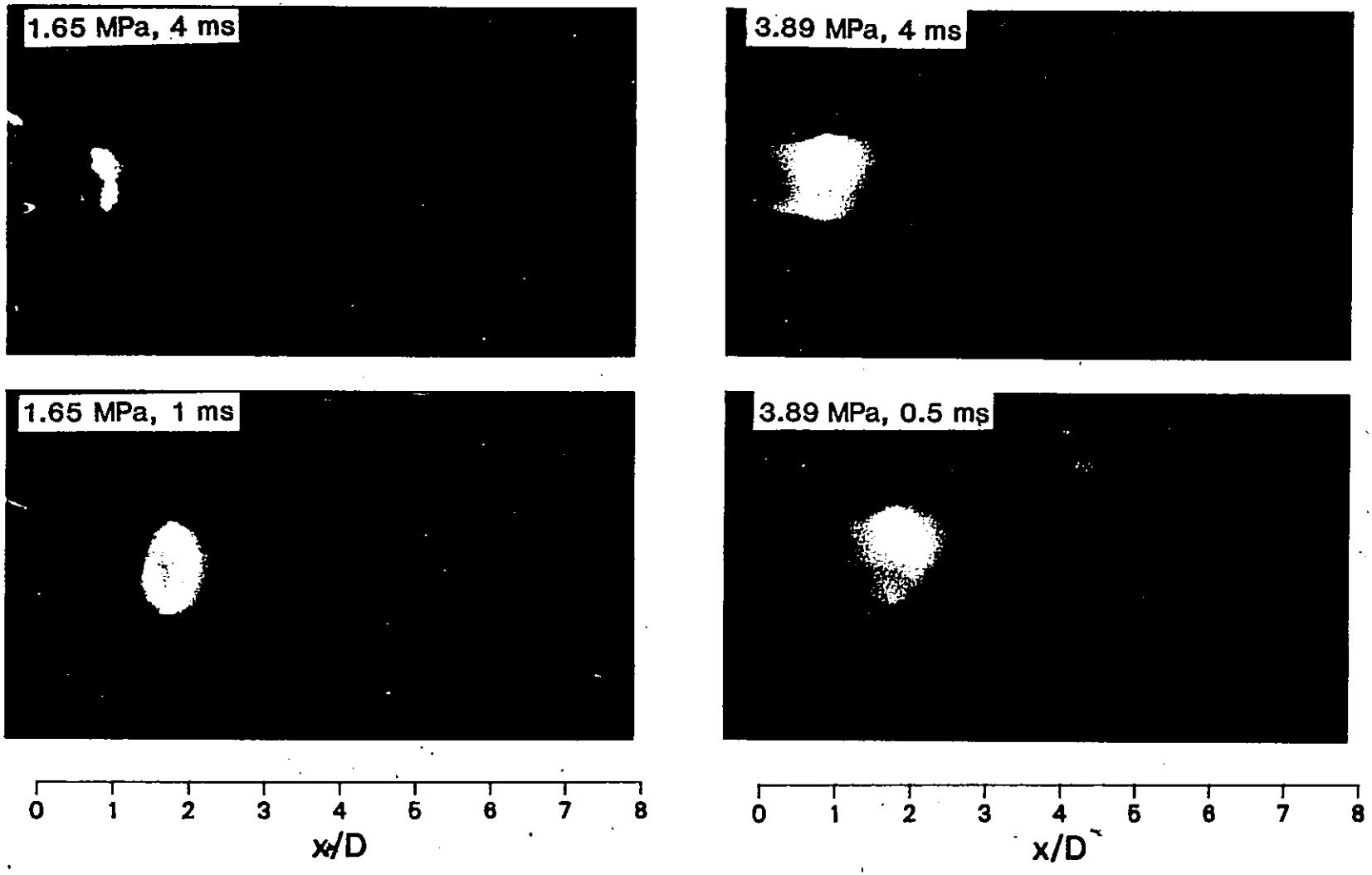

Plate 16a. Jet issuing from plain conical entry nozzle, D=4.01 mm, illuminated by transverse laser-sheet

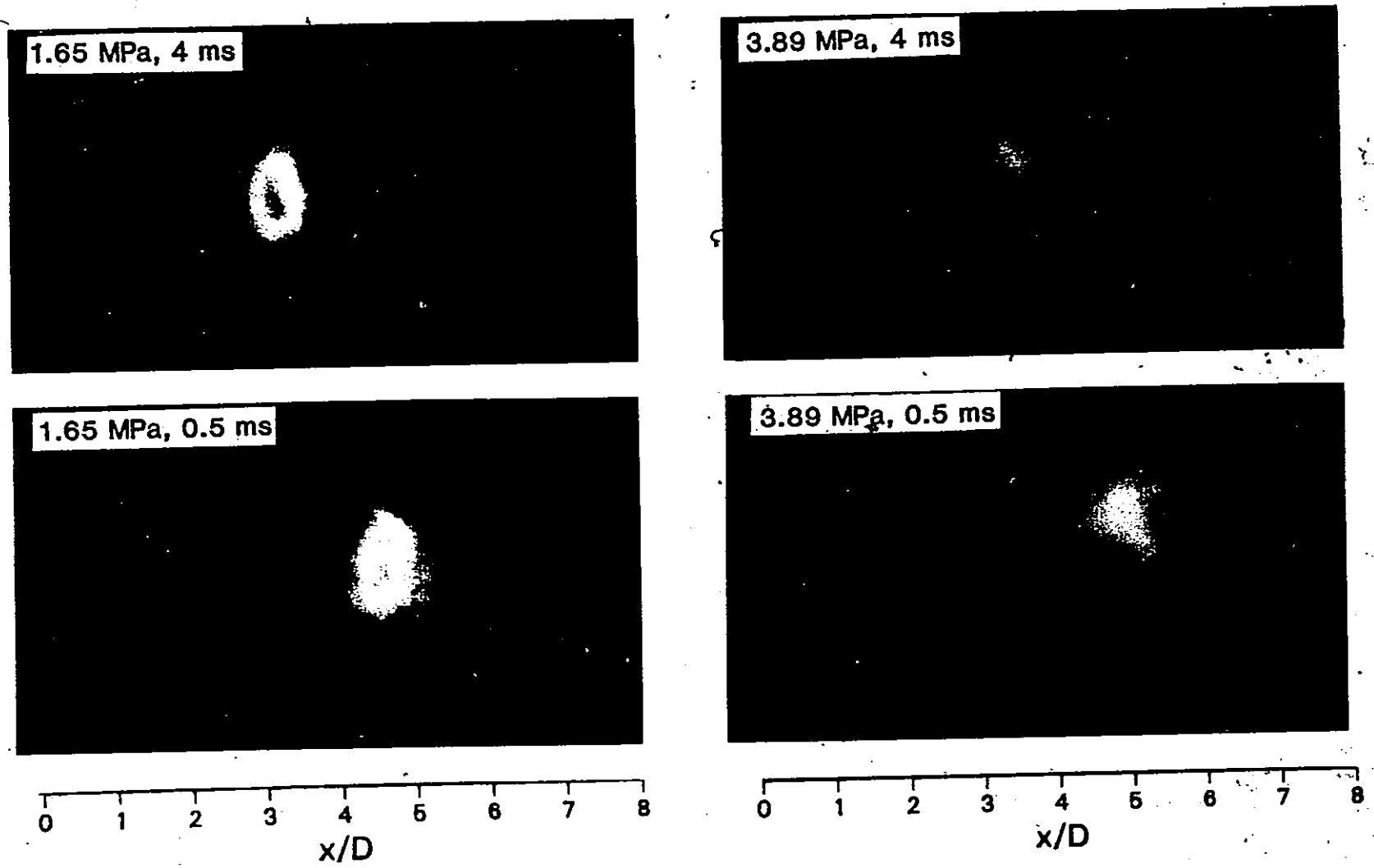

Plate 16b. Jet issuing from plain conical entry nozzle, D=4.01 mm, illuminated by transverse laser-sheet

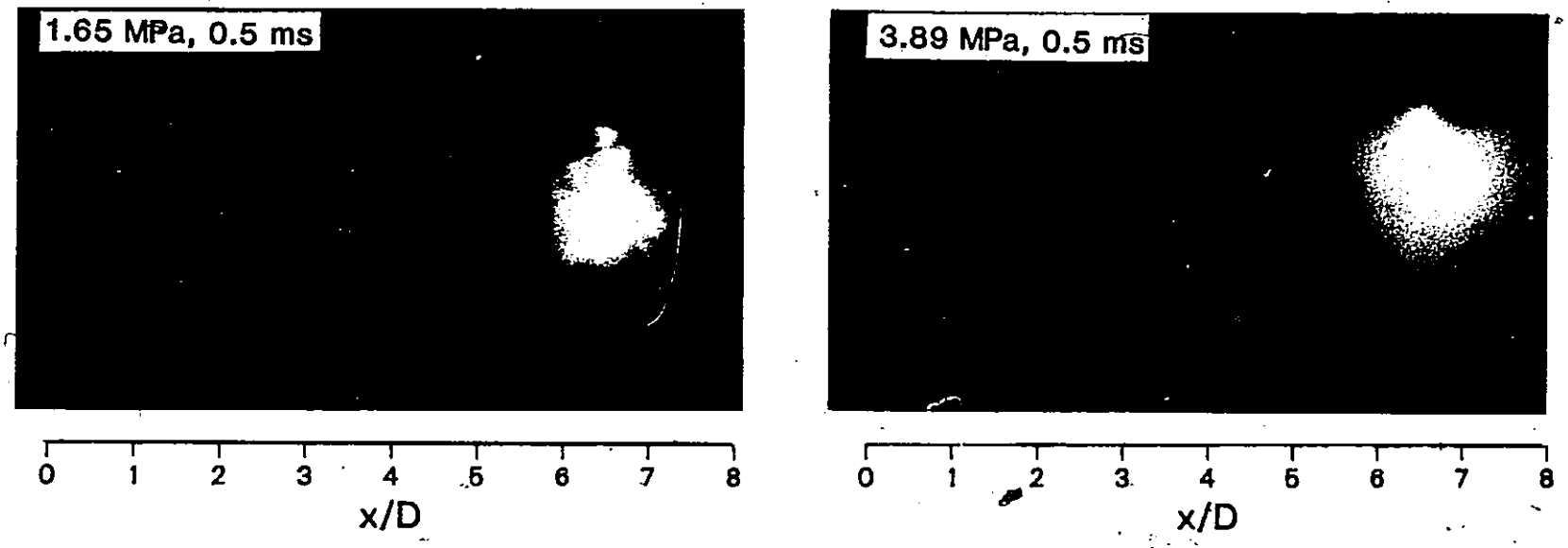

Plate 16c. Jet issuing from plain conical entry nozzle, D=4.01 mm, illuminated by transverse laser-sheet

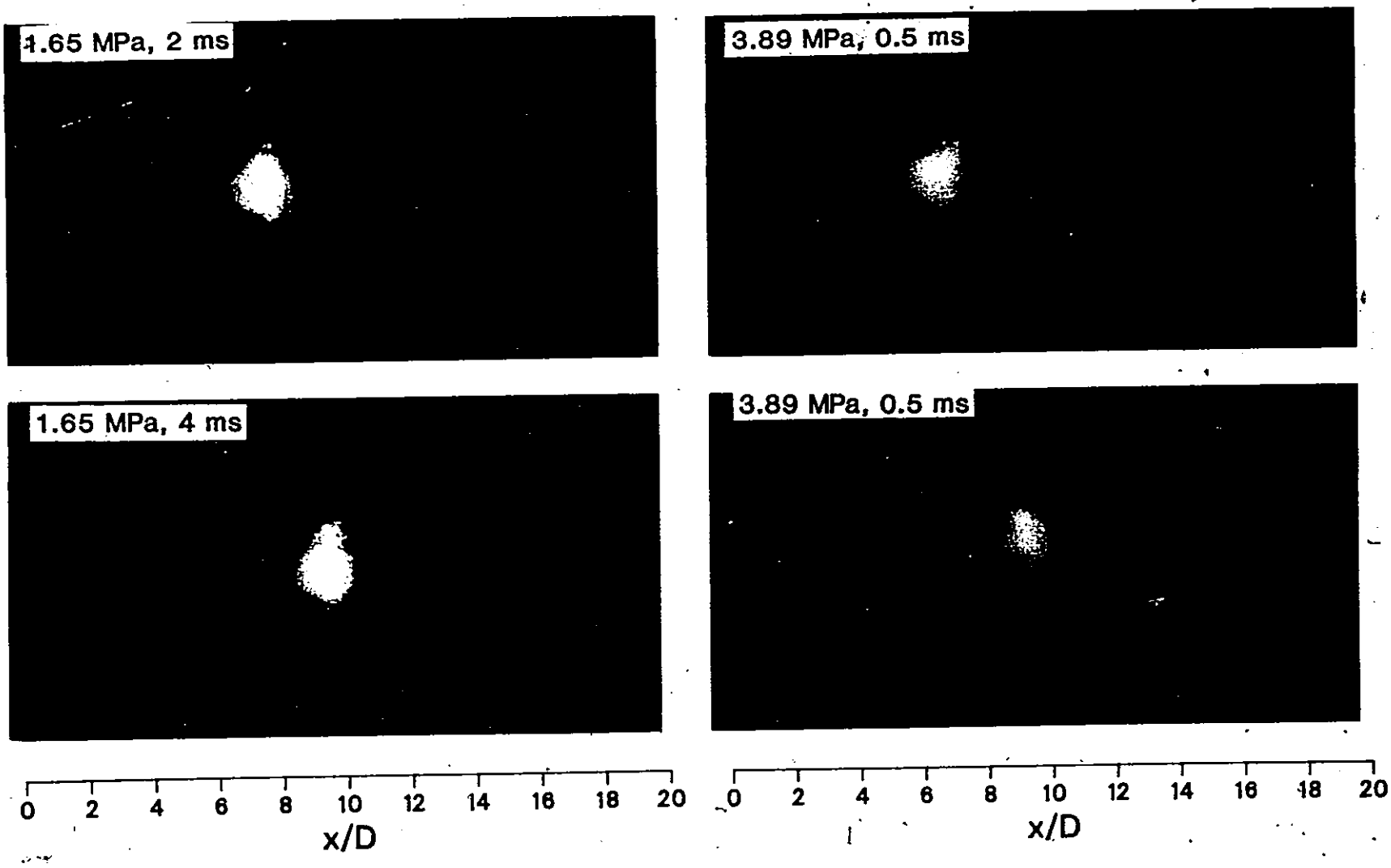

Plate 17a. Jet issuing from plain conical entry nozzle, D=4.01 mm, illuminated by transverse laser-sheet

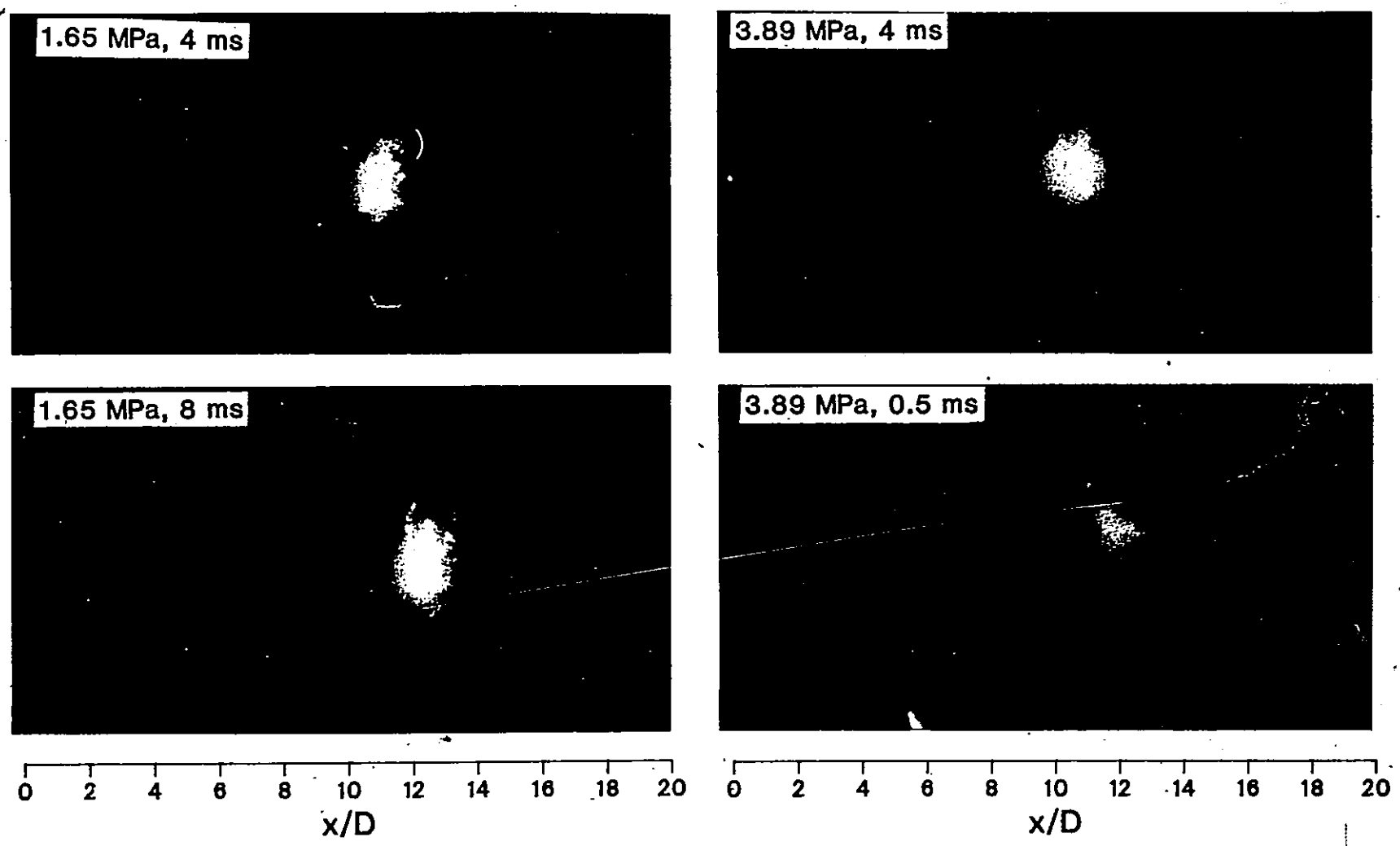

Plate 17b. Jet issuing from plain conical entry nozzle, D=4.01 mm, illuminated by transverse laser-sheet

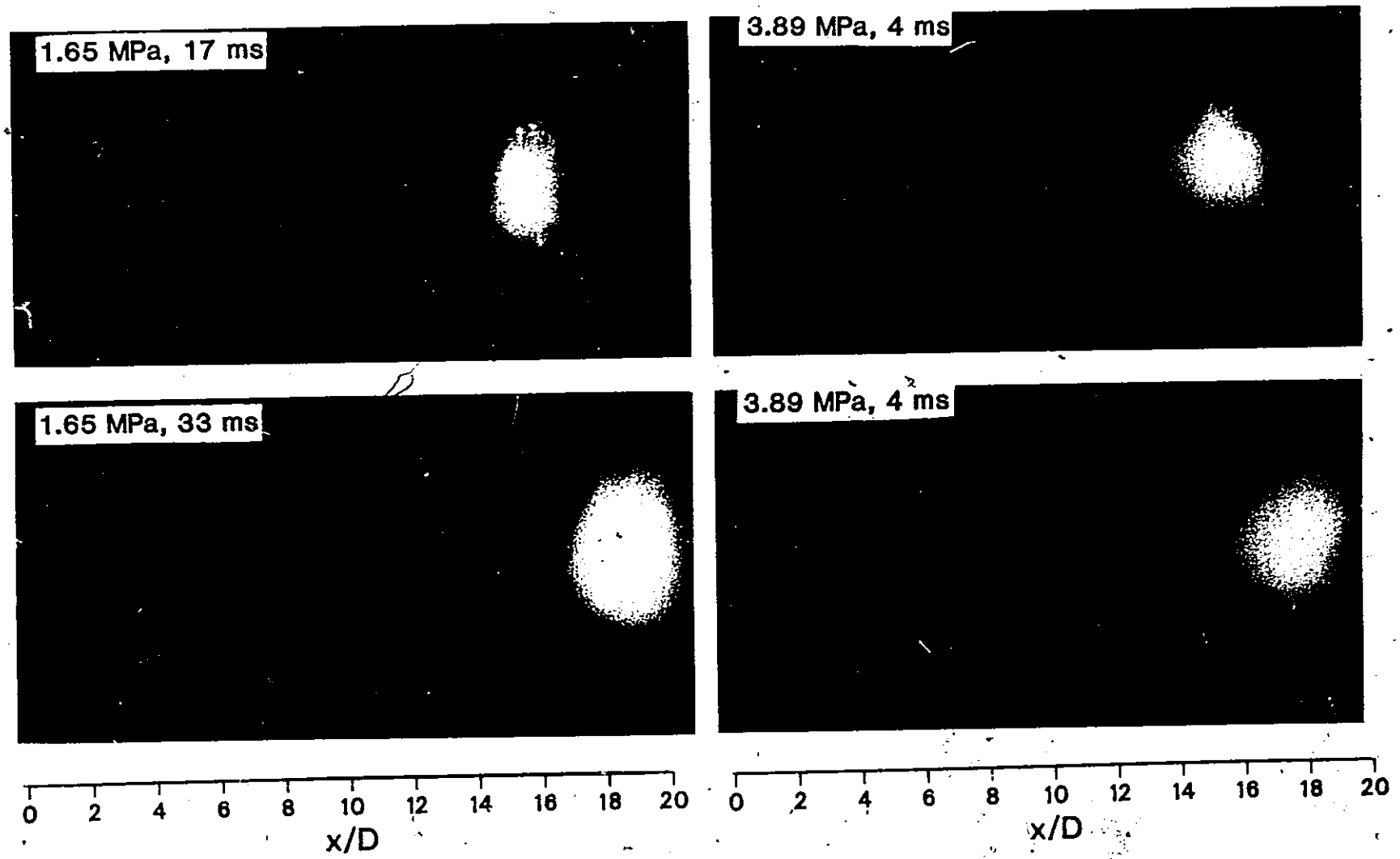

Plate 17c. Jet issuing from plain conical entry nozzle, D=4.01 mm, illuminated by transverse laser-sheet

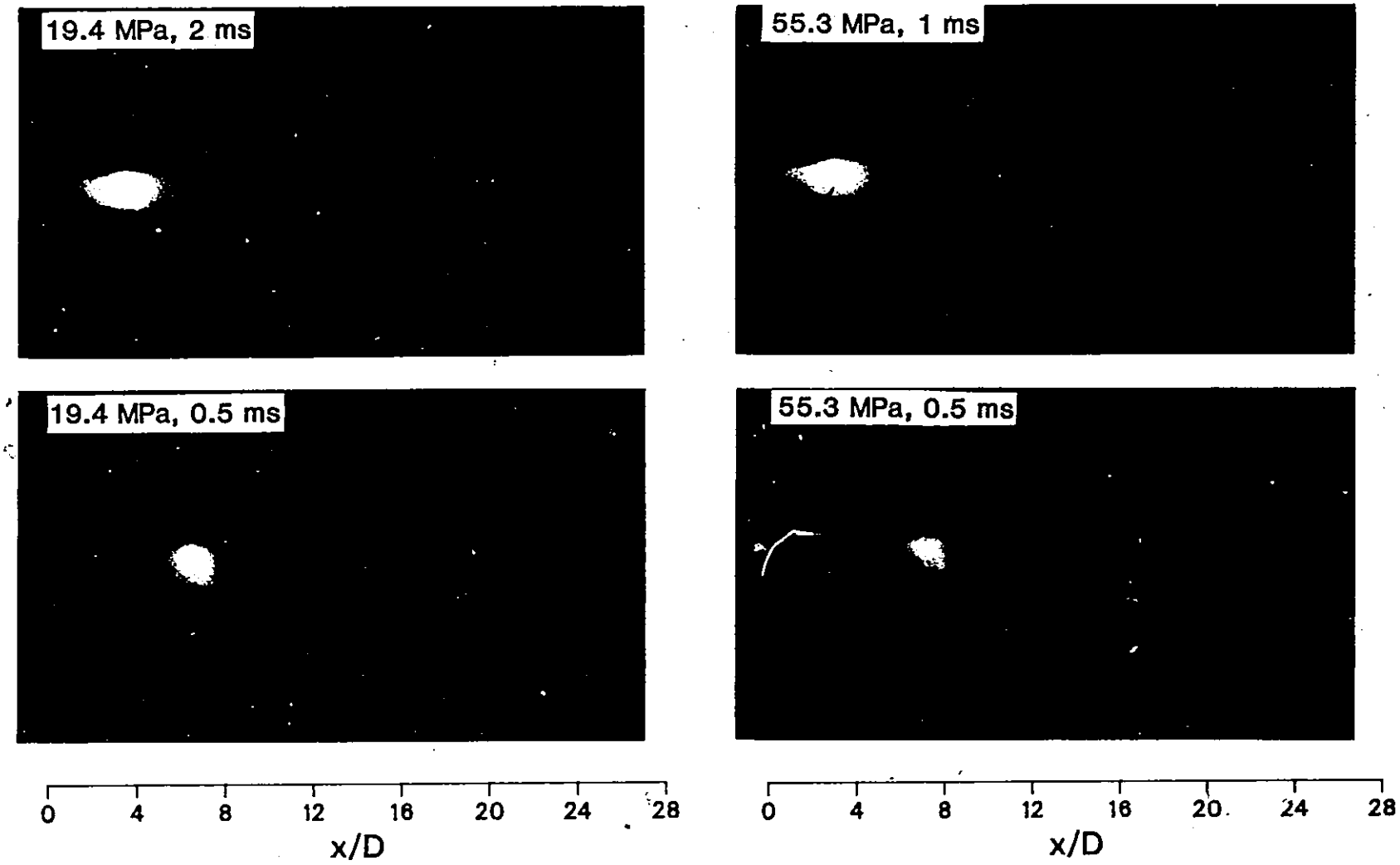

Plate 18a. Jet issuing from plain conical entry nozzle, D=1.02 mm, illuminated by transverse laser-sheet

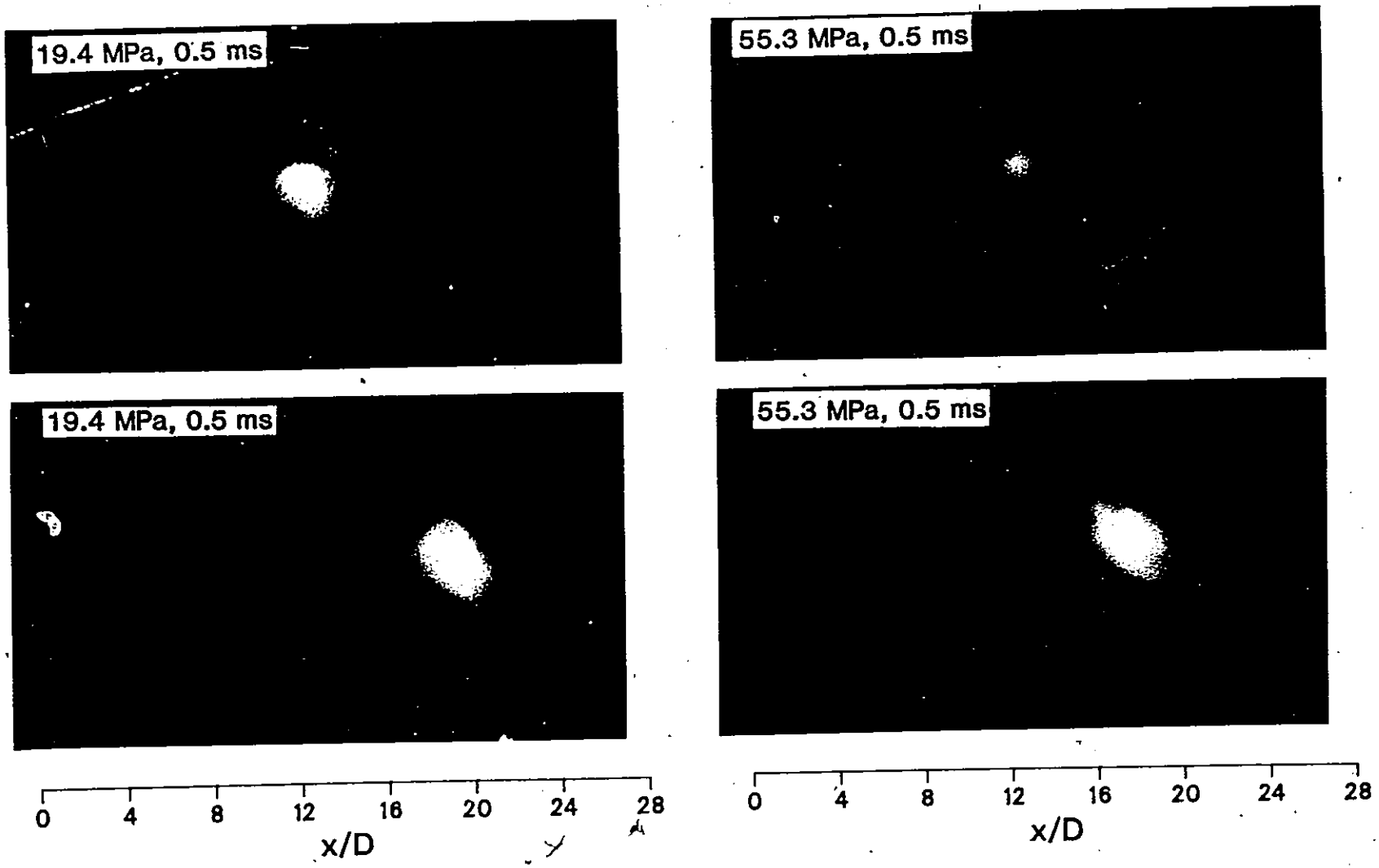

Plate 18b. Jet issuing from plain conical entry nozzle, D=1.02 mm, illuminated by transverse laser-sheet

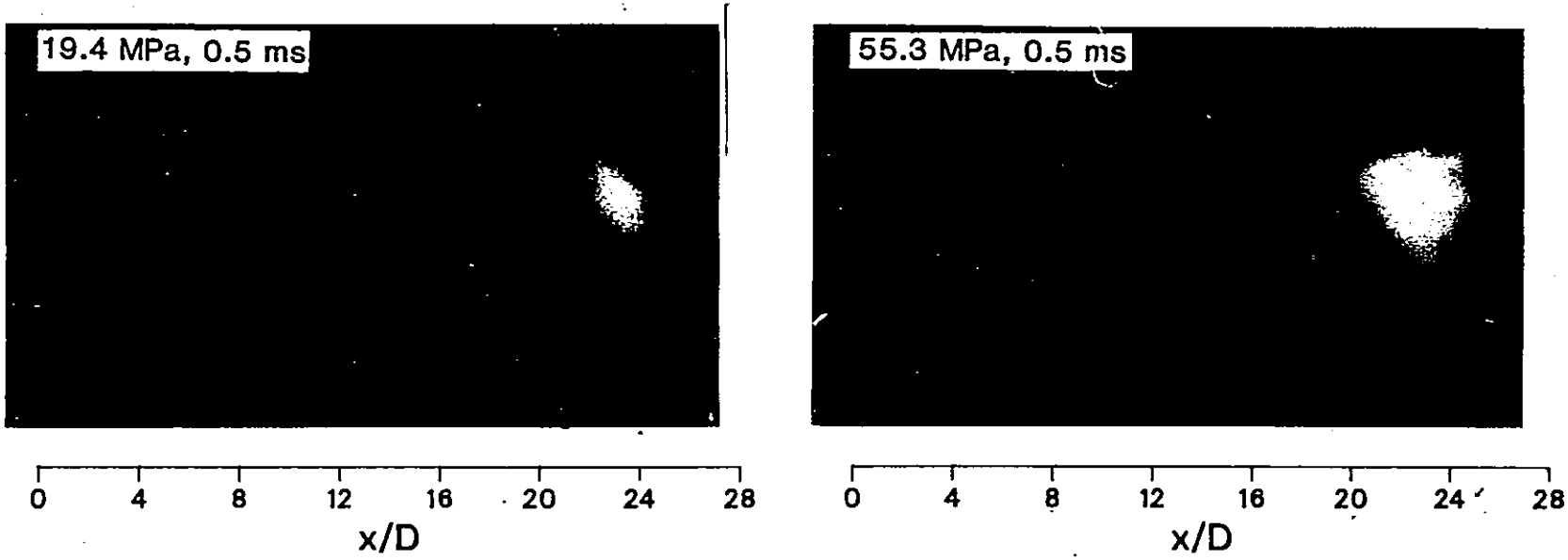

Plate 18c. Jet issuing from plain conical entry nozzle, D=1.02 mm, illuminated by transverse laser-sheet

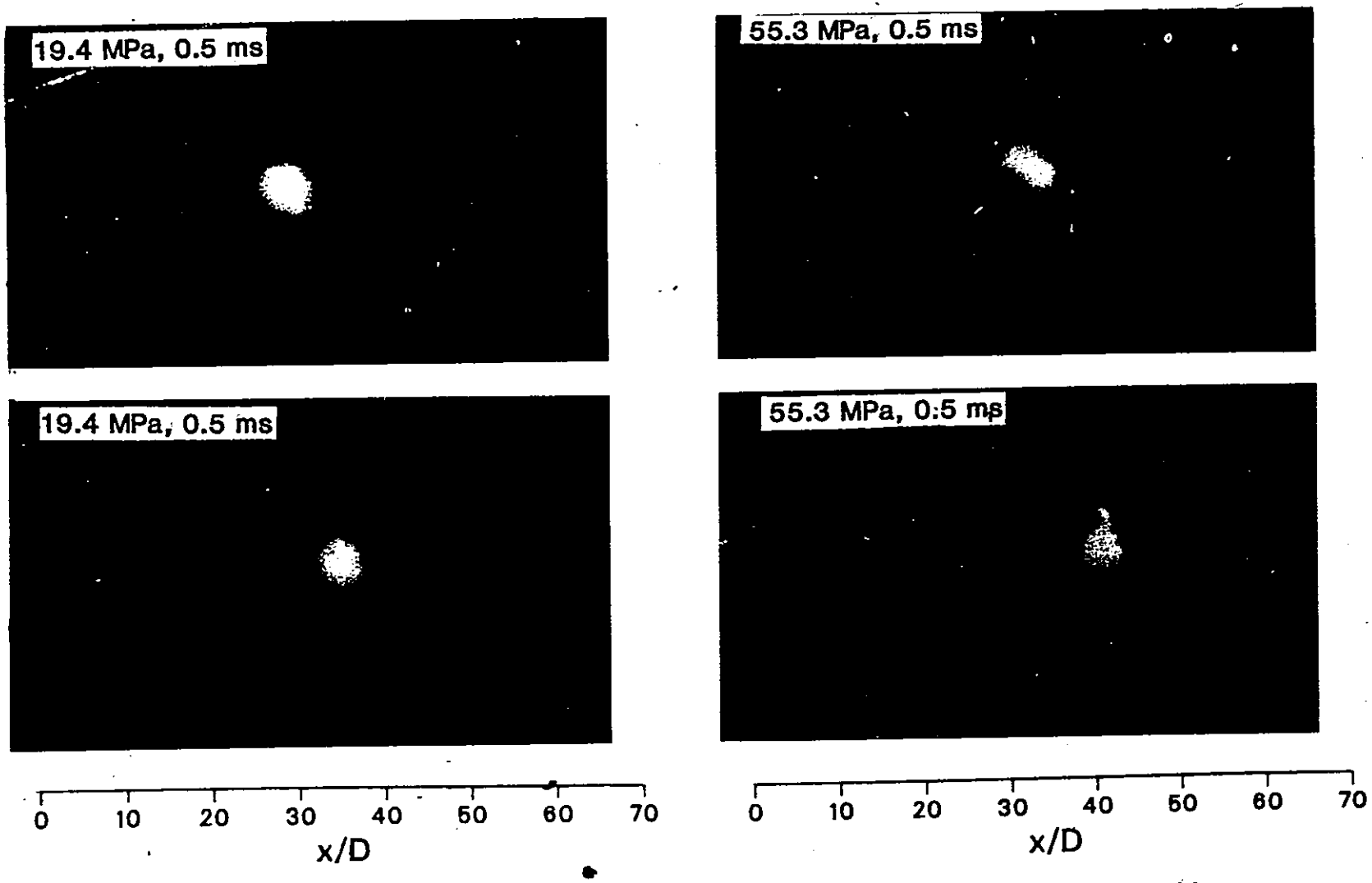

Plate 19a. Jet issuing from plain conical entry nozzle, D=1.02 mm, illuminated by transverse laser-sheet

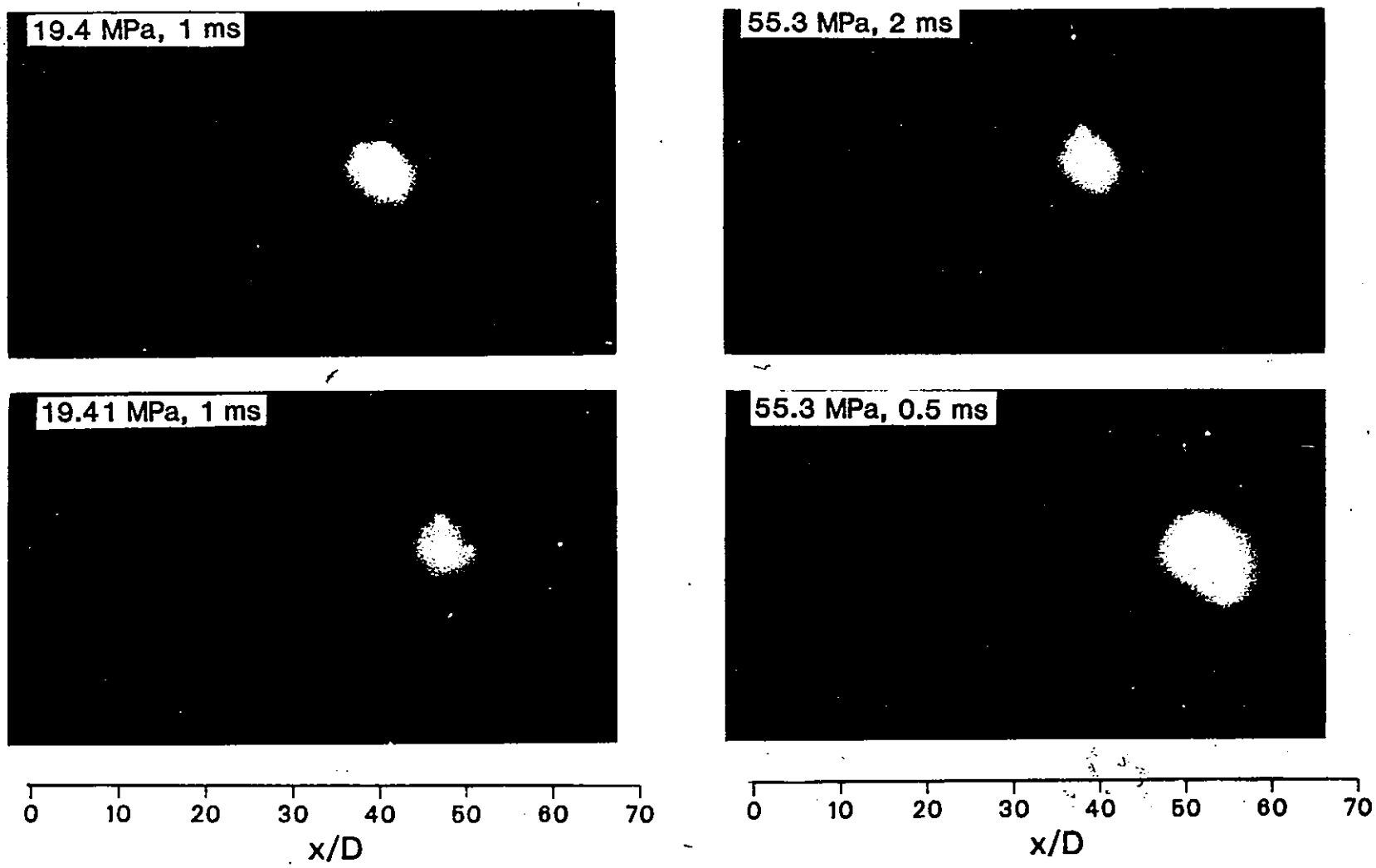

Plate 19b. Jet issuing from plain conical entry nozzle, D=1.02 mm, illuminated by transverse laser-sheet

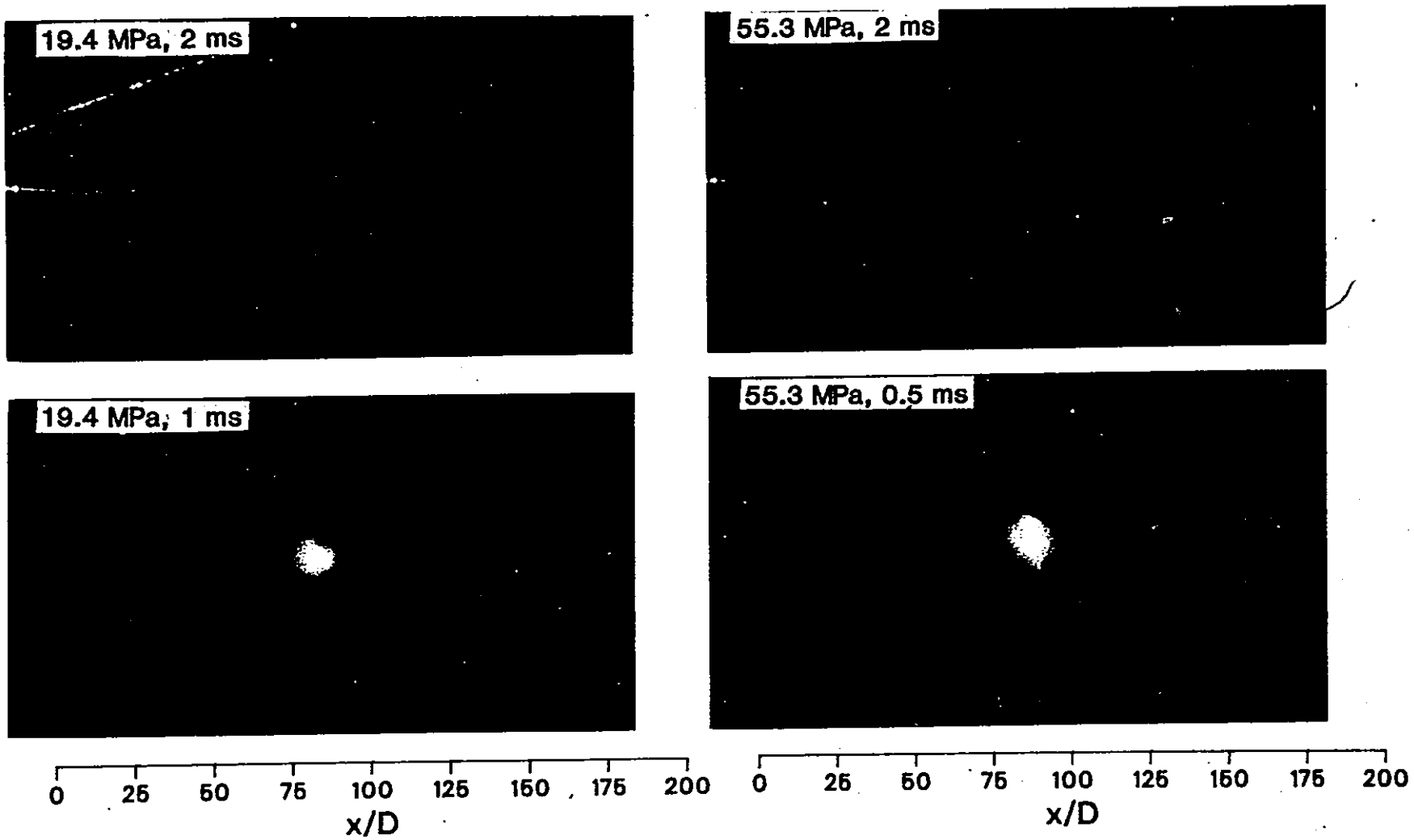

Plate 20a. Jet issuing from plain conical entry nozzle, D=1.02 mm, illuminated by transverse laser-sheet

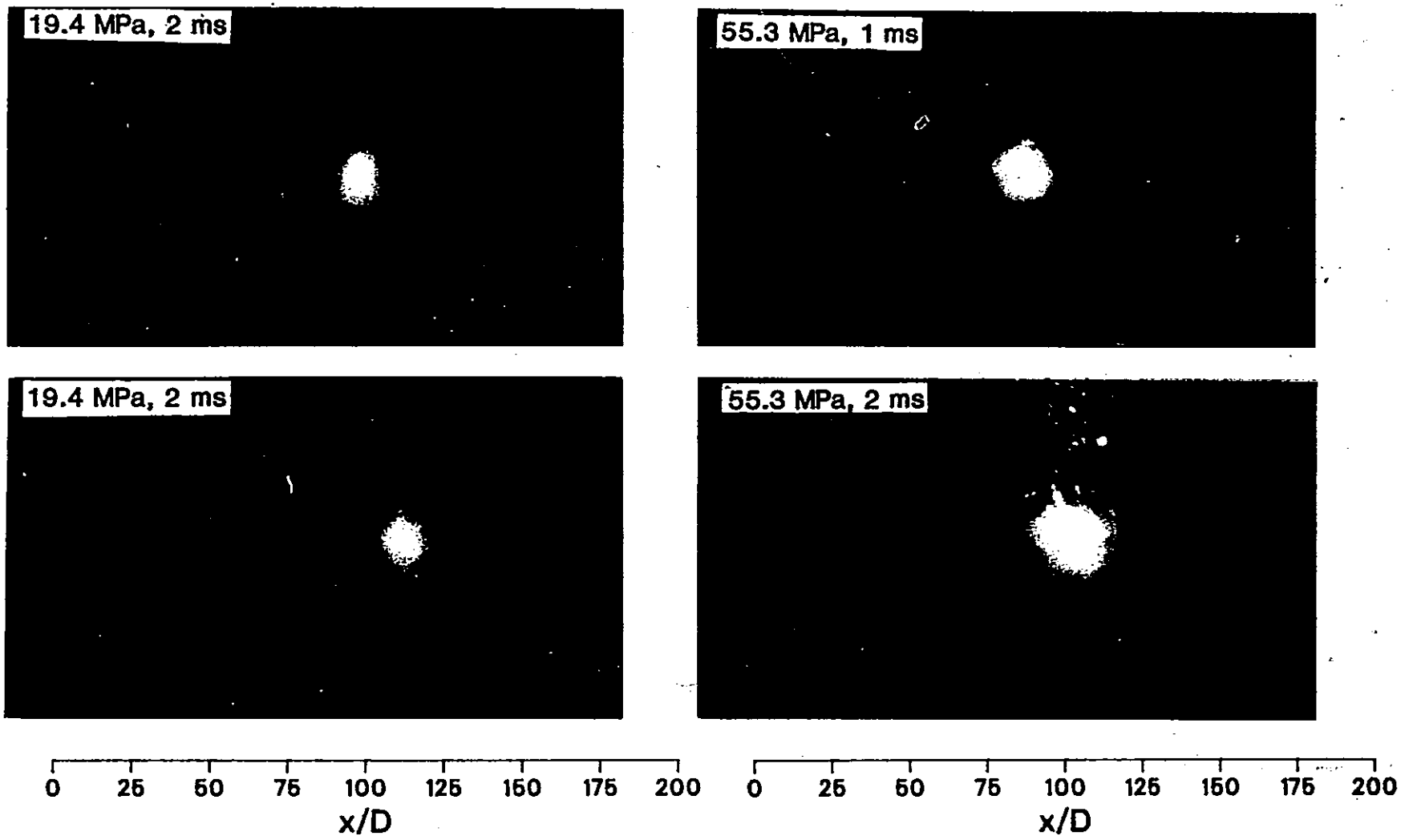

Plate 20b. Jet issuing from plain conical entry nozzle, D=1.02 mm, illuminated by transverse laser-sheet

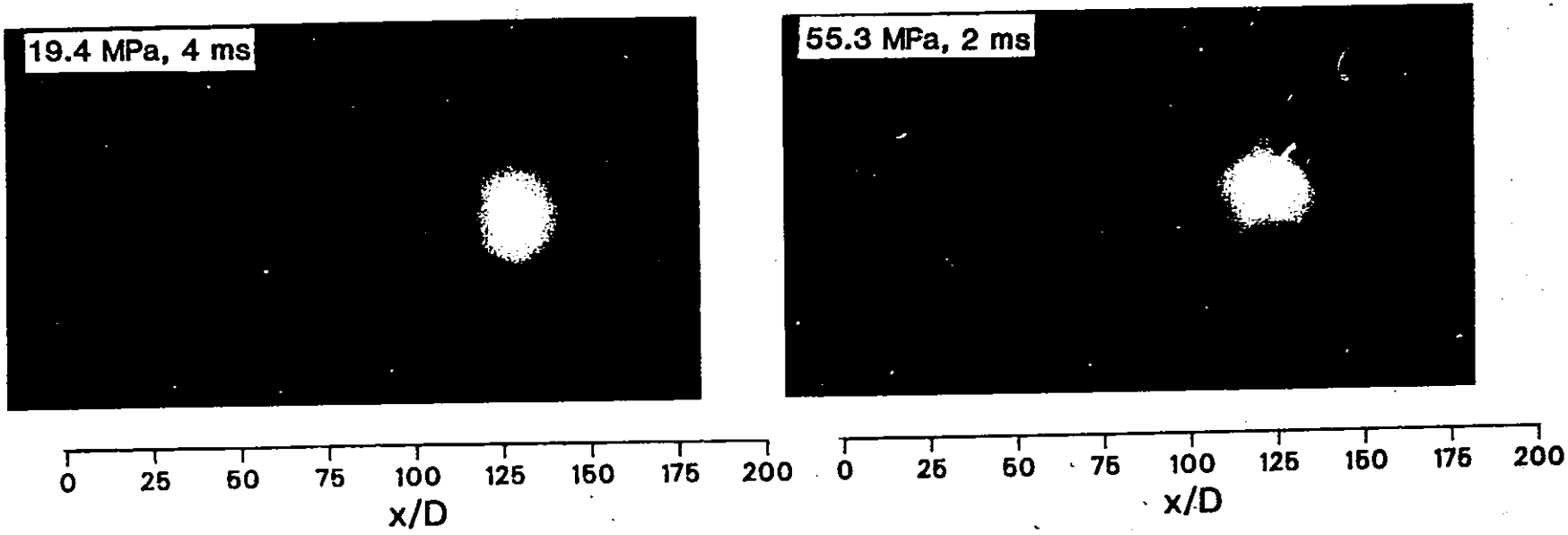

Plate 20c. Jet issuing from plain conical entry nozzle, D=1.02 mm, illuminated by transverse laser-sheet

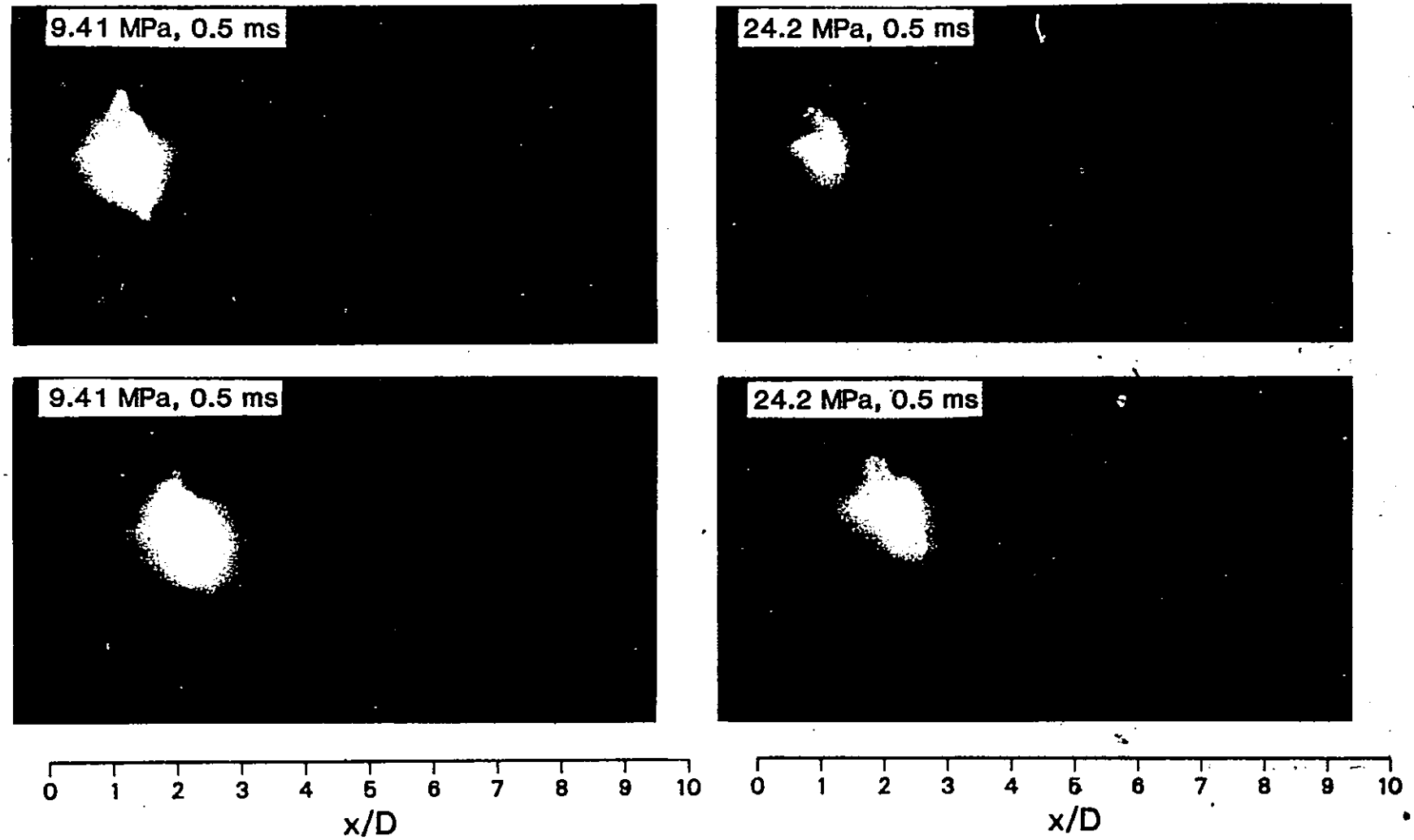

Plate 21a. Jet issuing from plain conical entry nozzle with pin insert, D_e=2.34 mm, illuminated by transverse laser-sheet

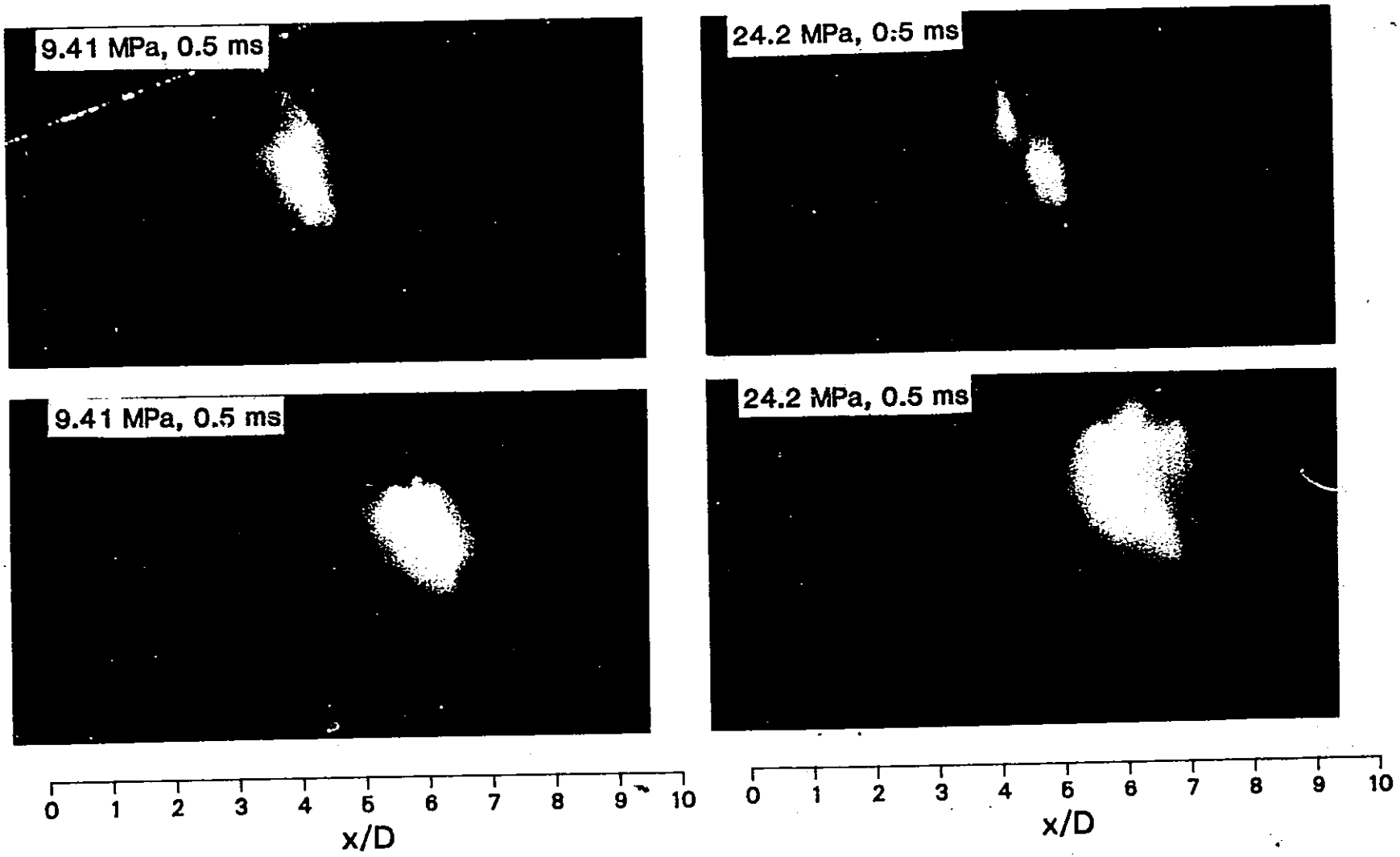

Plate 21b. Jet issuing from plain conical entry nozzle with pin insert, D_e=2.34 mm, illuminated by transverse laser-sheet

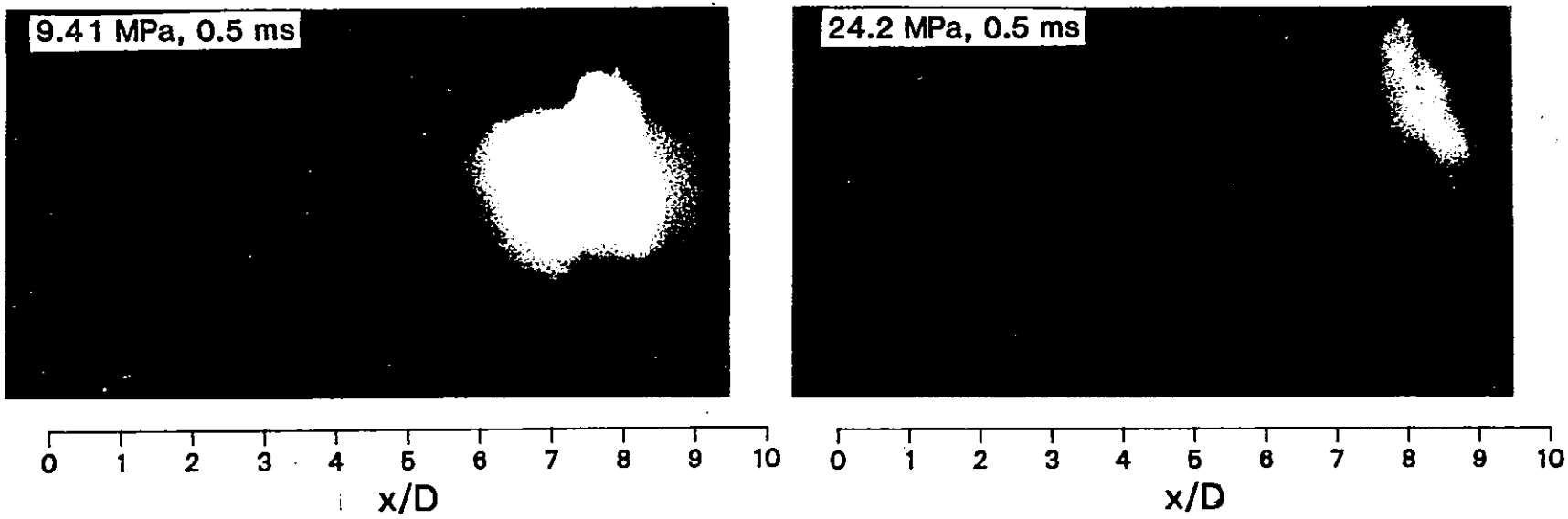

Plate 21c. Jet issuing from plain conical entry nozzle with pin insert, D_e=2.34 mm, illuminated by transverse laser-sheet

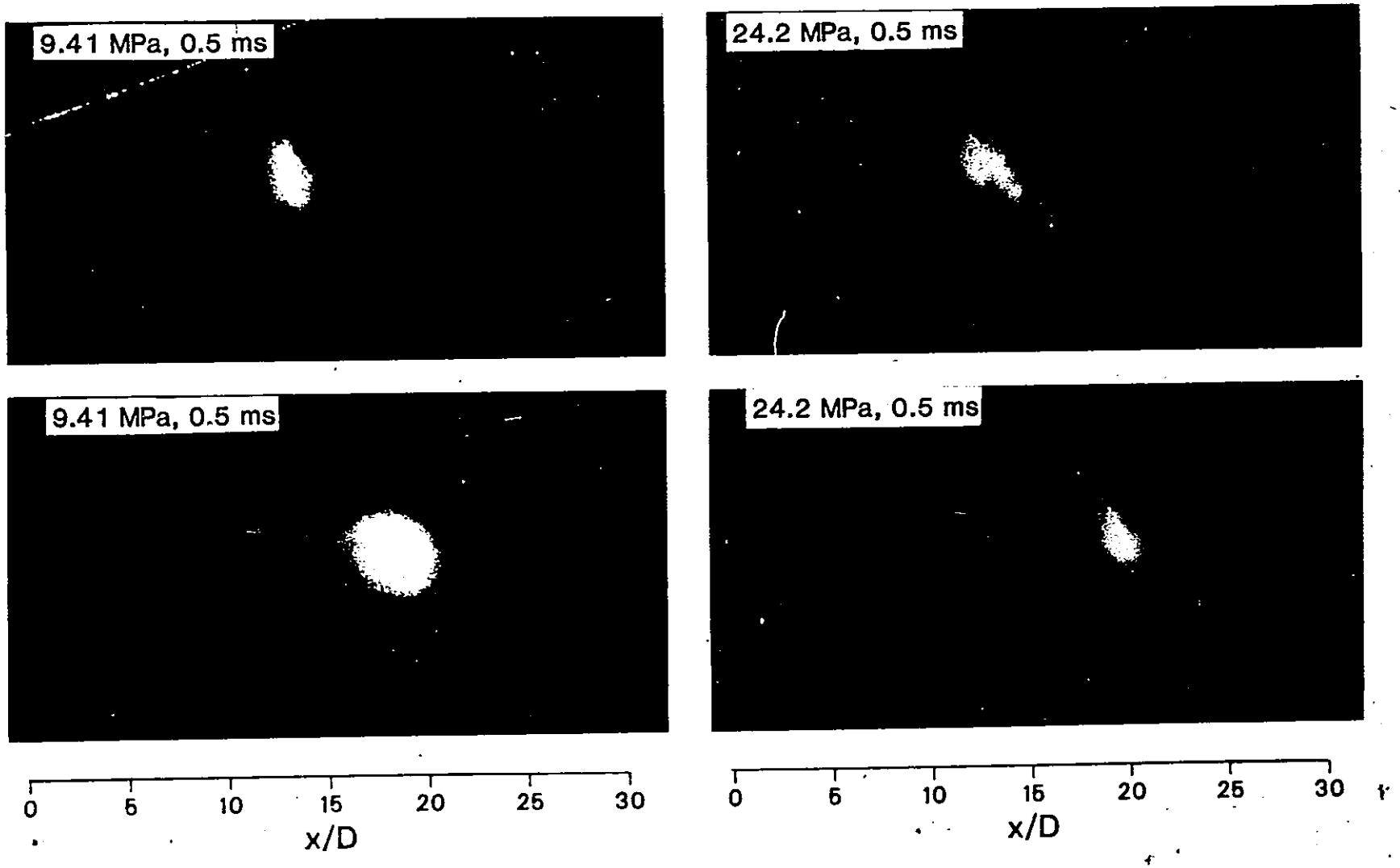

Plate 22a. Jet issuing from plain conical entry nozzle with pin insert, D_e=2.34 mm, illuminated by transverse laser-sheet

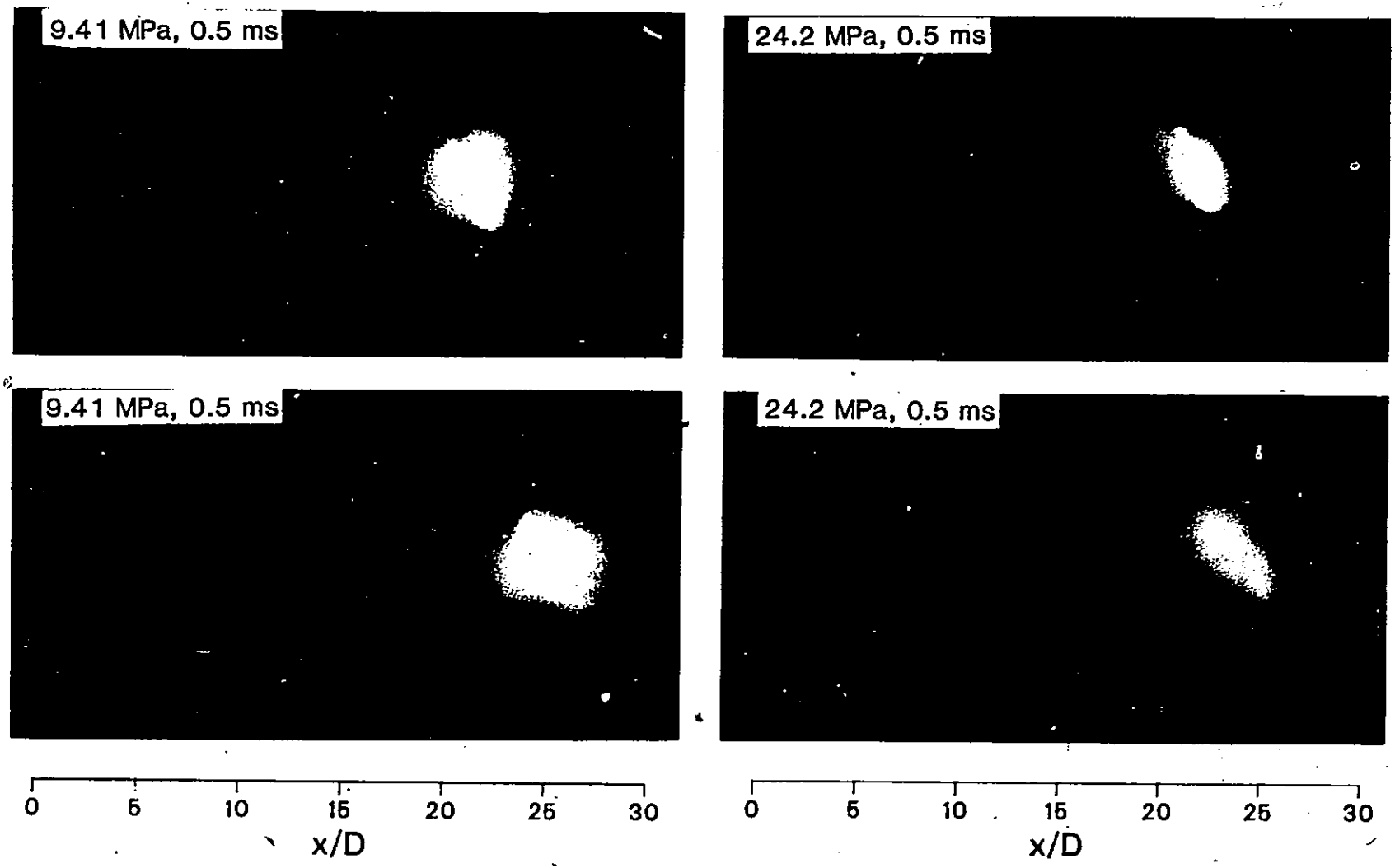

Plate 22b. Jet issuing from plain conical entry nozzle with pin insert, D_e=2.34 mm, illuminated by transverse laser-sheet

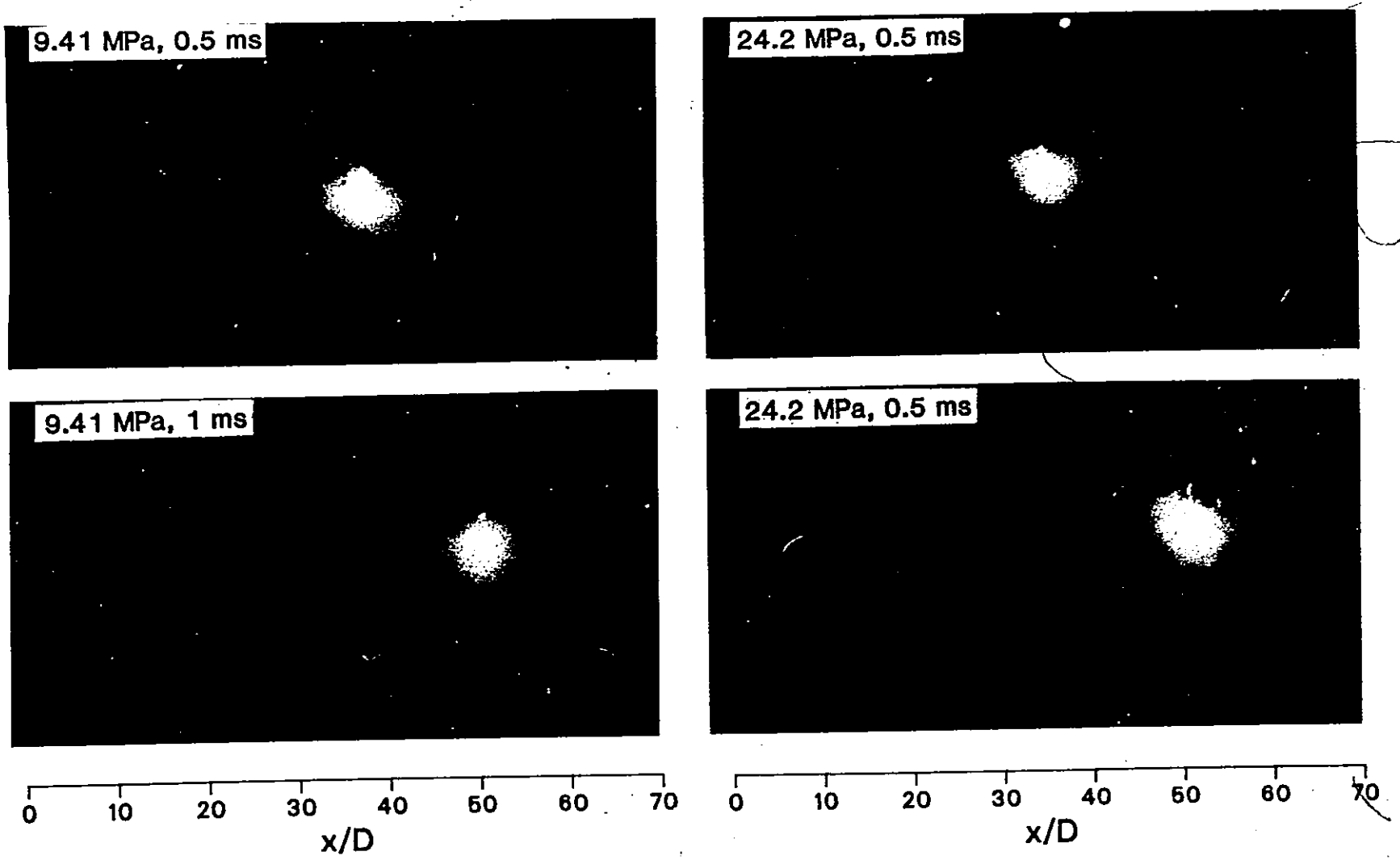

Plate 23a. Jet issuing from plain conical entry nozzle with pin insert, D_e=2.34 mm, illuminated by transverse laser-sheet

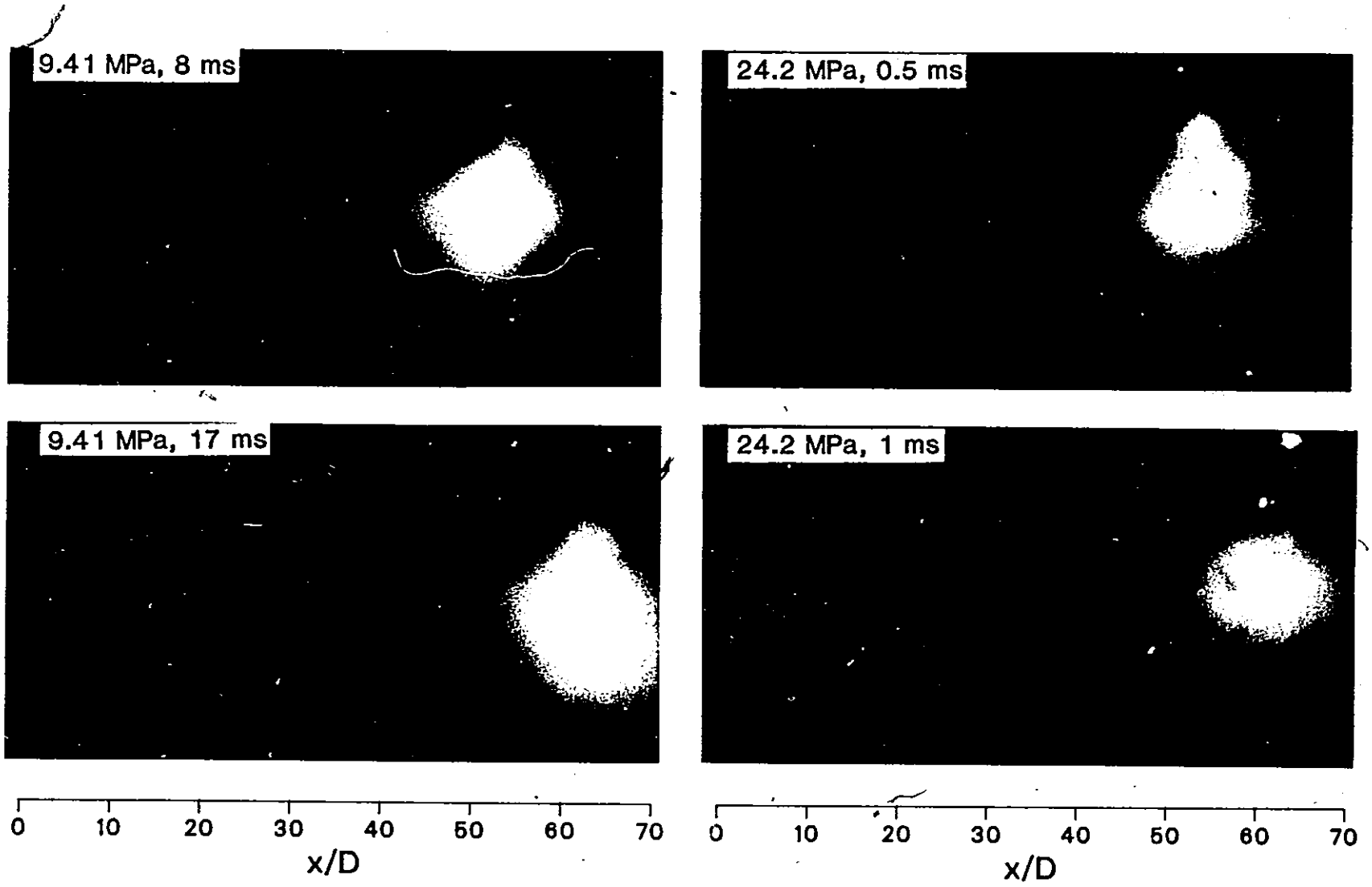

Plate 23b. Jet issuing from plain conical entry nozzle with pin insert, D_e=2.34 mm, illuminated by transverse laser-sheet

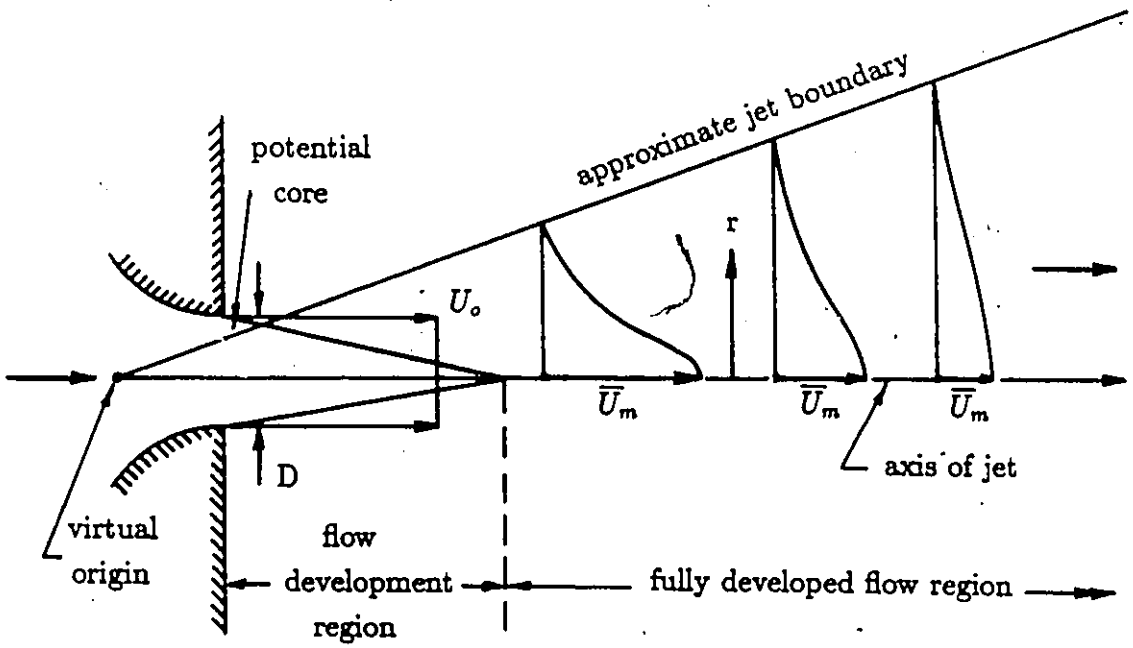

Figure 1. Sketch of a circular turbulent jet (Rajaratnam, 1976)

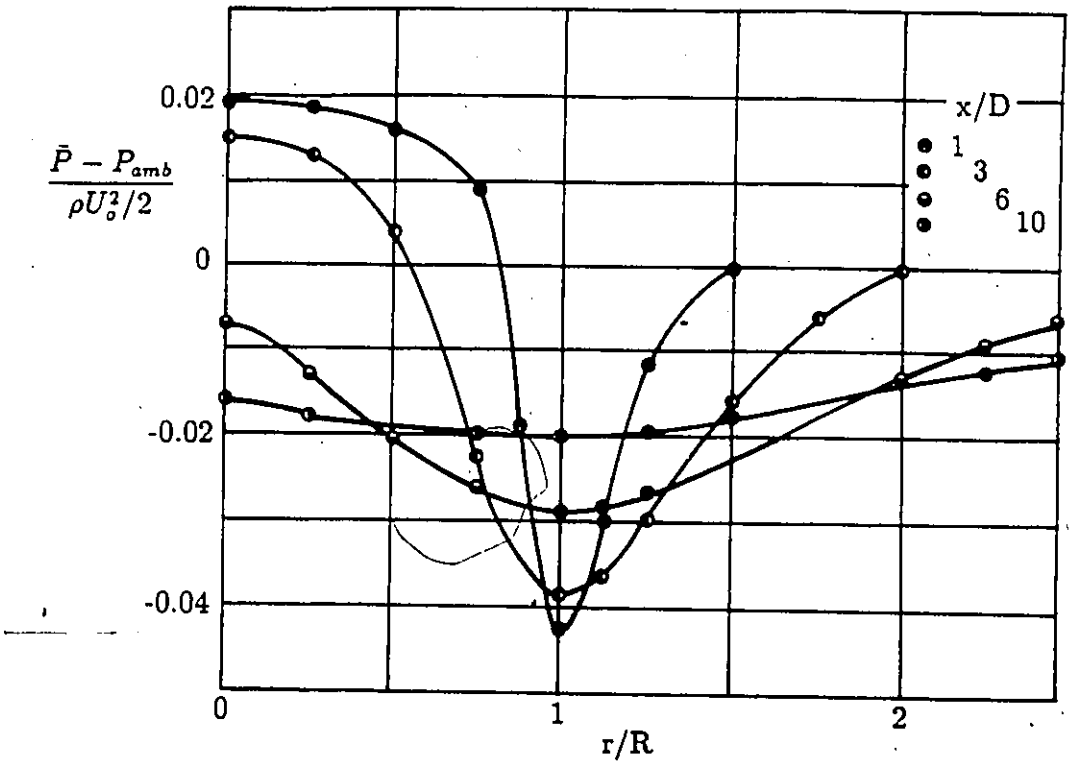

Figure 2. Mean pressure profiles (Sami et al., 1967)

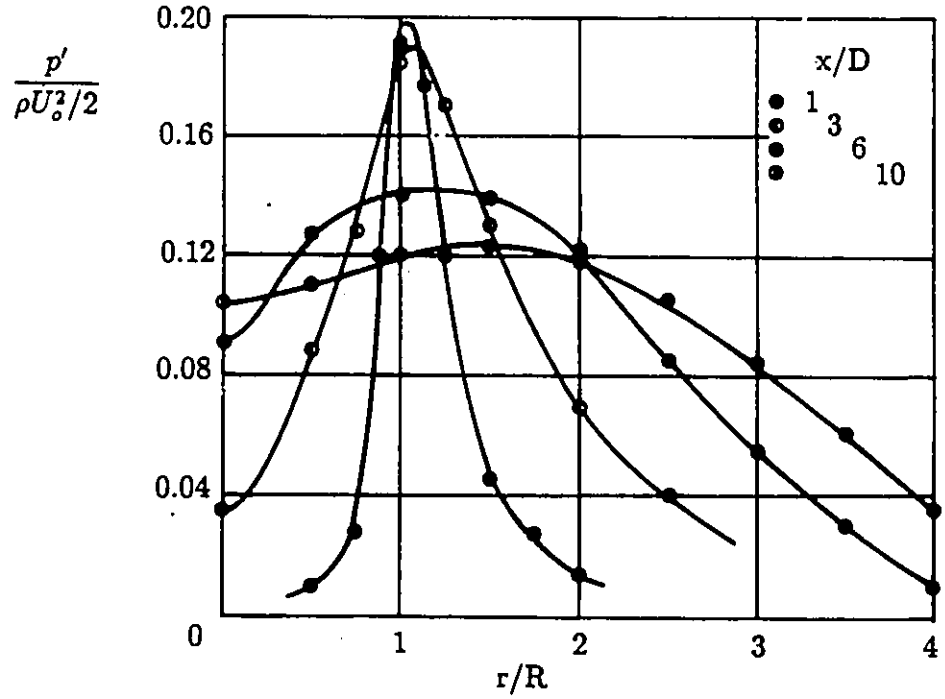

Figure 3. R.m.s. pressure fluctuation profiles (Sami et al., 1967)

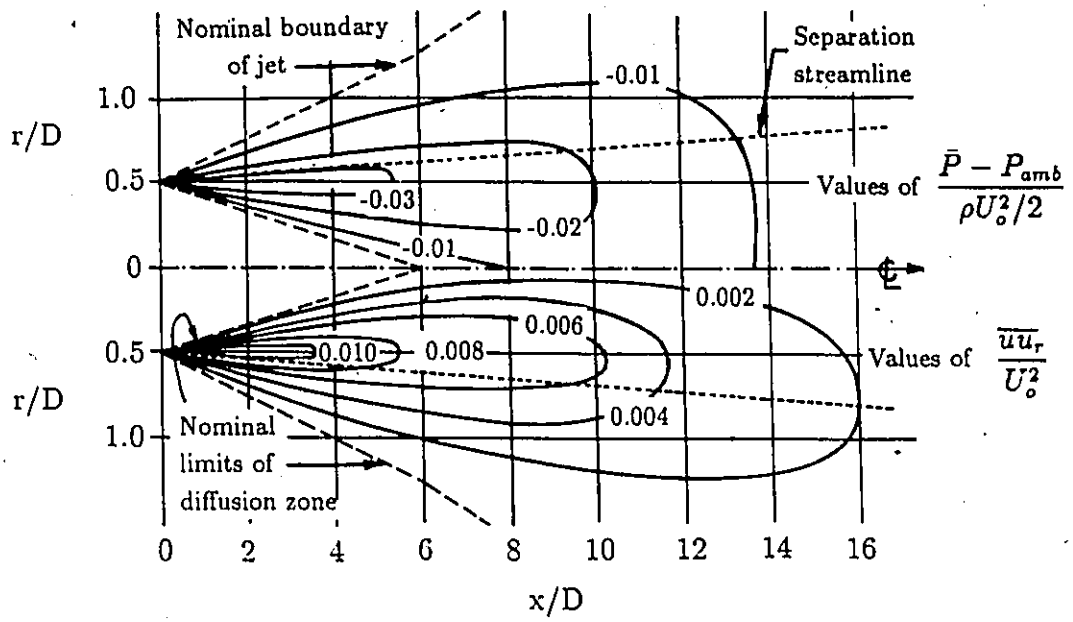

Figure 4. Distribution of mean pressure (above) and turbulent shear stress (below) in a circular jet (note scale distortion) (Rouse, 1966)

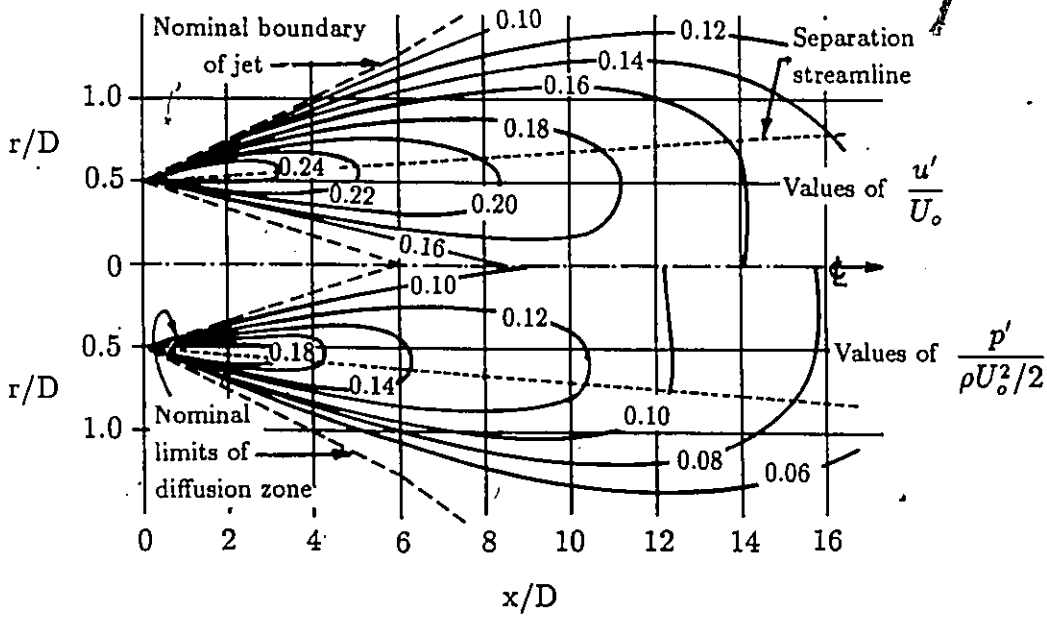

Figure 5. Distribution of velocity (above) and pressure (below) fluctuations (Rouse, 1966)

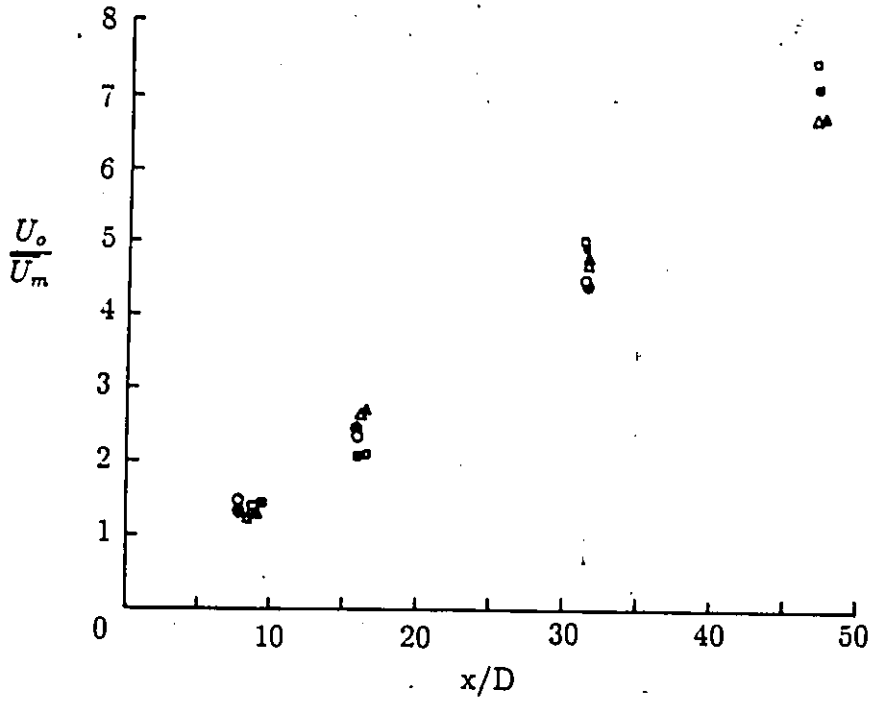

Figure 6. Centre-line velocity *vs* x/D (Barker, 1973).
Open symbols, water; filled symbols, Polyox.
○, U_o=122 cm/s; △, U_o=257 cm/s; □, U_o=340 cm/s

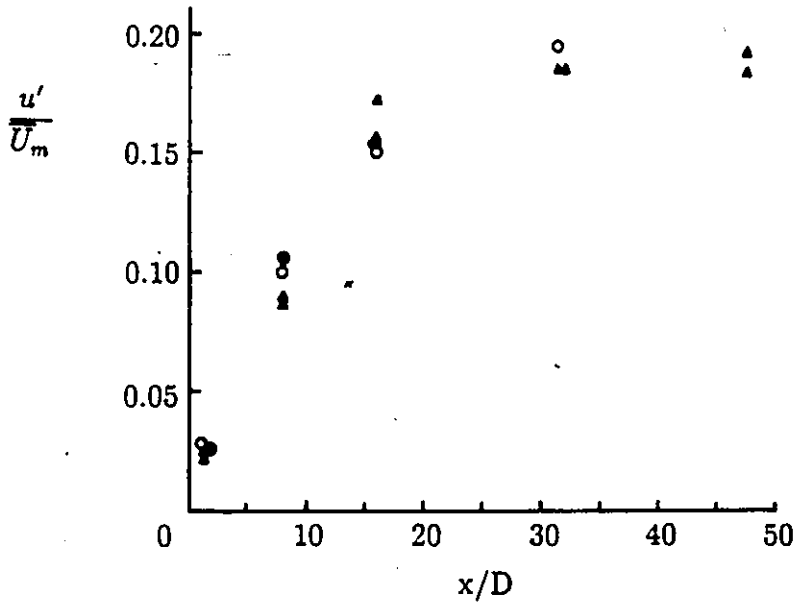

Figure 7. Turbulence level *vs* x/D (Barker, 1973). Symbols as in figure 6.

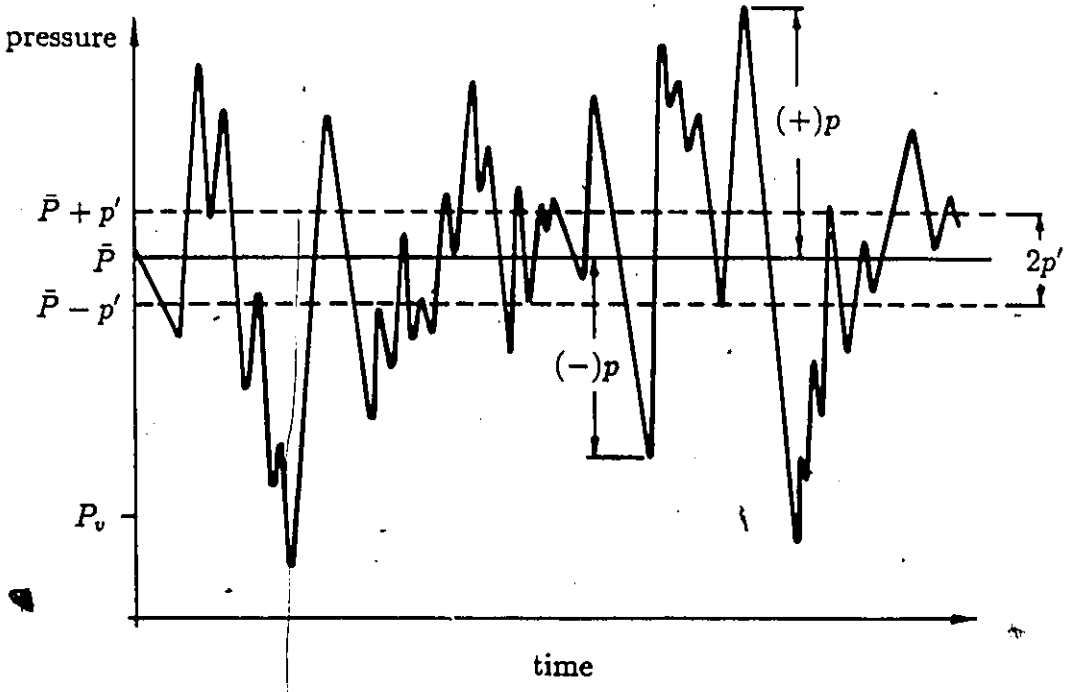

Figure 8. Fluctuating pressure at a point

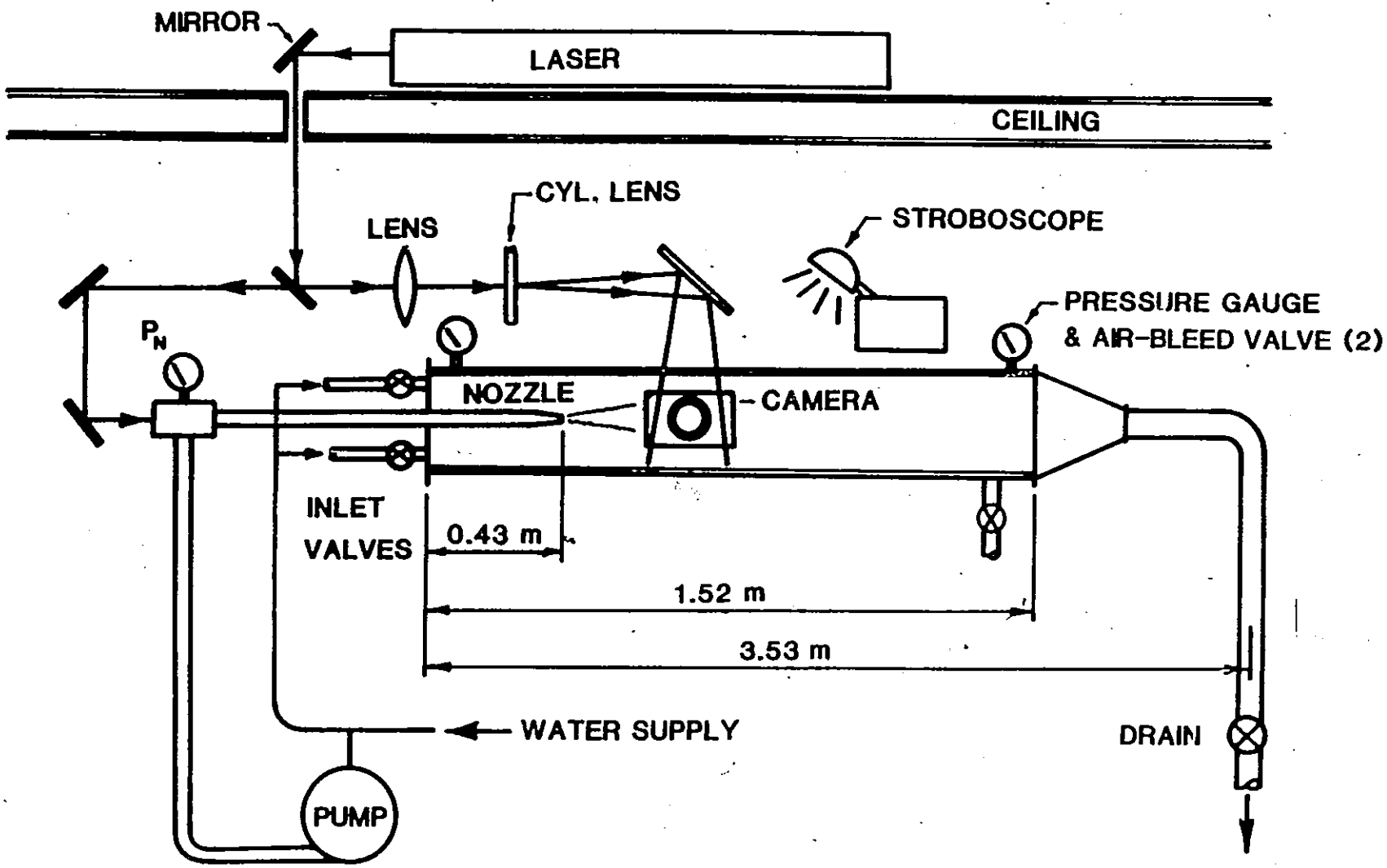

Figure 9. Experimental apparatus

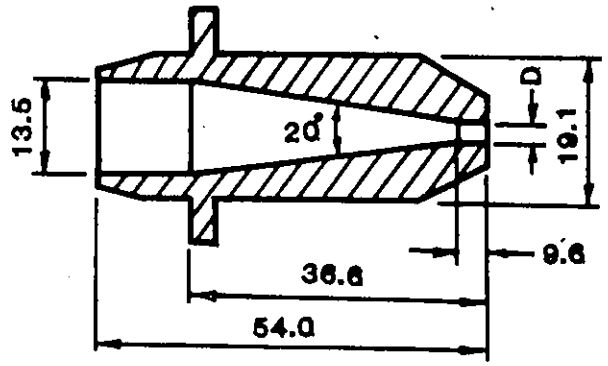

a) PLAIN CONICAL ENTRY NOZZLE
D = 4.01 mm

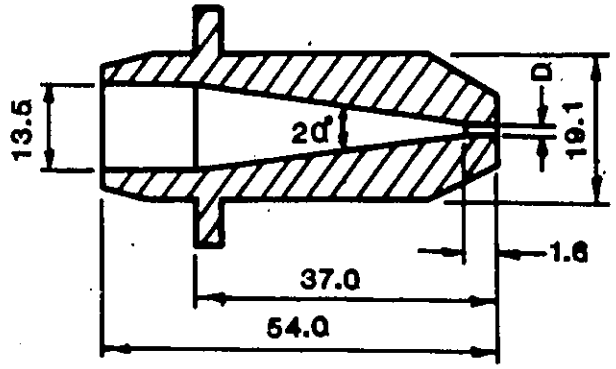

b) PLAIN CONICAL ENTRY NOZZLE
D = 1.02 mm

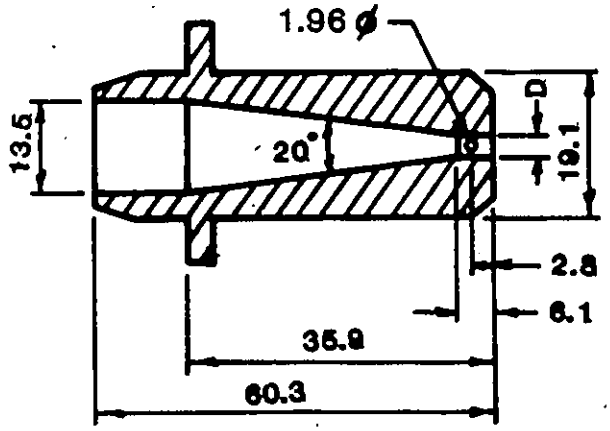

c) PLAIN CONICAL ENTRY NOZZLE WITH PIN INSERT
D_e = 2.34 mm
D = 3.05 mm

NOTE: ALL DIMENSIONS IN mm

Figure 10. Sketch of nozzles

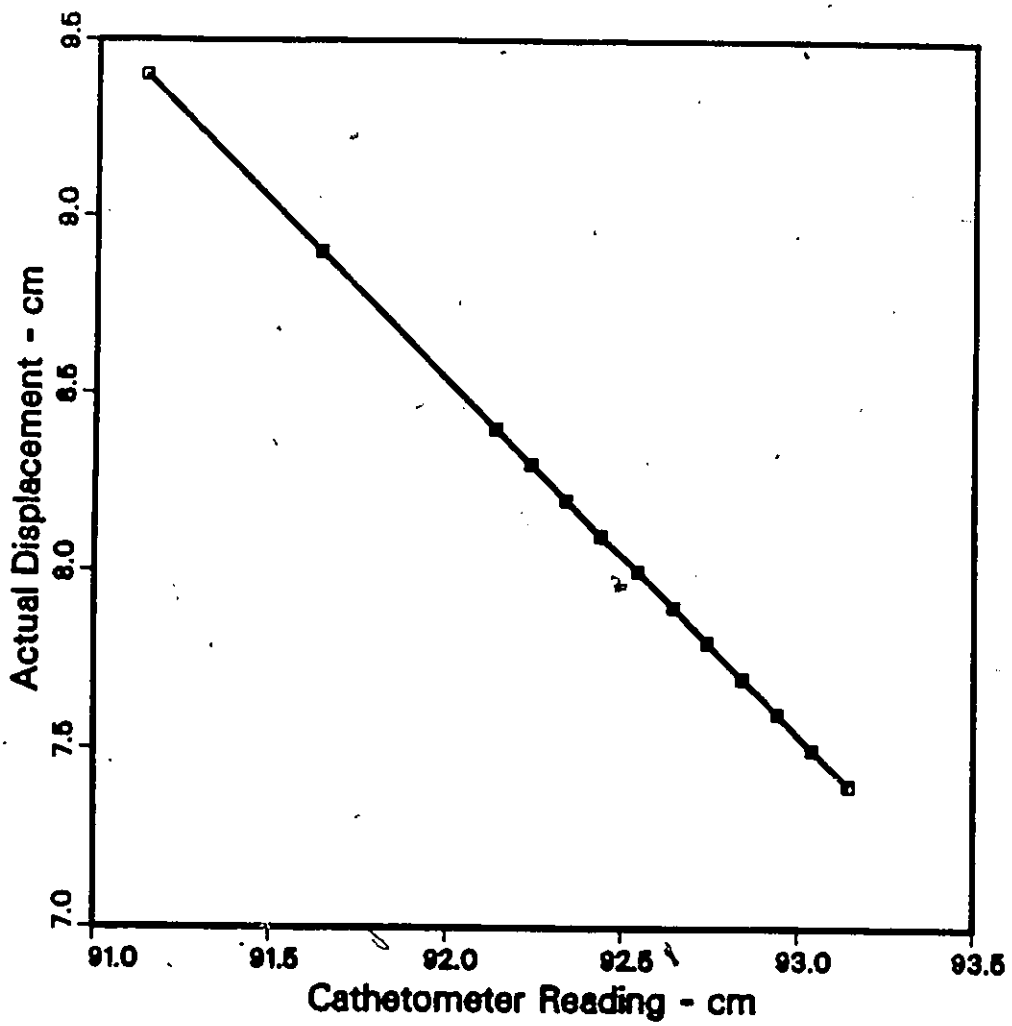

Figure 11. Cathetometer calibration curve

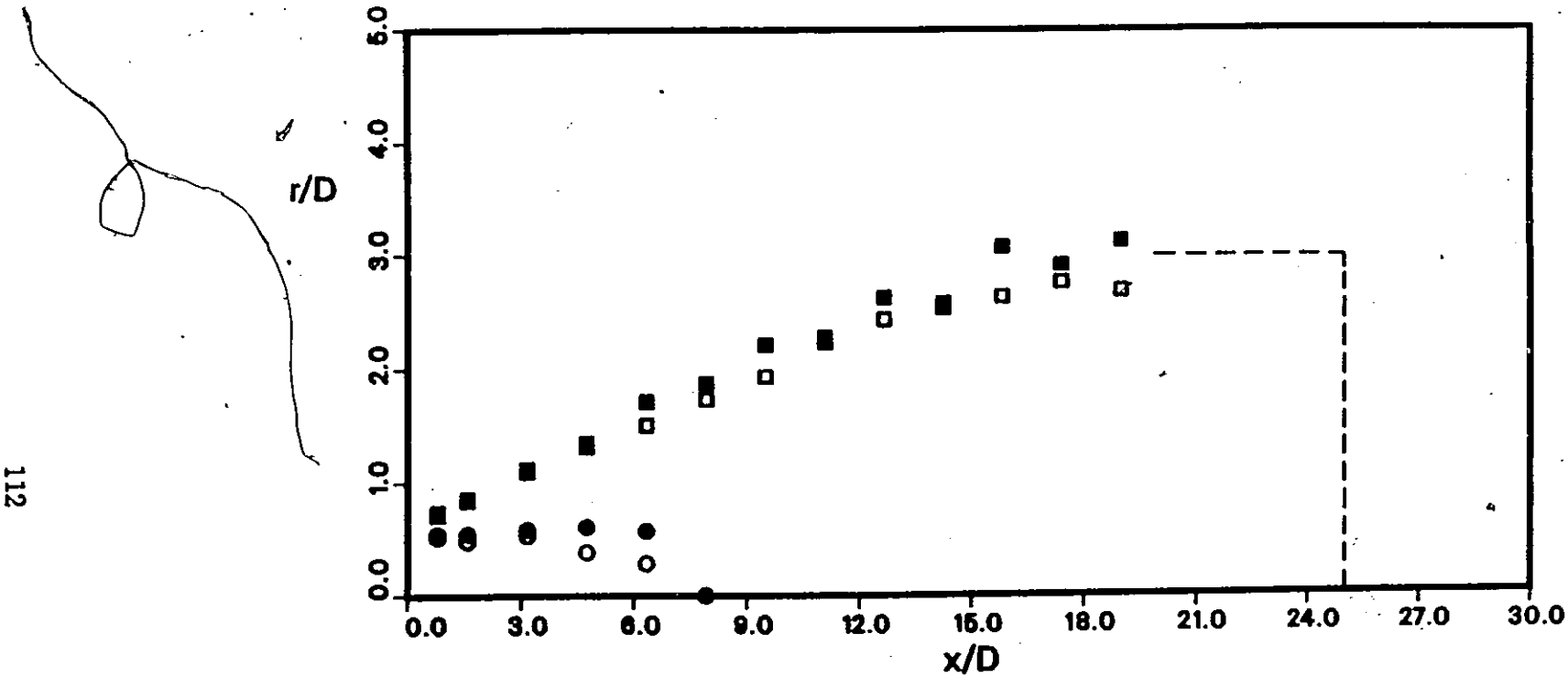

Figure 12. Cavitation region for jet issuing from plain conical entry nozzle, D = 4.01 mm; transverse laser-sheet illumination; outer boundary: □P_N=1.65 MPa, ■P_N=3.89 MPa; inner boundary: ○P_N=1.65 MPa, ●P_N=3.89 MPa

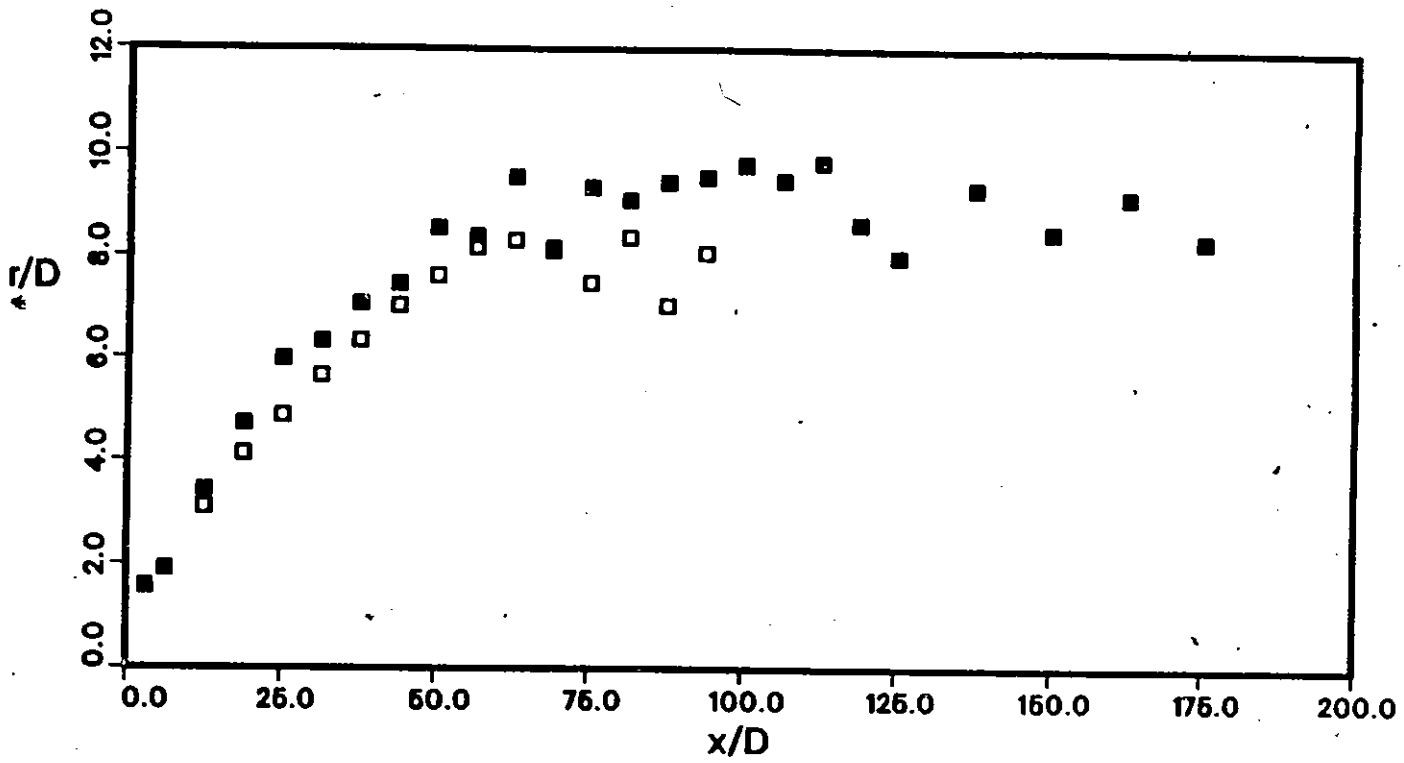

Figure 13. Cavitation region for jet issuing from plain conical entry nozzle, D = 1.02 mm; stroboscopic illumination; outer boundary: □P_N=19.4 MPa, ■P_N=55.2 MPa;

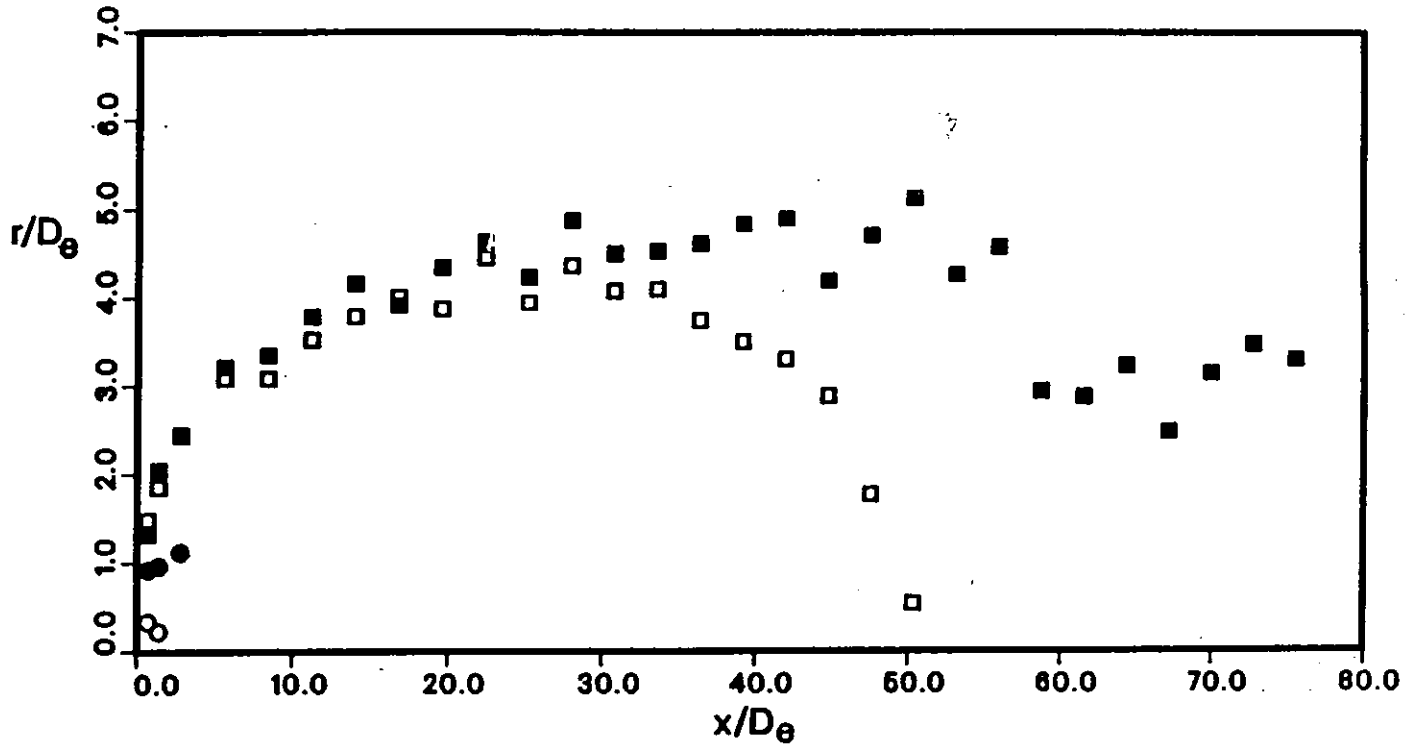

Figure 14. Cavitation region for jet issuing from plain conical entry nozzle with pin insert, D_e = 2.34 mm; stroboscopic illumination; outer boundary: □P_N=9.41 MPa, ■P_N=24.2 MPa; inner boundary: ○P_N=9.41 MPa, ●P_N=24.2 MPa

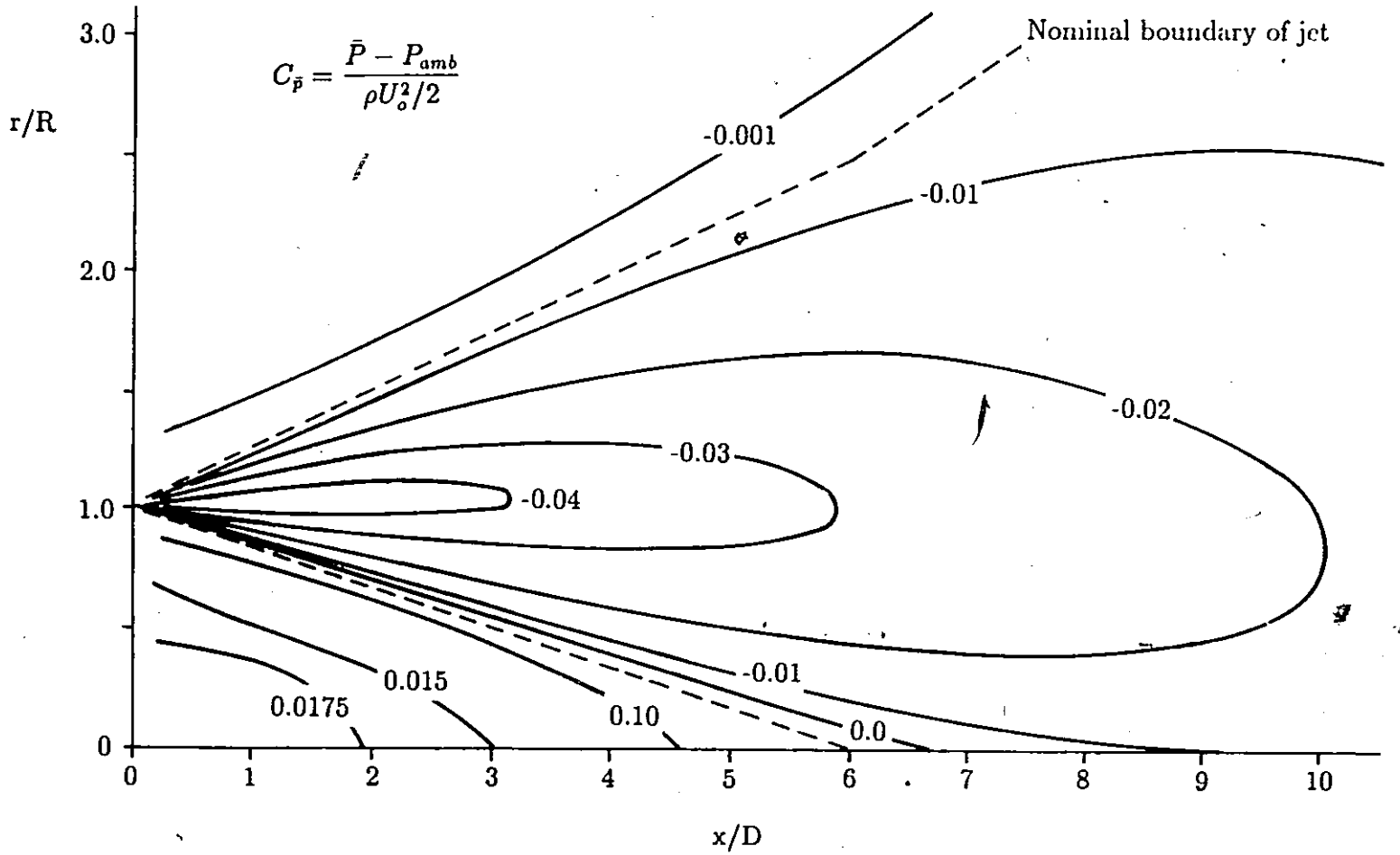

Figure 15. Distribution of mean pressure in a circular jet (Sami et al., 1967)

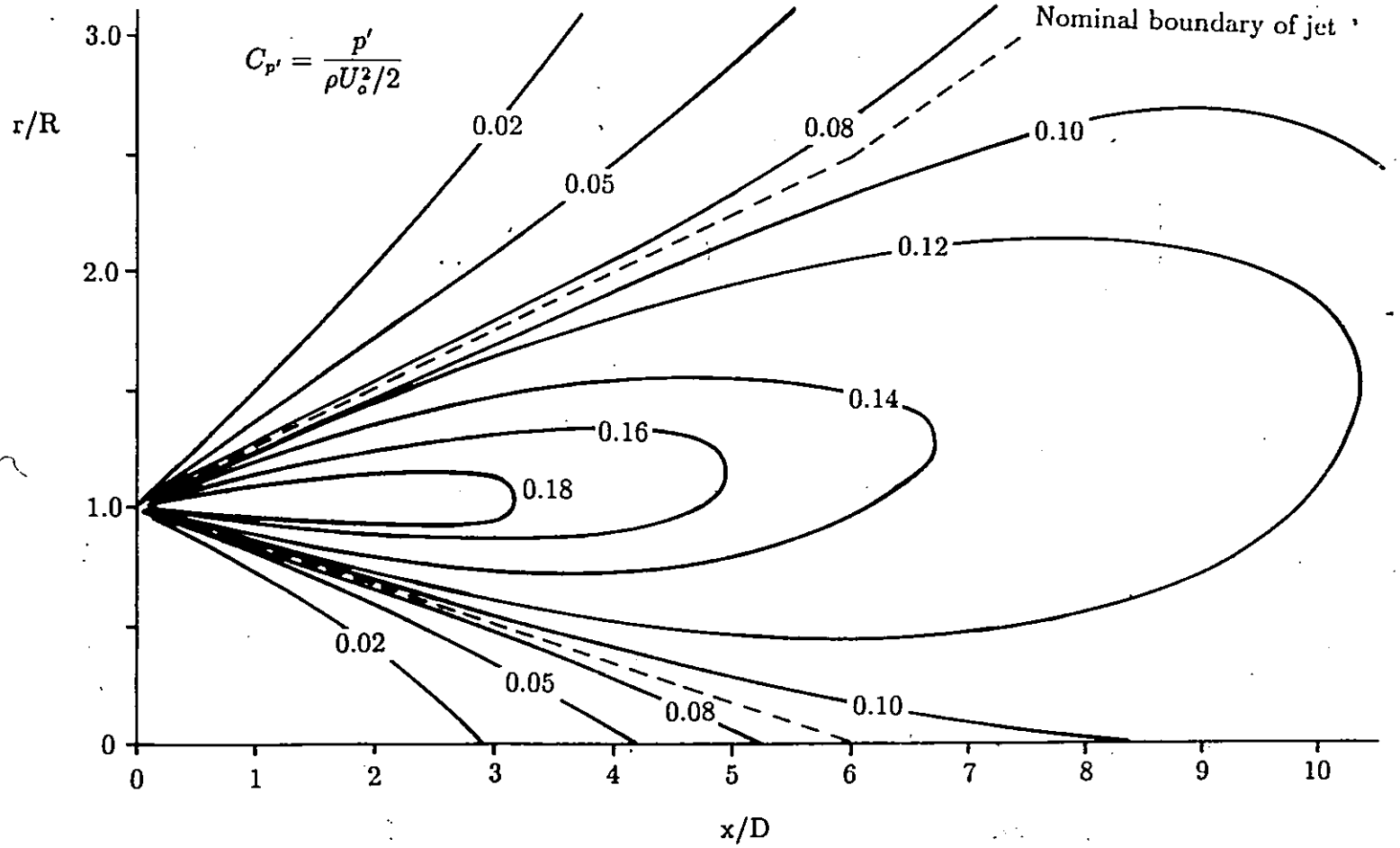

Figure 16. Distribution of r.m.s. pressure fluctuations in a circular jet (Sami et al., 1967)

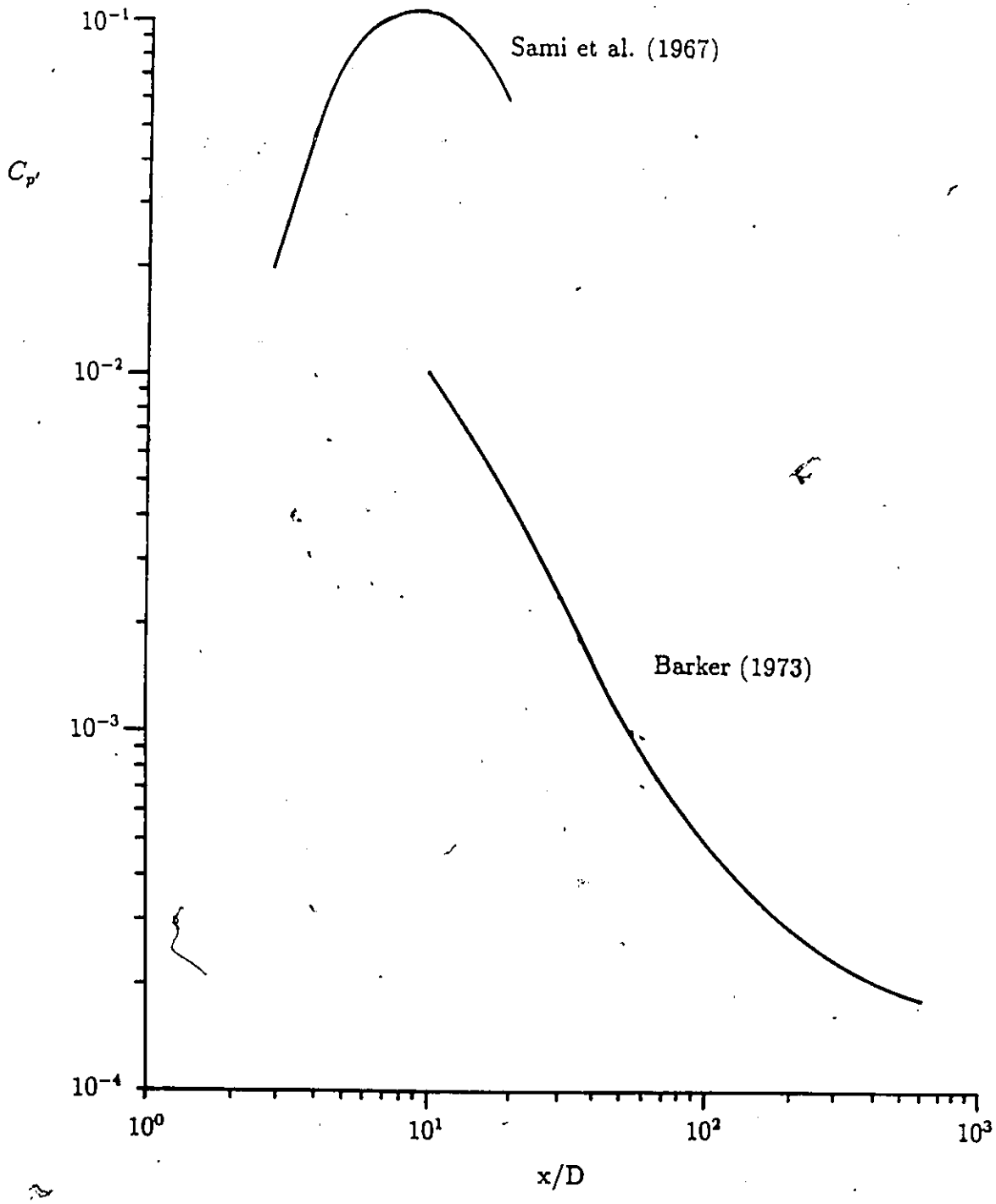

Figure 17. R.m.s. pressure fluctuations on jet axis

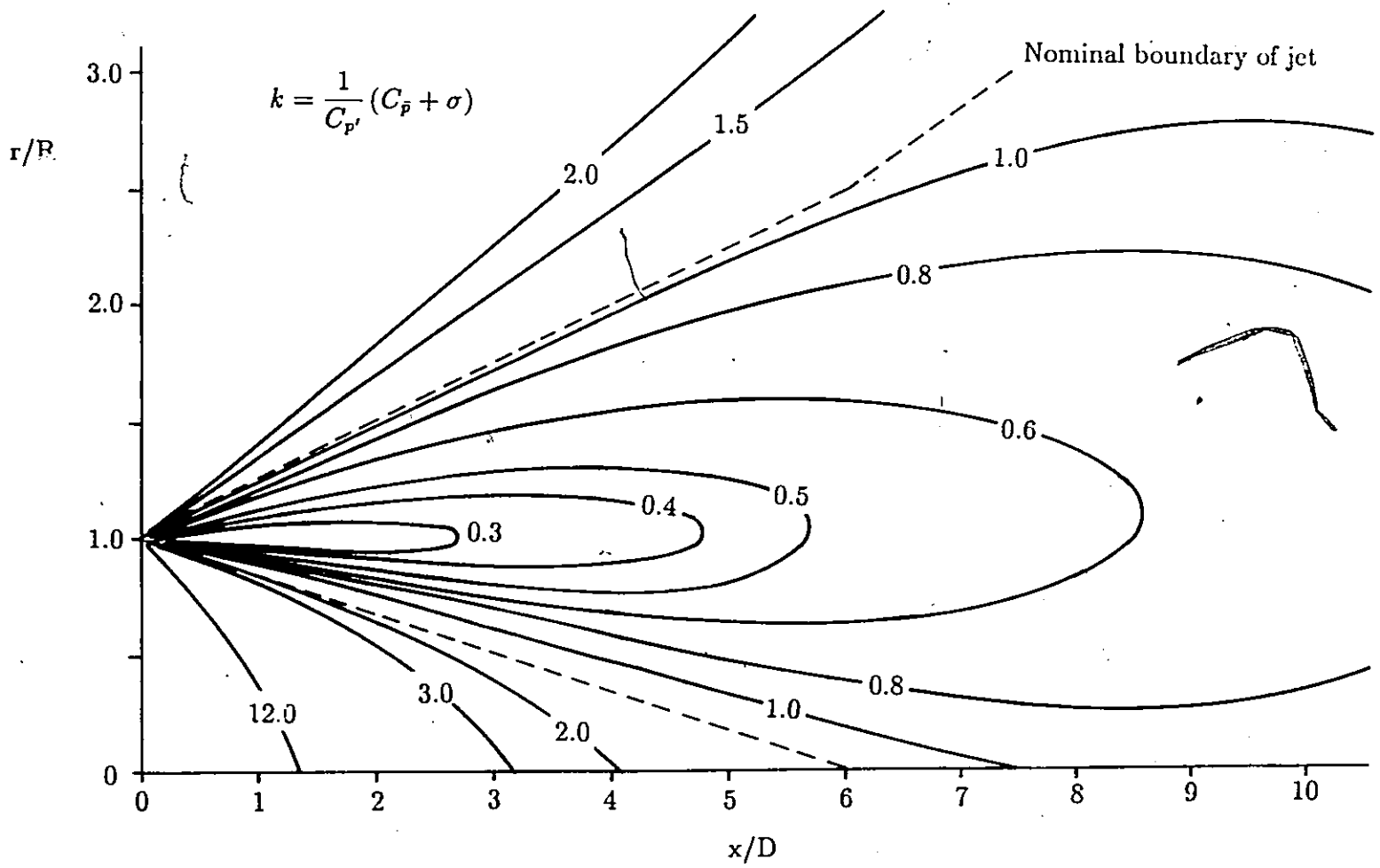

Figure 18. Distribution of the coefficient k for jet issuing from plain conical entry nozzle; D=4.01 mm, P_N = 1.65 MPa and U_o = 55.5 m/s

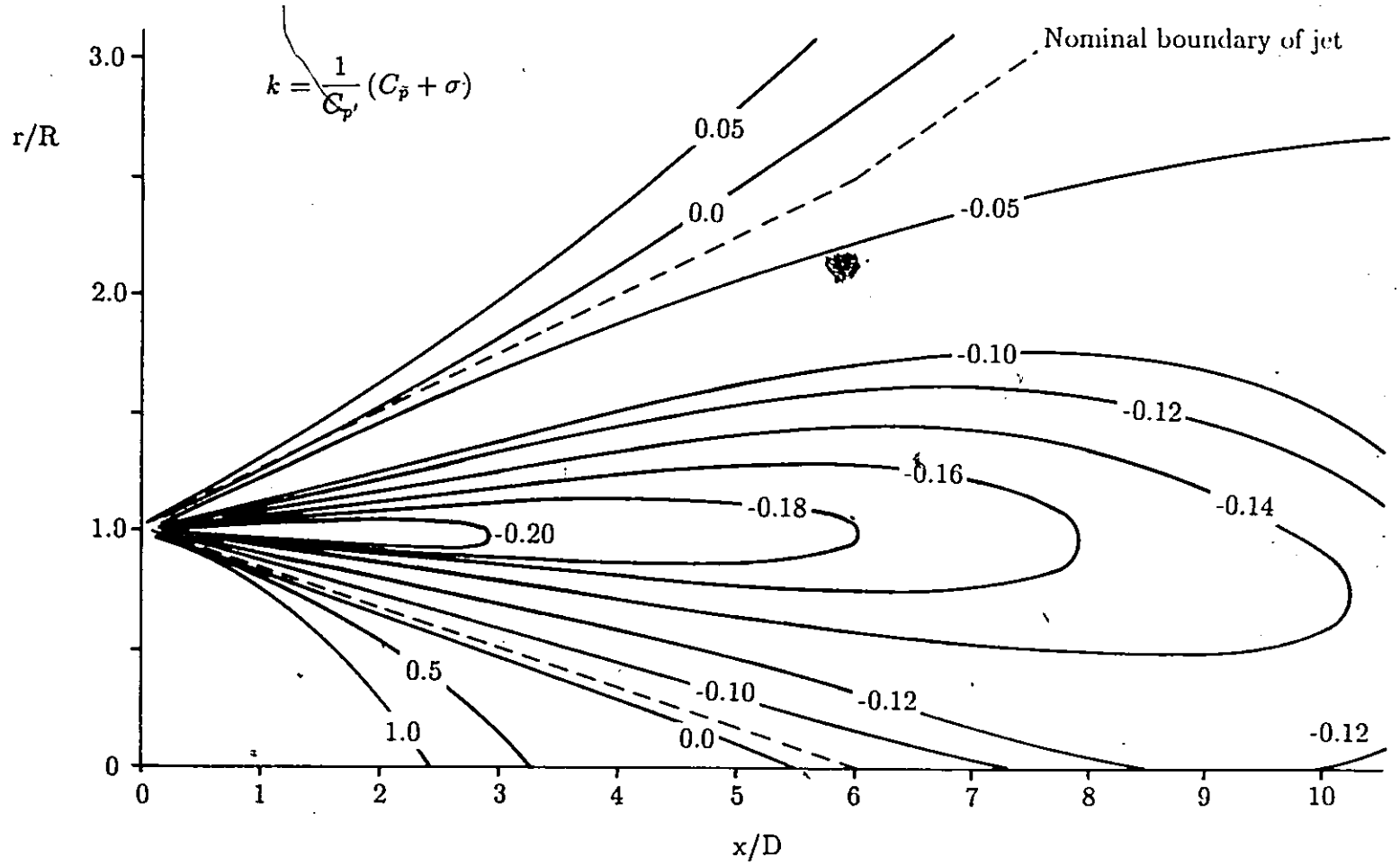

Figure 19. Distribution of the coefficient k for jet issuing from plain conical entry nozzle; D=1.02 mm, P_N = 55.2 MPa and U_o = 331. m/s

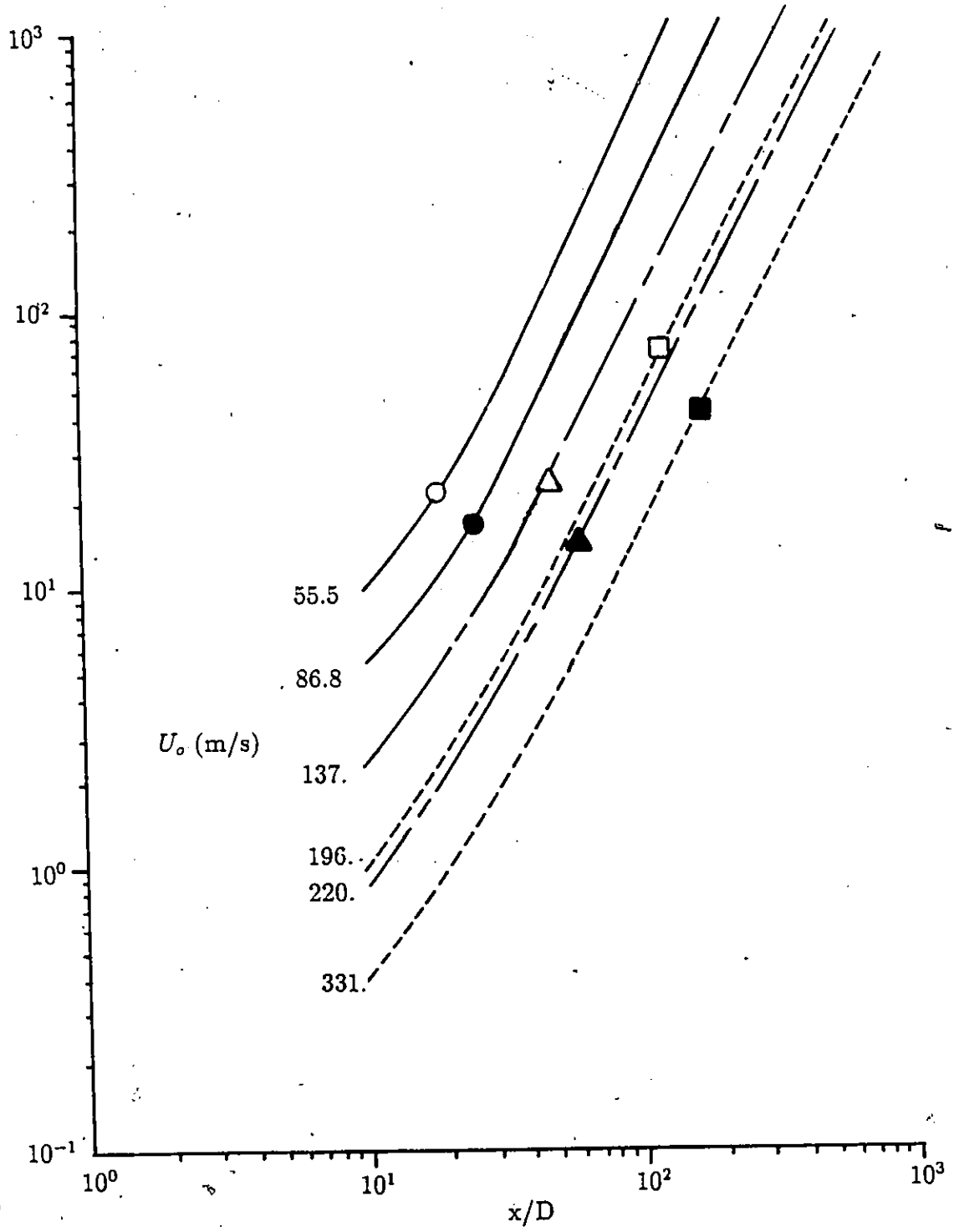

Figure 20. Estimates of the coefficient k along jet axis;
——— $D = 4.01$ mm, ○ $P_N = 1.65$ MPa, ● $P_N = 3.89$ MPa,
- - - - - - - $D = 1.02$ mm, □ $P_N = 19.4$ MPa, ■ $P_N = 55.2$ MPa;
nozzle with pin insert:
——— $D_e = 2.34$ mm, △ $P_N = 9.41$ MPa, ▲ $P_N = 24.24$ MPa;

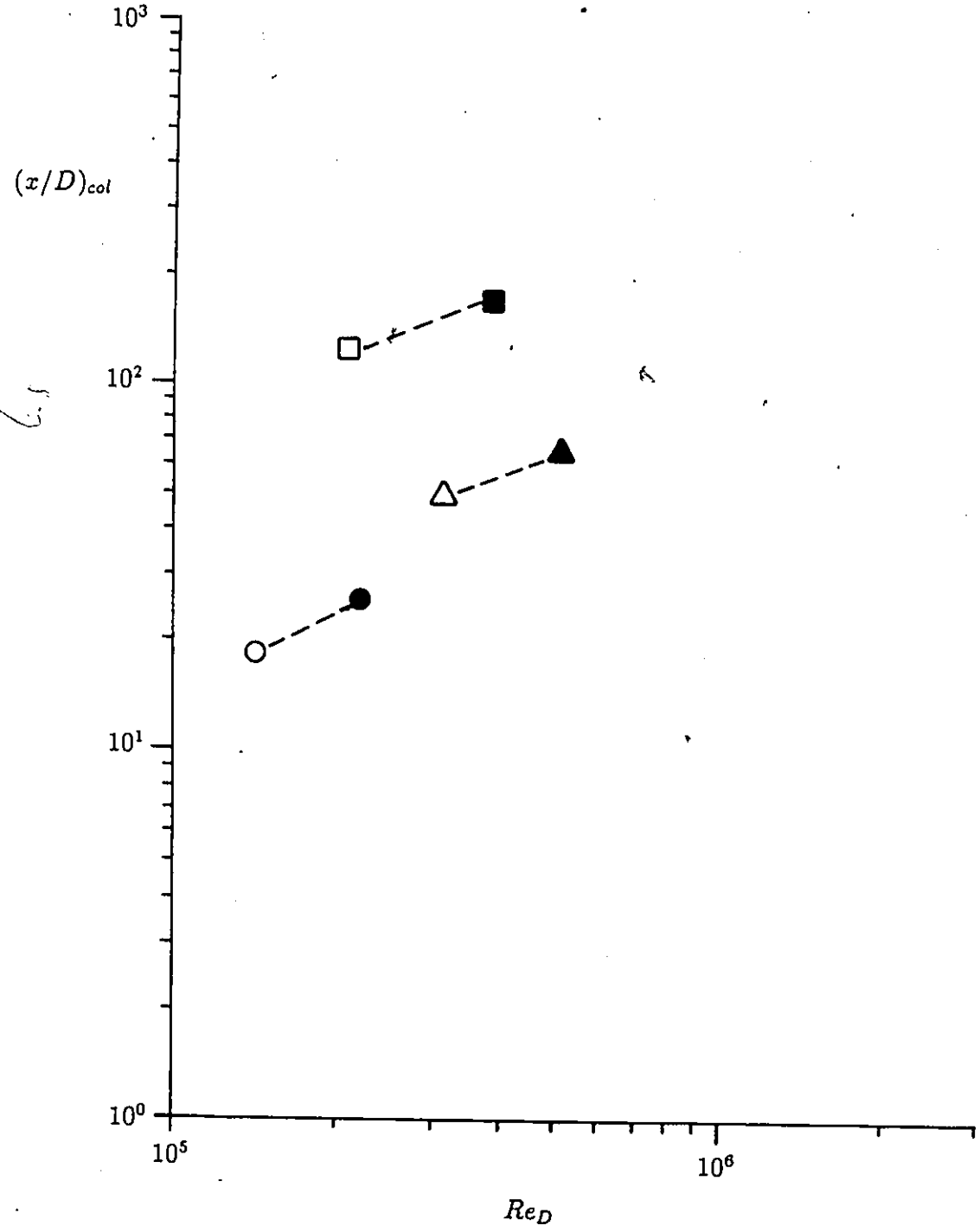

Figure 21. x/D *vs* Re_D;
D = 4.01 mm, ○ P_N = 1.65 MPa, ● P_N = 3.89 MPa;
D = 1.02 mm, □ P_N = 19.4 MPa, ■ P_N = 55.2 MPa;
nozzle with pin insert:
D_e = 2.34 mm, △ P_N = 9.41 MPa, ▲ P_N = 24.24 MPa.

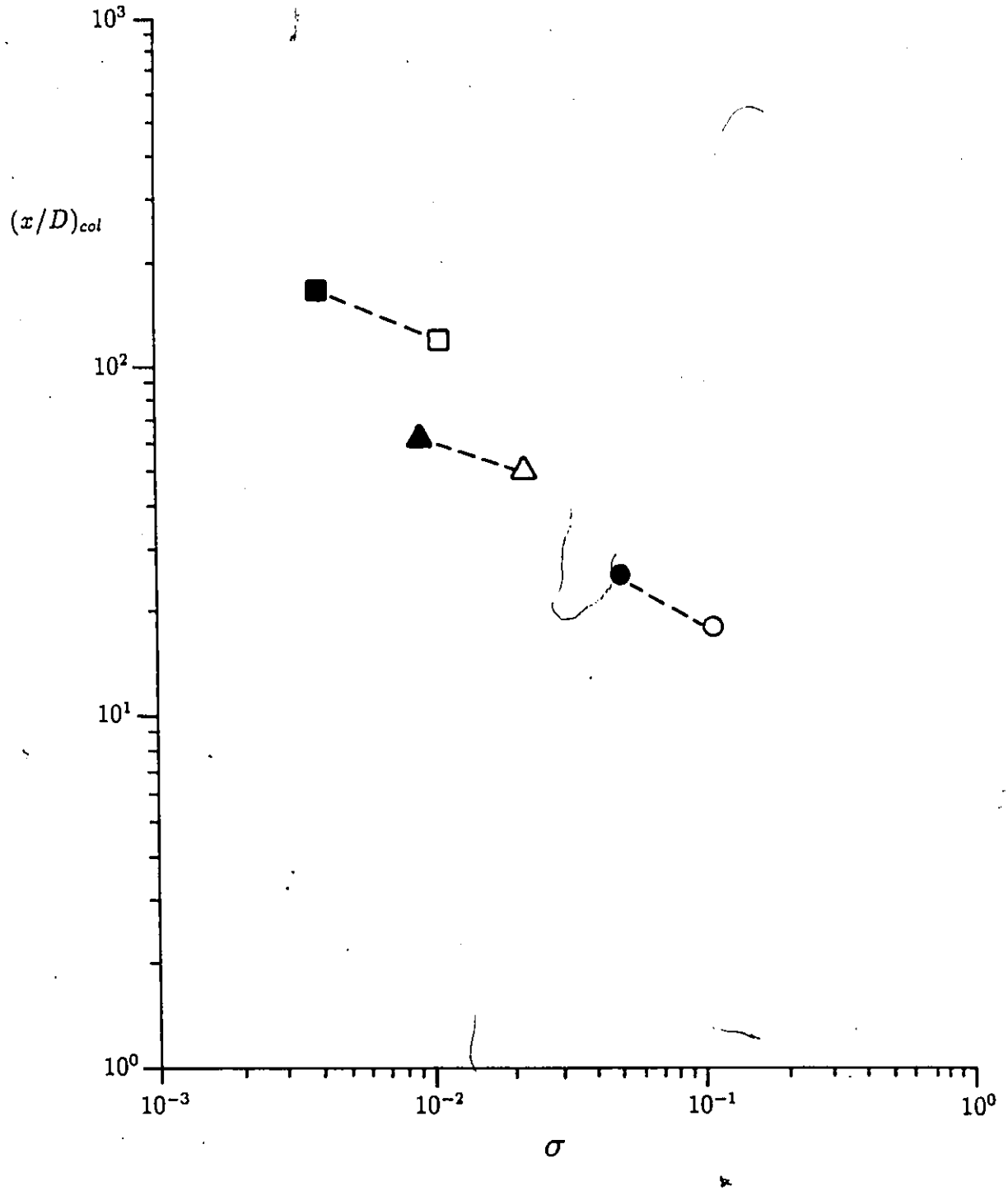

Figure 22. x/D *vs* σ;
D = 4.01 mm, ○ P_N = 1.65 MPa, ● P_N = 3.89 MPa;
D = 1.02 mm, □ P_N = 19.4 MPa, ■ P_N = 55.2 MPa;
nozzle with pin insert:
D_e = 2.34 mm, △ P_N = 9.41 MPa, ▲ P_N = 24.24 MPa.